



University of Strathclyde
Department of Electronic and Electrical Engineering

MSc in SMART GRIDS

Individual MSc Final Report

Analysis of information from the installed Dynamic Line Rating (DLR) systems, to define a deployment plan up to 2030

Beatriz Morales Montoya (RegNo 202260382)

Industrial Supervisor: David Santacruz

Academic Supervisor: Matteo Troncia

Glasgow
August 2023

This thesis is the result of the author's original research. It has been composed by the author and has not been previously submitted for examination which has led to the award of a degree.

The copyright of this thesis belongs to the author under the terms of the United Kingdom Copyright Acts as qualified by University of Strathclyde Regulation 3.50. Due acknowledgement must always be made of the use of any material contained in, or derived from, this thesis.



Beatriz Morales Montoya

17/08/23

Acknowledgments

First and foremost, I would like to express my heartfelt gratitude to my master's directors who have provided guidance and support throughout the completion of this project: David Santacruz and Matteo Troncia. Their unwavering assistance has been invaluable in making this endeavor possible. I would also like to extend my thanks to María Cerrato, who has been by my side from day one, offering constant support. Additionally, I am grateful to all my colleagues at SISCO for making the work environment enjoyable. Lastly, I want to acknowledge my family – my mother, father, brother, and grandmother – for their unwavering support not only during this project but always.

To all of them, thank you.

Table of contents

1. Introduction	8
2. State of the Art of Line Rating in Transmission Systems	13
2.1. Static Line Rating.....	13
2.2. Dynamic Line Rating.....	14
2.2.1. <i>Background of DLR</i>	16
2.2.2. <i>Benefits of Implementing DLR</i>	17
2.2.3. <i>Challenges of Implementing DLR</i>	18
2.3. Methods for Calculating DLR.....	21
2.3.1. <i>Direct</i>	23
2.3.1.1. Clearance or sag	24
2.3.1.2. Tension	25
2.3.1.3. Conductor temperature.....	25
2.3.2. <i>Indirect</i>	25
2.3.2.1. Comparison between IEEE and CIGRE standards	27
2.3.2.2. Differences between CIGRE 207 and CIGRE 601	28
2.4. DLR Technologies.....	28
2.4.1. <i>Dynamic Thermal Rating</i>	28
2.4.2. <i>Dynamic Smart Protection</i>	30
2.5. Iberdrola Current Situation	31
2.5.1. <i>Supplier 1</i>	31
2.5.2. <i>Supplier 2</i>	31
3. Final Master Thesis Description	33
3.1. Iberdrola Objective	33
3.2. Contributions and Limitations.....	34
3.3. Case Study	35
3.4. Project Objectives.....	36
3.4.1. <i>Analysis of the Standards</i>	36
3.4.1.1. Type of Formulation.....	36
3.4.1.2. Impact of the Altitude	36
3.4.1.3. Impact of Emissivity and Solar Absorption Coefficients.....	37

3.4.2. <i>Analysis of the Data Equipment</i>	37
3.4.2.1. Reliability Analysis	37
3.4.2.2. Input Data Analysis	38
3.4.2.3. Type of Calculation	38
3.4.2.4. Periodicity of the Rating	38
3.4.2.5. Emissivity and Solar Absorption Coefficients.....	39
3.4.2.6. Solar Radiation.....	39
3.4.2.7. Simplified Wind Calculation.....	39
3.4.2.8. Temperature Analysis	40
3.5. Methodology Used for the Analysis.....	40
3.5.1. <i>Standards' Formulas</i>	40
3.5.1.1. IEEE	41
3.5.1.2. CIGRE 601.....	46
3.5.1.3. CIGRE 207.....	53
3.5.2. <i>Analysis of the Standards</i>	60
3.5.2.1. Type of Formulation.....	60
3.5.2.2. Impact of the Altitude to the Line Ampacity.....	60
3.5.2.3. Impact of the Emissivity and Absorption Coefficients	61
3.5.3. <i>Analysis of the Data Equipment</i>	61
3.5.3.1. Reliability Analysis	61
3.5.3.2. Input Data Analysis	62
3.5.3.3. Type of Calculation	62
3.5.3.4. Periodicity of the Rating	63
3.5.3.5. Emissivity and Solar Absorption Coefficients.....	64
3.5.3.6. Solar Radiation.....	64
3.5.3.7. Simplified Wind Calculation.....	65
3.5.3.8. Temperature Analysis	65
4. <i>Results and Discussion</i>	67
4.1. Analysis of the Standards.....	67
4.1.1. <i>Type of Formulation</i>	67
4.1.1.1. Impact of the Wind speed	67
4.1.1.2. Impact of the Wind Direction.....	68
4.1.1.3. Impact of the Temperature	70
4.1.2. <i>Impact of the Altitude</i>	71

<i>4.1.3. Impact of the Emissivity and Absorption Coefficients.....</i>	73
4.2. Analysis of the Data Equipment.....	74
4.2.1. Reliability	74
4.2.2. Data Input: Weather Variables.....	76
4.2.2.1. Temperature measurements.....	80
4.2.2.2. Wind speed measurements	80
4.2.2.3. Solar radiation measurements.....	81
4.2.2.4. Key remarks on measurements reliability	81
4.2.3. Type Of Calculation.....	82
4.2.3.1. Suppliers' Ampacity Compartion	82
4.2.3.2. Ampacity Calculation Using Suppliers' Input Data.....	85
4.2.4. Periodicity of the Rating.....	86
4.2.5. Emissivity and Solar Absorption Coefficients	87
4.3. Solar Radiation.....	91
4.4. Simplified wind calculation	92
4.5. Temperature analysis	98
4.5.1. Day of Lower Temperature.....	98
4.5.2. Day of Higher Temperature	101
5. Conclusions.....	103
6. PLAN 2030.....	108
7. Bibliography.....	113
ANNEX I: Alignment with the Sustainable Development Goals (SDGs).....	117

Table of Figures

Figure 1: Different control levels.....	9
Figure 2: Ampacity given by DLR vs SLR [5].	15
Figure 3: Sag and clearance of a line [32].....	24
Figure 4: Line sensor.....	29
Figure 5: Weather monitoring station	29
Figure 6: Functional architecture of DSP.....	33
Figure 7: Proposed functional architecture DSP+DTR.....	34
Figure 8: Wind speed analysis Rs=0.04	67
Figure 9: Wind speed analysis Rs=0.08	68
Figure 10: Wind direction analysis	69
Figure 11: Temperature analysis	70
Figure 12: Impact of the altitude in the ampacity calculation.....	71
Figure 13:Temperature and Wind speed of the Supplier 1, Supplier 2 and Open-Meteo data sets.....	78
Figure 14: Solar radiation of the Supplier 1, Supplier 2 and Open-Meteo data sets.	79
Figure 15: Dynamic rating values given by both Suppliers and static rating of the line a) include Supplier 2' points missing an input data b) excluding these points	84
Figure 16: Ampacity comparison between ampacity calculated with actual line coefficients and ampacity calculated with IEEE recommended coefficients.	89
Figure 17: Difference between ampacity calculated with actual line coefficients and ampacity calculated with IEEE recommended coefficients.	89
Figure 18: Ampacity comparison between ampacity calculated with actual line coefficients and ampacity calculated with CIGRE 601 recommended coefficients.	90
Figure 19: Difference between ampacity calculated with actual line coefficients and ampacity calculated with CIGRE 601 recommended coefficients.	90
Figure 20: Solar radiation estimated by different ways and Solar radiation measured with the sensor.....	91
Figure 21: Wind simplification using Supplier 1 data input.	93

Figure 22: Ampacity with wind simplification using Supplier 1 data input.	94
Figure 23: Wind simplification using Supplier 2 data input.	95
Figure 24: Ampacity with wind simplification using Supplier 2 data input.	96
Figure 25: Wind simplification using historical data from Open-Meteo as data input.	96
Figure 26: Ampacity with wind simplification using historical data from Open-Meteo as data input.	97
Figure 27: Comparation between temperature measured and predicted with coefficient applied for the day 23/01/2023.....	99
Figure 28: Comparation between the ampacity calculated with measured temperature and the ampacity calculated with temperature predicted with coefficient applied for the day 23/01/2023.....	100
Figure 29: Comparation between temperature measured and predicted with coefficient applied for the day 24/06/2023.....	101

Table of Tables

Table 1: Advantages and disadvantages of direct and indirect methods.	23
Table 2: Advantages and disadvantages of DTR.....	30
Table 3: Advantages and disadvantages of DSP.	31
Table 4: Comparison between the two Suppliers.	32
Table 5: Parameters of the line.	35
Table 6: C parameter for Solar Azimuth calculation.	43
Table 7: Coefficients B and n for smooth conductors.	50
Table 8: Coefficients B and n for ACSR Conductors with $R_S \leq 0.05$	50
Table 9: Coefficients B and n for ACSR Conductors with $R_S > 0.05$	50
Table 10: A and m coefficients.....	52
Table 11: Coefficients B and n.	57
Table 12: A and m coefficients.....	59
Table 13: Parameters for ampacity calculation.	60
Table 14: Parameters used for the altitude analysis.....	60
Table 15: Coordinates	62
Table 16: Absorption and emissivity coefficients recommended by CIGRE 601 and IEEE standards.....	64
Table 17: Decrement in ampacity between 0 and 1500 meters of altitude.	72
Table 18: Decrement in ampacity when increasing 500 meters in altitude	72
Table 19: Ampacity values (A) varying the solar absorption and emissivity coefficients with different temperature of service using the IEEE standard for ampacity calculation.	73
Table 20: Ampacity values (A) varying the solar absorption and emissivity coefficients with different temperature of service using the CIGRE 601 standard for ampacity calculation. 73	73
Table 21: Ampacity values (A) varying the solar absorption and emissivity coefficients with different temperature of service using the CIGRE 207 standard for ampacity calculation. 73	73
Table 22: Reliability analysis for Supplier 1	75
Table 23: Reliability analysis for Supplier 2	75
Table 24: Statistical results of both Suppliers and Open-Meteo data set inputs	77

Table 25: Similar and different measurements.....	82
Table 26: Statistical results of the ampacity values given by both Suppliers.	82
Table 27: Difference between the ampacity suppliers' value and the ampacity calculated by using their input data.....	85
Table 28: Difference between the ampacity supplier 2 value and the ampacity calculated by using their input data.....	85
Table 29: Statistics of the time in minutes when the ampacity given different frequencies (15 min, 39 min, and 1 hour) exceeds the real-time ampacity.	86
Table 30: Comparison of ampacity values using default and actual coefficients - Average absolute difference	88
Table 31: Absolute percentage difference between the estimated and the measure solar radiation values.....	92
Table 32: Differences between the simplified and non-simplified approaches.	98
Table 33: Differences between the parameterized methods and the non-parametrized one for the day 23/01/2023.....	100
Table 34: Differences between the parameterized methods and the non-parametrized one for the day 24/01/2023.....	102

1. INTRODUCTION

Nowadays, energy is not only indispensable in our lives, but also a key factor in development. In the past, energy was extracted from non-renewable sources like coal, natural gas, and oil, emitting greenhouse gases into the atmosphere when burned. The visible effects of climate change, such as rising temperatures, continuous heatwaves, and extreme weather events, have heightened society's concern about combating climate change. This is evident in the commitments made by countries, particularly in the EU, to reduce fossil fuel consumption and improve energy efficiency, as demonstrated by the Paris Agreement's goal of reducing emissions by at least 55% compared to 1990 [1].

To achieve these ambitious targets and accommodate the growing demand for energy, there has been a revolution in power systems. This new paradigm involves increasing the use of renewable energy sources, promoting self-consumption, integrating distributed generators, adopting electric vehicles, and electrifying the economy in general terms [2]. However, this transition from traditional power systems to one that integrates these new components presents challenges in both operation and network planning.

The integration of variable renewable sources poses previously unseen scenarios in transmission lines, such as reverse power flow. As an example, in Spain, the Spanish Transmission System Operator (REE) projects that 50% of the energy generated by 2023 will come from renewables [3]. This shift presents multiple technical and social challenges that need to be addressed, including the current network's capacity not being adequately prepared for the increased integration of renewables.

From the perspective of integrating Distributed Energy Resources (DERs), they need to be connected to the distribution grid, whereas in the past, renewables were typically connected to the transmission grid. This shift requires distribution companies to develop additional control mechanisms, essentially taking on the role of a Distribution System Operator (DSO), which is equivalent to the Transmission System Operator (TSO) but at

the distribution level. In other words, they become a system operator rather than just being a distributor.

To optimally integrate renewables and harness their full potential, increasing the transmission and distribution capacity of the grid is essential. This can be achieved by implementing new infrastructure, elevating voltage levels, utilizing low-loss or high-capacity conductors, modifying tower designs, and adopting dynamic management strategies [4]. While constructing new lines may seem like a straightforward solution, is not the more effective as its complexity, time-consuming, and cost, making it unsuitable for rapid network expansion [5]. Furthermore, the traditional solution of repowering the network to increase power capacity through equipment replacement is not sufficient to address the network's expansion, connection and flexibility needs [6]. As results, it raises the necessity of exploring alternative solutions beyond the traditional approach.

In response to the challenges posed by traditional power grids, smart grids, also known as intelligent grids, have emerged as a revolutionary solution. These types of grids utilize advanced technology and real-time data to improve grid management and optimize the existing network. Advances in control and automation of the power system have driven this transformation [7]. Figure 1 shows the different levels of control in the power system thanks to smart grids.

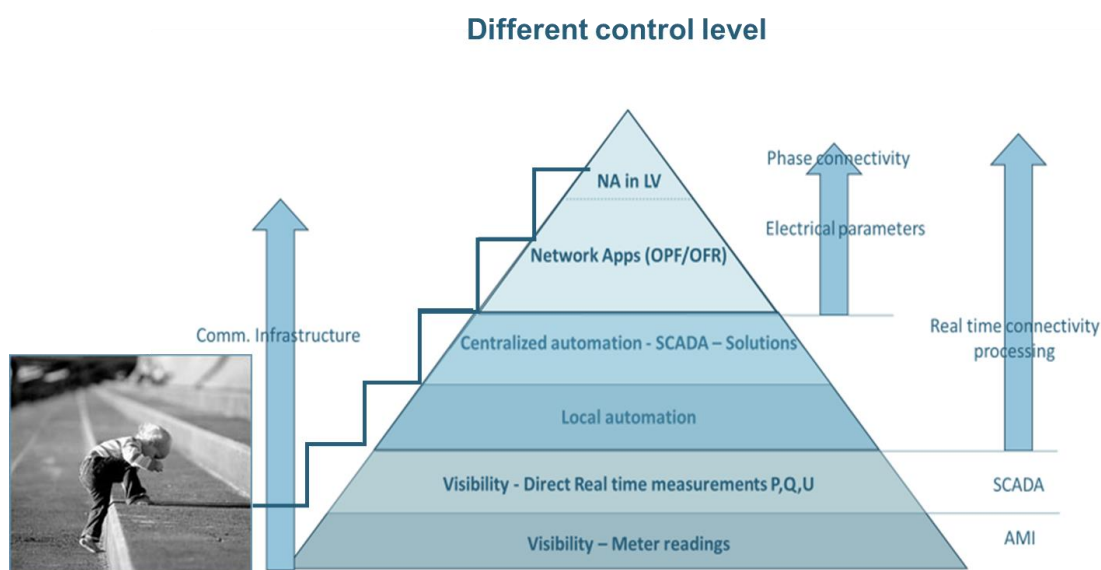


Figure 1: Different control levels.

At the base of the pyramid representing different levels of control lies the Advanced Metering Infrastructure (AMI). Thanks to these systems, grid operators have greater visibility of customer energy consumption patterns and grid performance, as they collect all information in real time.

The next pillar upon which smart grids are built is the Supervisory Control and Data Acquisition (SCADA) systems. SCADA enabled direct real-time measurements of critical grid parameters such as power, voltage, and reactive power [7]. This enhanced monitoring capability facilitated remote control and coordination of grid operations, improving the overall efficiency and reliability of power transmission and distribution.

The subsequent level is local automation, which refers to intelligent automation or automated processes at the distribution Low voltage/Medium voltage (LV/MV) substations based on downstream measurements. This enables real-time connectivity processing.

The SCADA-implemented network applications are situated on the top level of the control pyramid. These programmes, including the Optimum Power Flow (OPF) and the Optimal Frequency Response (OFR), are essential to the reliable and optimum control of the power system.

The Optimum Power Flow (OPF) is an optimization procedure which aim to find the best operating conditions for the electrical power system considering technical and economic aspects [8]. It takes into account all the variables and constraints of the system. Its purpose is to minimizing generation and transmission costs, maximizing system efficiency, and ensuring that all technical and operational constraints are met.

On the other hand, the Optimal Frequency Response (OFR) focuses on maintaining the frequency of the power system within acceptable limits to ensure stable and reliable operation [9]. It uses control algorithms to match generation and load in real-time, optimizing the system's frequency response to changes in demand or disturbances.

OPF and OFR largely rely on accurate and updated data to perform their calculations and adjustments in real-time. This is where the Dynamic Line Rating (DLR) comes into play.

Based on ambient conditions such as temperature, solar radiation, and wind speed, the DLR gives real-time information regarding about the transmission line's capacity [10]. This information is crucial for the OPF, as it enables taking into account the lines' actual capacity rather than just using conservative fixed values for line ratings.

The integration of DLR through OPF in smart grids enables the optimization of network capacity while maximizing the utilization of existing infrastructure. Numerous studies illustrate the successful optimization of line ratings, such as the case presented in [11] within the German power system, [12] in the Australian power system, and [13], which indicates that an enhancement in static rates can be accomplished approximately 85% of the time. Additionally, various studies showcase how DLR can facilitate the integration of renewables [4],[14],[15]. DLR stands as a pivotal innovation within the smart grid framework, enabling real-time data utilization to enhance decision-making and more efficient management of the power system.

The activity described in this document is a final master thesis, that has been carried out in collaboration with i-DE, Redes Eléctricas Inteligentes, the Distribution System Operator of Iberdrola's group. It consists in a statistical analysis of the information from the Dynamic Line Rating (DLR) testing systems already installed in some transmission lines as a pilot project. DLR enables the optimization of existing line capacity based on weather conditions, and the primary objective of its implementation at Iberdrola is to enhance grid flexibility through reconfiguration. This study analyses and evaluate different DLR technologies, the impact of the weather variables, different standards for the calculation of the rating, DLR equipment, challenges with its deployment and future approaches. It is done with the ultimate purpose of defining a 2030 plan for the deployment of this technology for Iberdrola group.

The parameters considered for sensitivity are the weather variables, the altitude above the sea, the roughness of the conductor, the periodicity of the rating, the absorption and emissivity coefficients, and safety coefficient among others. After carrying out the statistical analysis of the data, it is noted that these devices do not exhibit complete reliability and recommendations for the future deployment are given.

The document is structured as follows: Section 2 provides an overview of DLR, its background, the benefits of its implementation in the overall power system, and the challenges for its consolidation. It also explains the different methods of ampacity calculation, the various technologies that can be used, and the current situation of Iberdrola. In Section 3, the project outlines Iberdrola's objectives regarding DLR, the goals of this project along with its contributions and limitations, the methodology, and the case study. Section 4 presents the results, and Section 5 provides the conclusions drawn. The final part, Section 6 offers recommendations for Iberdrola when developing their 2030 plan.

2. STATE OF THE ART OF LINE RATING IN TRANSMISSION SYSTEMS

2.1. STATIC LINE RATING

Until now, systems operators have managed the network using a static limit for the maximum current that the network can carry [13]. This limit is a single rating for the whole year that remains unchanged, or at most two different ratings for summer and winter. To set these limits, the worst-case conditions are considered: no wind and the highest temperature. This conservative approach is known as Static Line Rating (SLR). It is intended to always operate the grid safely, but almost always results in underutilization of the grid's true capacity [16].

The IEEE 738, "Standard for Calculating the Current-Temperature Relationship of Bare Overhead Conductors", is used to calculate the SLR. This standard makes conservative considerations about the atmospheric environment of the line and considers that these environmental conditions remain static. Thus, changing or favourable meteorological variables are never taken into account [17]. This approach is intended to restrain too rapid temperature increases that could lead to undesired degradation processes and increased sagging. Consequently, considering the cooling effects on the conductors to be negligible, situations such as low wind speed, intense solar radiation and increased ambient temperature are taken into account when determining the rated power of the line.

As a consequence of the conservative nature of SLRs, the network's potential capacity is often not fully utilized. Consequently, conductors are frequently thermally limited when actual weather conditions would allow for larger ampacities. This leads to inefficient use of the grid's capacity, with the utilized ampacity often falling 10% below the actual ampacity for most of the year [18].

An illustrative example is the restriction of connecting PV panels or wind farms to the grid because the line to which they are to be connected reaches its static capacity limit [14]. This restriction occurs even when actual network and environmental conditions

would permit a higher capacity based on the real line rating. In the context of wind farms, this becomes advantageous since these locations experience frequent winds, resulting in consistently higher capacity than a static rating [19]. Thus, the fixed limit imposed by SLRs can hinder the integration of renewable energy sources.

It can be said that the traditional SLR approach worked well until the intermittent renewable energy generating units spread widely, as well as of the implementation of the Integrated Electricity Market (IEM), which allows for the trading and sharing of electricity across the regions. In this way, a so-called bottleneck effect occurs on some transmission lines, where their capacity reached, causing constraints on power flow. Consequently, there is a need to increase the transmission capacity of these critical lines [5]. This emphasizes the importance of a more adaptable and dynamic approach to transmission capacity calculation to accommodate evolving energy generation and market dynamics.

2.2. DYNAMIC LINE RATING

The advancement of the traditional Static Line Rating (SLR) is the Dynamic Line Rating (DLR). As mentioned above, SLR is limited to considering only the worst conditions. In contrast, DLR takes into account real-time weather conditions such as ambient temperature, wind speed, wind direction and solar radiation as well as line-specific characteristics such as load, ground clearance, conductor sag, conductor voltage and conductor temperature [20]. Providing a dynamic and precise evaluation of a transmission line's ampacity, which is the maximum current it can carry safely.

Unlike SLR, which remains the maximum capacity of the line fixed, DLR defends that is not static. Instead, it responds in real time to its immediate environment. Thanks to this dynamic nature, it enables a more accurate calculation of ampacity, enabling optimized power flow through the line and allowing for capacity increases when conditions permit. The calculated ampacity using this approach is notably greater during nearly 95% based on simulations and practical examples, [5], as Figure 2 shows. This emphasises how significantly DLR may improve the effectiveness, adaptability, and general performance of power transmission systems.

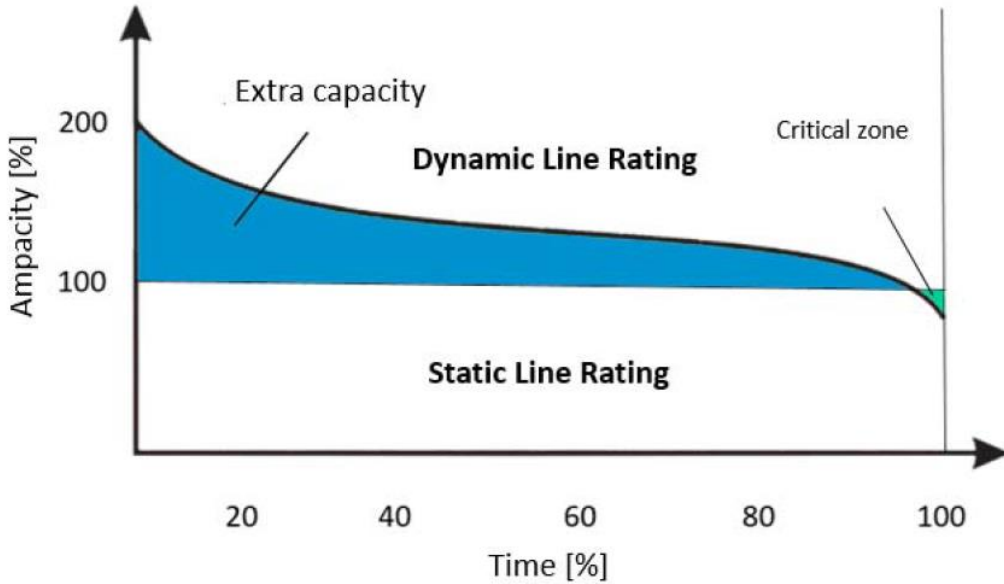


Figure 2: Ampacity given by DLR vs SLR [5].

Multiple benefits raise from this transformative solution. Firstly, it can address the problem of integration renewables sources into the grid as it reduces the need for constructing new transmission lines. Furthermore, DLR offers empowering to grid operators as there is an increased network flexibility. Through the use of Optimal Power Flow (OPF) techniques, DLR facilitates the redispatch of power, enhancing grid operation and adaptability [21]. More detail of these benefits is explained later in this document.

The implementation of DLR through OPF represents a pivotal advancement in grid management, ushering in a new era of optimized power flow and efficient resource utilization within smart grids. Addressing the integration of intermittent energy sources and the ongoing demand for electricity necessitates a more flexible grid [22]. DLR provides this flexibility by enhancing transmission line capacity while maintaining safety protocols. As a result, DLR not only solves existing challenges but also paves the way for a more resilient and adaptable energy landscape.

2.2.1. BACKGROUND OF DLR

Until now, as it has mentioned in Spain and traditionally all over the word the static limits have been utilised [23]. But since Oncor Electric Delivery Company (Oncor) demonstrated in 2016 that the capacity transmission of the lines increases by 6%-14% for 84%-91% of the time [24], more countries have signed up to implement this technology. Several transmission system operators (TSOs) in Europe, Amprion (Germany), Terna (Italy), RTE (France) and Elia (Belgium), are using DLR to operate the cross-border transmission capacity with the aim of increasing the amount of power that can be traded between nations on the European market. As a result of this, in 2017–2018, when there was a significant demand for electricity during cold weather, the thermal limitations were raised by 20% [25]. Another more recent example is Energinet, the Danish TSO, which has implemented DLR on around 20 of its power lines, aiming to install it on all of their lines by the end of the year. They have calculated that capacity can be improved by 30%, with the benefit of delivering increased electricity supply estimated at DKK 400 million (US\$57 million) by 2030 [26]. Also, National Grid, one of the largest world utilities, [27] is also deploying this technology in the US in order to unlock 600 MW of additional capacity and save £1.4 million in network operating costs per year based on the results from the US networks.

Furthermore, the Agency for the Cooperation of Energy Regulators (ACER), in its recent decisions, has been actively incorporating DLR methodologies into its regulations, particularly in the context of core capacity calculation. ACER is driving the adoption of DLR for determining maximum current intensity. In fact, ACER's decision 2019, number 70 [28] explicitly states: “In order to maximise the available capacity on the CENECs, the Agency reinforced the obligation for the Core TSOs gradually to replace the seasonal limits to calculate I_{max} with a dynamic limits, which ensures that I_{max} represents the maximum current under expected ambient conditions for a given market time unit” and “When benefits outweigh costs, TSOs should install such equipment within three years”.

2.2.2. BENEFITS OF IMPLEMENTING DLR

There are multiple papers that explain in detail the benefits of implementing DLR in the power systems [20], [29], [25] and [17]. Next, a summary is provided for the most important ones.

- **Improved Grid Operations and Reliability:** DLR enhances grid flexibility, allowing for higher currents during emergencies, leveraging the thermal inertia of conductors. This provides additional system adaptability and ensures reliable power delivery for both base and peak loading. DLR technology contributes to more cost-effective power generation dispatch and aids in system planning by forecasting power-carrying capacity. It enhances grid resilience, crucial for maintaining a secure power supply. In cases of substation or power line failures, DLR enables the rerouting of power through alternative transmission paths, safeguarding grid integrity [25].
- **Reduced Need for Operator Intervention:** DLR along with OPF, reduces the need for manual intervention by providing real-time thermal rating information, automating decision-making processes and optimizing grid operation.
- **Reduced Congestion on Power Lines:** As there is an increased capacity of the lines, there is a reduction of the congestion.
- **Reduced Curtailment of Variable Renewable Energy (VRE):** There is a positive correlation between wind production and transmission capacity potentially available from overhead lines. As wind generation increases, the enhanced cooling effect on overhead conductors allows for greater transmission capacity. This alignment enables more wind energy to be transmitted during higher wind periods, reducing generation curtailments and optimizing resource utilization.
- **Facilitated Rapid Access to Renewable Energy:** DLR accelerates the integration of distributed energy resources, streamlining the integration of variable renewable energy (VRE) sources like wind and solar. This facilitates quicker access to clean energy, saving time and resources that would otherwise be required for the construction of new transmission lines.

-
- **Enhanced Utilization of Distributed Generation:** DLR reduces curtailment of distributed generation production, that in most cases is renewable, in maximizing the use of locally generated power.
 - **Reduced Capital Costs and Investments:** Optimized asset utilization through DLR minimizes the need for new infrastructure investments as new lines, leading to cost savings and improved cost efficiency of power lines. Considering alternative methods such as DLR allows to optimise investments, avoiding those that are unnecessary.
 - **Financial Benefits to Consumers and Market Participants:** By increasing transmission capacity and optimizing power flow, the cost of connecting generators to the grid is reduced, particularly facilitating the entry of renewable energy sources. The higher presence of renewables in the market dispatch would lead to a decrease in energy costs, ultimately benefiting consumers. Furthermore, if DLR is employed with forecasting, it facilitates more efficient day-ahead and real-time markets by providing more accurate estimations of expected transmission capacity. This enables more effective power trading activities.
 - **Reduced Carbon Footprint:** The reduction of the carbon footprint is not only attributed to allowing greater consumption of distributed energy, often from renewable sources. It is also due to the reduction of line extensions, which further contributes to minimising this footprint.

2.2.3. CHALLENGES OF IMPLEMENTING DLR

To enable the successful implementation of this new technology, several key factors are essential, which could be categorized as challenges to overcome [25], [20].

- **Data collection and digitization of the grid:** DLR relies on real-time monitoring of transmission line status and employs communication systems to transmit collected data to a central data centre for processing. Integrating this data with industry standards and algorithms enables "real-time" ampacity ratings. Challenges arise in collecting data, which can be achieved through sensors or meteorological sources like Agencia Estatal de Meteorología (AEMET). The latter approach has a drawback as measurements are not collected on-site directly

from the line, but rather obtained from the nearest weather station, introducing a margin of error. Conversely, sensor-based data collection on the line presents its own set of challenges, including high installation and maintenance costs, susceptibility to interference, and uncertainties associated with measurements. Additionally, robust communication and control systems are essential for effective DLR operation.

- **Thermal aging:** In the implementation of DLR, the focus on maximizing the thermal capacity of transmission lines can accelerate the process of thermal aging in conductors. By operating cables closer to their thermal limits, higher temperatures are generated in the conductors, which can expedite the degradation of their properties over time. This process of thermal aging can reduce the efficiency and lifespan of the conductor, which in turn can impact the accuracy of real-time ampacity calculations and the safe operation of the electrical grid.
- **Reliability and security:** Ensuring the reliability and security of DLR technology requires thorough validation and verification of its used technologies. Uncertainties can stem from sources like measurement and model inaccuracies. Detecting accurate weather data is critical, and missed data due to equipment failures poses another issue. Sensor calibration is necessary for precision. The broader security analysis of the power grid might be insufficient when integrating DLR, demanding careful evaluation. There's a financial risk of exceeding line limits, which can be costly. Moreover, if a line breaks, its operation halts until replacement, incurring substantial expenses. One solution involves utilizing temperature or sag sensors to verify calculated ampacities based on weather conditions. Alternatively, weather forecast data and machine learning algorithms can be employed.
- **Integration into system operation:** At first glance, for system operators, there might appear to be only drawbacks, as implementing DLR could potentially compromise the security and reliability of the system. Consequently, they might be reluctant to adopt it. Therefore, incentives must be provided for such technologies (indeed, they are already recognized as retributable investments) to

encourage system operators to overcome their reservations and install a DLR system.

- **Variability of ampacity:** It is a challenge when implementing DLR in the power system. Dispatching based on highly variable real-time ratings is impractical due to constraints in generation dispatch and load response. To address this, strategies like averaging ratings over time, constraining rating ranges, and clustering dynamic values into finite states can be employed to minimize rating variability and enhance the feasibility of DLR integration.
- **Application Development:** DLR's potential is limited without a dedicated application to safely implement its capacity enhancements within the power system. For instance, calculating that an additional 100 Amperes can be added to a line is meaningless if the overall power system cannot accommodate this increase, as demand must always match generation. Therefore, a secure application is essential to ensure the safe application of increased capacity. Developing an application like the Optimal Power Flow (OPF) is necessary for effective DLR utilization.
- **Difficulty to calculate the economic benefit:** While the substantial reliability advantages of implementing DLR are acknowledged, accurately quantifying the economic value attributed to enhanced reliability poses a significant hurdle [20].
- **Calculation algorithms:** Suppliers can use various standards established by regulatory bodies and standardization entities in the electricity field to calculate ampacity. Standards from organizations such as the International Council on Large Electric Systems (CIGRE) [30] and the Institute of Electrical and Electronics Engineers (IEEE) [31] are commonly used for calculating ampacity in overhead conductors. It is important to note that uncertainties exist in these calculations, particularly when temperatures approach the conductor's limit. The accuracy of these calculations relies on input data, including the physical properties of the conductor, geographical information about the line's location, and atmospheric variables [25].
- **Regulation:** Traditionally, regulations based on investment costs, such as rate of return and cost-plus regulation, have been prevalent for making grid operation and

investment decisions. However, these approaches have limitations and may not effectively encourage efficient utilization of existing infrastructure. To address these limitations, regulators have introduced regulations focusing on operational expenditures (OPEX) to incentivize transmission system operators (TSOs) to enhance operational practices and reduce the need for new physical infrastructure investments. These regulations incorporate incentives like rewards and penalties, motivating TSOs to achieve transmission capacity targets set by regulators and allowing them to share in the "extra profit" if these targets are exceeded. Embracing such OPEX-based solutions, like DLR, promotes innovative approaches to power system operation. DLR optimizes the utilization of current transmission lines, potentially reducing or eliminating the need for capital expenditures (CAPEX) in new infrastructure. In vertically integrated power systems, DLR adoption also enables power system operators to dispatch power from their renewable energy assets more cost-effectively, thereby enhancing returns on their power generation portfolios [25].

- **Critical Spans identification:** The temperature of the conductor fluctuates along the line primarily due to variances in wind distribution. The ampacity of the transmission line is established based on the segment that experiences the least cooling effect, known as the critical span. On a transmission line, there may be multiple critical spans. As a result, pinpointing the locations and quantities of devices necessary to monitor these vital spans presents a challenge during the implementation of the DLR system [20].

2.3. METHODS FOR CALCULATING DLR

Two distinct methods for calculating DLR are available, they differ in the monitoring system used to collect the input variables for the calculation. The indirect method relies on weather conditions variable inputs, and the direct method is based on the measurement of line characteristics such as clearance, sag, tension, or conductor temperature.

In Table 1, it is outlined the advantages and disadvantages of each approach. The indirect method offers simplicity, cost-effectiveness, and reliability, requiring no sensor

installation on the line itself. However, it may lack precision in representing worst-case conditions and introduces uncertainty in ampacity estimation due to indirect determination based on theoretical models. On the other hand, the direct method provides accurate measurements of physical quantities but involves field data analysis, calibration, and potential inaccuracies in certain scenarios.

Method	Advantages	Disadvantages
Indirect Method	<ul style="list-style-type: none"> -Simplicity: No need for sensors on the line. -Cost-Effectiveness: Low installation and maintenance cost. -Reliability: Highly reliable, minimal for special calibrations. -Investigative Potential: Allows investigation of estimated temperature reasons. - Multi-Purpose Suitability: Enables short-term and long-term load capacity forecasts. 	<ul style="list-style-type: none"> -Precision Limitations: May not accurately represent worst conditions. -Uncertainty: As it is an indirect estimation, the line temperature and ampacity determined indirectly, introducing potential errors. -Limited Environmental Data: Meteorological stations provide data only for specific areas, without local variations. - Environmental Variability: Wind speed and direction variations affected by terrain and obstacles.
Direct method	<ul style="list-style-type: none"> -Precise Measurement: Provides accurate measurement of physical quantities (e.g., temperature, sag). 	<ul style="list-style-type: none"> - Calibration and Analysis: Requires field data analysis and calibration for accurate results.

<i>Method</i>	<i>Advantages</i>	<i>Disadvantages</i>
Direct method		<ul style="list-style-type: none"> - Limited Representative Data: Data related to the measured span may not represent average conditions along the entire line. - Inaccuracies: Large errors may arise for lightly loaded lines or small conductor temperature rises over ambient. - Maintenance Challenges: High maintenance costs and potential line interruption requirements. - Cost: More expensive to acquire and install.

Table 1: Advantages and disadvantages of direct and indirect methods.

Considering the trade-offs, the indirect method, particularly using weather stations, emerges as the best solution due to its crosschecking capabilities and ability to forecast load capacity in both short- and long-term perspectives. The accuracy of local weather forecasts becomes pivotal in ensuring the success of this approach [23].

2.3.1. DIRECT

The line rating is calculated based on direct measurement power line characteristics such as ground clearance, conductor sag, tension, and conductor temperature. Point sensors for direct conductor temperature offer insights from specific locations, potentially missing worst-case points. Conversely, **conductor tension and sag monitoring systems provide a comprehensive view of weather conditions across the entire transmission line, allowing calculation based on average conductor temperature conditions.**

2.3.1.1. Clearance or sag

The Figure 3 shows key components of a transmission line: the span, the sag and the clearance. The span is the distance between the two towers that support the conductor. The sag is the vertical distance between the span and the conductor, while the clearance is the height of the conductor above the ground. Various methods are employed to measure sag, including conductor inclination, vibration frequency, target monitoring, and clearance assessed through technologies like sonar, laser, microwave, magnetic field, optical sensors, ultrasonic, and radar [20], [23].

While some systems utilize sag or clearance in conjunction with average temperature for DLR calculations, their primary purpose lies in verifying the accuracy of the calculated line rating. During line design, clearance or sag is carefully determined to ensure safety, preventing potential contact between the conductor and people or animals. This determination is made based on the worst-case scenario, often involving minimal wind and maximum temperature. If the sag exceeds permissible limits before reaching the design temperature, it signals a problem that needs attention, as the sag should ideally stay within specified bounds until the design temperature is reached. In this way, clearance and sag serve as critical checks on design and safety considerations.

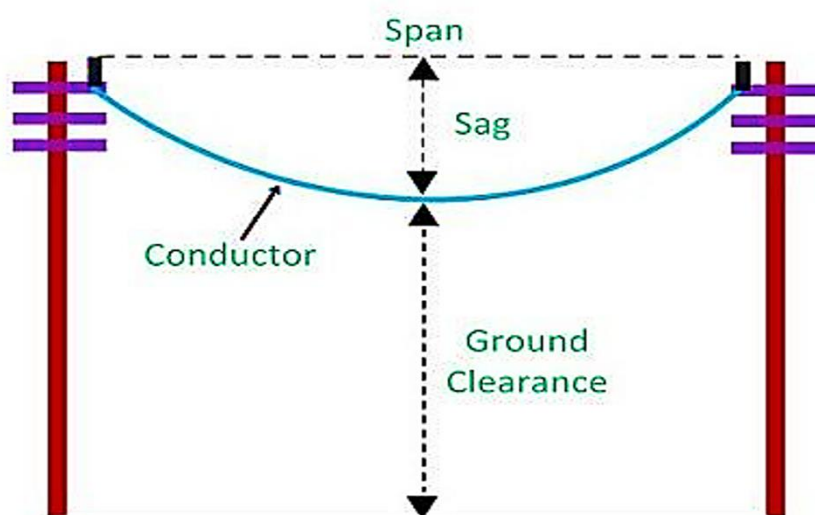


Figure 3: Sag and clearance of a line [32].

2.3.1.2. Tension

Conductor tension can be assessed either at a specific point along the line or at its termination. Analysing the tension in the conductor facilitates the determination of its sag and consequent core temperature [20]. Alternatively, real-time tension measurements can be translated into an equivalent wind speed, enabling the computation of line ampacity through the utilization of the heat balance equation [23].

2.3.1.3. Conductor temperature

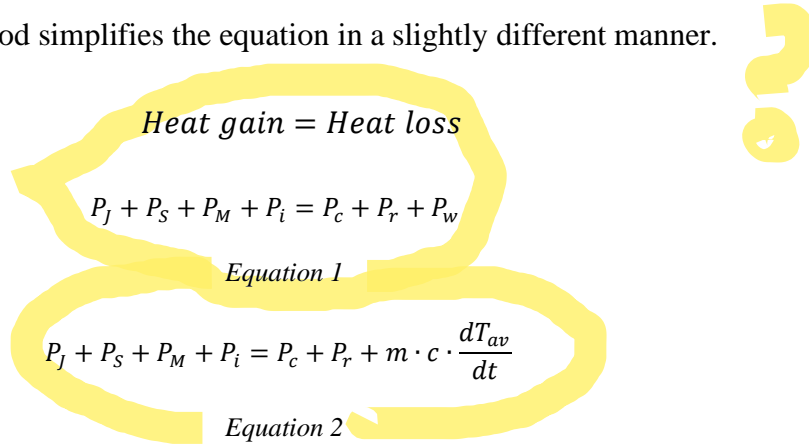
The conductor temperature can be measured using temperature sensors, optical fibers, or infrared thermal cameras [23]. It is crucial to recognize that conductor temperature fluctuates from one span to another, primarily due to substantial variations in wind speed and direction along the transmission line. Temperature sensors are usually positioned at specific points, capturing the surface temperature of the conductor rather than the average temperature across the whole span. As a result, converting these recorded temperatures to corresponding sags or positions is vital to precisely assess the real-time conductor position.

2.3.2. INDIRECT

It uses the weather data as input to calculate the line rating. This data can be collected either from sensors installed in the line or from forecast meteorological source as AEMET. The ampacity calculation through weather variables is based on the basic heat balance equation, where the gained heat is equal to the lost heat. It also depends on ohmic losses, skin effect, conductor type and the geographical location. These factors can be categorised into two main groups: the physical properties of the conductor and the atmospheric conditions in which it operates. Various standards govern the calculation of ampacity using this approach, with the most prominent and relevant ones for this project being IEEE, CIGRE 207, and CIGRE 601 (an updated version of CIGRE 207).

There are two equations of heat balance assuming the weather variables constant, both in IEEE and CIGRE, the steady-state and the non-steady-state one. The steady-state models operate under the assumption that the conductor is in a state of thermal equilibrium, with no heat being stored within the conductor, Equation 1. On the other hand, the non-steady-

state modelling approach considers that the conductor can store heat and is either accumulating more heat or dissipating the stored heat, Equation 2. This non-steady-state model is more suitable for capturing the short-term variations in weather conditions and line loading. In both standards CIGRE and IEEE [30], [31] utilize the thermal equilibrium or heat balance equation to estimate the ampacity or temperature of the conductor. However, each method simplifies the equation in a slightly different manner.



$$\text{Heat gain} = \text{Heat loss}$$

$$P_J + P_S + P_M + P_i = P_c + P_r + P_w$$

Equation 1

$$P_J + P_S + P_M + P_i = P_c + P_r + m \cdot c \cdot \frac{dT_{av}}{dt}$$

Equation 2

Where P_J, P_S, P_M, P_i are the Joule, solar, magnetic, and corona heating respectively (W/m); P_c, P_r, P_w the convective, radiative and evaporative cooling (W/m); m represents the mass of the conductor (kg), c represents the specific heat capacity of the conductor (J/(kg°C)), and T_{av} represents the average temperature of the conductor (°C).

Both standards have a consensus in neglect the evaporation cooling and corona heating. Corona heating become meaningful when there are high wind speed and humidity, but during such times the convective effect become more much significant, making the corona heating irrelevant. The temperature of a conductor can be significantly impacted by the heat loss brought on by evaporation. However, due to the rarity of the entire line being wet and the difficulties in precisely determining its influence, this element is typically ignored in thermal rating calculations.

The calculated temperatures are very similar between the two standards. Furthermore, according to multiple studies, the temperature error ($|T_{\text{measured}} - T_{\text{calculated}}|$) is less than 5°C 85% of the time [19].

Numerous studies have conducted comparisons between these standards, including [33], [10], [34], [19] and [11]. below, there is a summary of the main differences in their

calculations. Additionally, the distinction between CIGRE 207 and CIGRE 601 is explained.

2.3.2.1. Comparison between IEEE and CIGRE standards



- Conductor heating

As the magnetic and the corona heating effects are neglected as mentioned before, solar and joule effect are the two remains effects that affect the temperature of the conductor.

The conductor's temperature-dependent DC resistance is calculated in a similar way in both standards, the only difference is that IEEE standard does not include an AC to DC current conversion, whereas the CIGRE model includes.

The solar heating depends on many variables as the coefficient of absorption of the conductor, line's orientation and latitude, the hour and day of the year, and atmospheric clarity. It is necessary to calculate the position of the sun and the solar intensity. The solar intensity, direct and diffuse can be measured by a sensor. However, the installation and upkeep of such sensors come with substantial expenses. Given that the sensor's impact on the final result is not particularly significant, both standards offer an alternative calculation method to estimate global solar radiation.

Due to the cyclic magnetic flux produced by the spiralling current around the steel core, ACSR conductors become magnetically heated. The amount of aluminium encasing the steel core and current flow are two elements that affect heating. The skin effect, magnetic heating, and losses related to ACSR conductors are all taken into account by an approximative correction equation built into the CIGRE model. The IEEE standard, in contrast, ignores both magnetic losses and the skin effect.

- Conductor cooling

The cooling of the conductor is produced by the convective and radiative effects.

Both standards use the same calculation for the radiative cooling, considering the gradient of the temperature between the conductor surface and the ambient, the diameter of the conductor and the emissivity coefficient.

The major difference between these two standards lies in the approach to calculating convective cooling. CIGRE employs Morgan correlations relying on the Nusselt number, while IEEE utilizes McAdams correlations grounded in the Reynolds number [19]. Furthermore, the CIGRE standard accounts for the conductor's surface roughness, which the IEEE standard does not consider. This inclusion intensifies the impact of forced convection on the conductor. Consequently, the IEEE standard is generally viewed as a more conservative approach to convection cooling calculation.

2.3.2.2. Differences between CIGRE 207 and CIGRE 601

In the context of evolving line rating methodologies, a comparison between CIGRE 207 and CIGRE 601 reveals distinct advancements. CIGRE 207, while initially displaying certain limitations, has served as a platform for improvement. CIGRE 207 recommends more detailed calculation methods for high current density scenarios. Another inherent drawback lies in its neglect of natural convection during calm wind conditions, thereby compromising overall line capacity. On the other hand, CIGRE 601 demonstrates improvements in AC resistance calculations, offering a more realistic depiction of conductor temperature distribution, both axially and radially. Moreover, CIGRE 601 addresses the limitations of its predecessor by enhancing its convection model for low wind speeds and incorporating a flexible solar radiation model [30]. R DY

2.4. DLR TECHNOLOGIES

Independently of the standard used for calculating the line rating, there are multiples technologies used for DLR. The ones of interest for Iberdrola are: Dynamic thermal rating (DTR) and Dynamic Smart Protection (DSP). The ultimate goal of both is to calculate ampacity, but how this is done can vary significantly from one to the other. It is important to have a deep understanding of them at the time of develop the deployment system plan for DLR, as each has its own advantages and disadvantages.

2.4.1. DYNAMIC THERMAL RATING

This method involves the installation of line meter on the proper line, Figure 4, or sensors on the tower that hold the line, Figure 5. These sensors act as weather stations, gathering

on-site real-time measurements. There is an external calculation system offered by a third-party supplier.



Figure 4: Line sensor.



Figure 5: Weather monitoring station.

One notable advantage of this solution is that it allows for the collection of actual measurements from the line itself or near the line thanks to the fact that the sensor is installed near the line or in the line. It is possible also to install a clearance or sag sensor or a conductor temperature sensor, to give a validation of the ampacity calculated, ensuring that the value is reliable for the line operate safety. Additionally, these measurement devices are typically considered as regulated equipment.

However, a drawback is that the ampacity calculation process is external, making it non-parametrizable. Accessing the data, which includes weather variables and rating calculations is also more difficult as it relies on an external source.

<i>Technology</i>	<i>Advantages</i>	<i>Disadvantages</i>
DTR	On-site measurement Clearance calculation Regulated equipment	Non-parameterizable external calculation Data access in external system

Table 2: Advantages and disadvantages of DTR.

2.4.2. DYNAMIC SMART PROTECTION

In this technology, meteorological data is collected externally from a meteorological source as for example AEMET instead of measuring it on-site with sensors. The collected data is then processed within the company itself, indicating that the calculation of the rating is performed by the company rather than relying on an external supplier. One of the advantages of this approach is that the calculation is internal, allowing for parameterization and easier access to the data, including the ability to predict future values. However, a disadvantage is that the input data for the calculation comes from external sources, and, that it does not directly involve real-time measurements from the actual transmission line.

<i>Technology</i>	<i>Advantages</i>	<i>Disadvantages</i>
DSP	Internal calculation Parameterizable Future data	External input data Not measured on site

<i>Technology</i>	<i>Advantages</i>	<i>Disadvantages</i>
	Data access	

Table 3: Advantages and disadvantages of DSP.

2.5. IBERDROLA CURRENT SITUATION

Iberdrola has DLR pilot equipment from two different suppliers installed on their high/medium voltage overhead lines.

The project was initially initiated in 2021 with Supplier 1 installing DTR on two 132 kV overhead lines to showcase viability and assess the technology's potential. In 2022, the deployment by Supplier 1 expanded to five more power lines. Additionally, a second supplier, Supplier 2, was engaged to concurrently advance the pilot test and explore new data collection methods that could complement or enhance the ongoing solution.

As an alternative approach, the company has also developed a DSP. In this setup, meteorological variables from the nearest weather stations are transmitted by a meteorological source. Utilizing this data, Iberdrola internally calculates ampacity.

The subsequent sections explain in more detail the equipment installed by the two different suppliers.

2.5.1. SUPPLIER 1

Supplier 1's equipment is comprised of sensors for each atmospheric variable to be measured: wind speed, wind direction, solar radiation, and ambient temperature. These sensors are positioned on the towers supporting the power lines. To calculate ampacity using atmospheric variables, Supplier 1 employs the CIGRE 207 standard. It provides minute-by-minute ratings.

2.5.2. SUPPLIER 2

Supplier 2's equipment exclusively employs a cable vibration sensor, which is located in the line, to derive effective wind speed and sag values. The remaining meteorological

data is obtained through a weather subscription service, utilizing a Weather API to access external variables. The concept of "effective" wind refers to the wind speed equivalent at a 90-degree angle to the cable, which has the most substantial impact. The supplier provides line ratings at five-minute intervals.

Table 4 summarizes the main characteristic of each supplier's equipment.

<i>Aspect</i>	<i>Supplier 1</i>	<i>Supplier 2</i>
Input data collection	Wind speed, wind direction, temperature, solar radiation sensors on line towers	Cable vibration sensor on the line
Standard	CIGRE 207 standard	Unknown
Wind Consideration	Real wind direction	Calculates "effective" wind at 90°
Rating Frequency	Minute by minute	Every 5 minutes

Table 4: Comparison between the two Suppliers.

3. FINAL MASTER THESIS DESCRIPTION

3.1. IBERDROLA OBJECTIVE

The optimal solution proposed by I+DE Iberdrola for future DLR development is to combine both solutions: DTR and DSP. This approach would involve having an internal calculation by Iberdrola and another by an external provider, allowing for a comparison of ratings. This combination aims to leverage the advantages of each method.

Figure 6 illustrates the functional architecture of the DSP system. Utilizing atmospheric data obtained from a meteorological service, such as AEMET, and electrical parameters for each segment of the line collected from the GENESIS database (containing electrical inventory data) and Spectrum (providing the current system topology), the rating of each segment is calculated using CIGRE 601 and IEEE standards. The most restrictive rating is selected, which becomes the line's rating and is communicated to Spectrum. Spectrum serves as the control system, and through applications like OPF, the optimal utilization of this additional capacity within the system is determined.

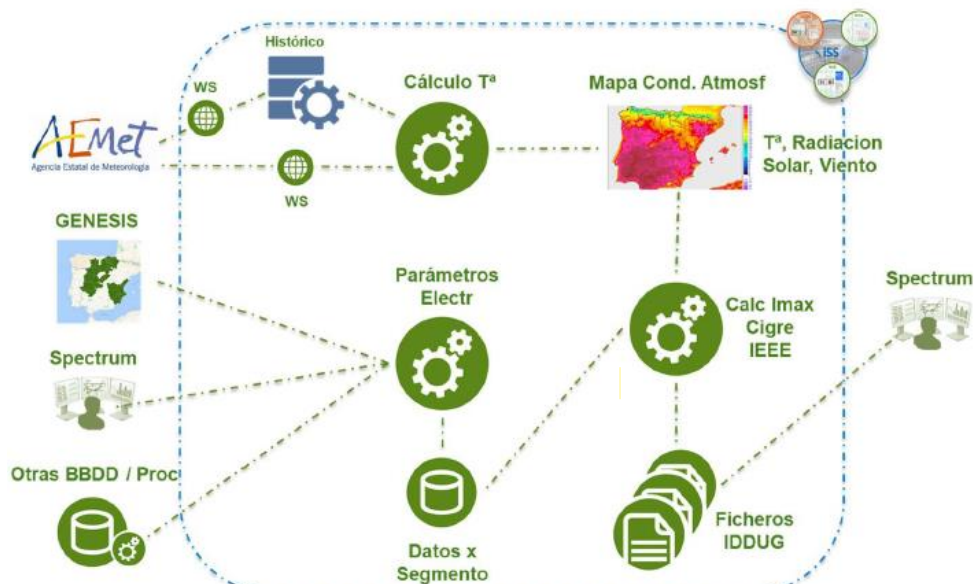


Figure 6: Functional architecture of DSP.

Similarly, the functional architecture proposed for the DSP+DTR system operates. Atmospheric variables are collected from both the DTR equipment and the meteorological service. Using these data, the rating is calculated and sent to the control system, as depicted in Figure 7.

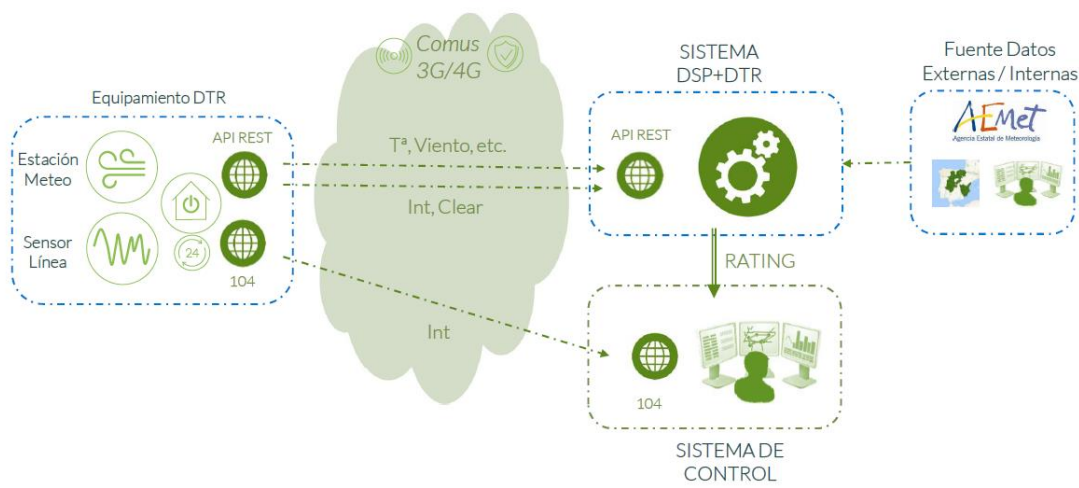


Figure 7: Proposed functional architecture DSP+DTR.

3.2. CONTRIBUTIONS AND LIMITATIONS

This project contributes to analysing the data from the pilot DTR systems installed by the two different suppliers. Access to data is limited to the year 2023, and equipment reliability, which tends to experience frequent failures, must be taken into account.

The analysis is conducted with the future prospect of using the calculated ratings as input data for OPF calculations, necessitating the examination of variables like periodicity and safety coefficients. Specifically, this project focuses on a single transmission line, which will be elaborated on in more detail in the below section. This line is chosen because both suppliers have their equipment installed on it, enabling a comparison of results.

The 2030 plan is not intended to be a detailed plan but rather a set of guidelines and recommendations outlining the steps to be taken for its implementation.

3.3. CASE STUDY

The overhead line examined in this project is the Rocamora to Carrús line, situated in the municipality of Elche. The static line rating is 200 A, and it operates at 132 kV. The line employs two types of conductors: LA 280 HAWK and LA-298HEN.

The Table 5 outlines the parameters utilized for ampacity calculation.

Temperature of service	65 °C
Nominal diameter D	22.4 mm
Outer layer thread diameter d	3.2 mm
R_T (25°C)	1,20E-04 Ω/m
R_T (75°C)	1,44E-04 Ω/m
Latitude	38 °
Average altitude above sea level	47 m
Emissivity coefficient	0.5
Absorptivity coefficient	0.6
Roughness	0.0833

Table 5: Parameters of the line.

On this line, Supplier 2 has installed two vibration sensors, while Supplier 1 has deployed five sets of sensors.

The analysis conducted on this line is carried out is divided into two groups. The first group is based on a sensitivity analysis on parameters values modified artificially. These parameters are wind speed, wind direction, temperature, roughness, altitude above the sea

level, absorptivity and emissivity coefficients. The second group is the analysis of the pilot equipment, and also, this data is used to study the periodicity, possible simplifications of wind, and security coefficient for the temperature.

3.4. PROJECT OBJECTIVES

As mentioned before, the project is divided into two groups. In this section, it is explained the objectives of each analysis.

3.4.1. ANALYSIS OF THE STANDARDS

The goal is to adjust specific parameters to observe their effects on the ultimate rating calculation. This process entails performing a sensitivity analysis on various standards to discern how alterations in parameters impact the calculated rating. This approach yields insights into which variables carry greater significance, aiding in determining the most suitable sensors for installation. It also helps determine whether knowledge of the actual line characteristics is necessary or if recommended parameters suffice, as well as whether an elevation terrain atlas is needed.

3.4.1.1. Type of Formulation

One of the primary objectives of the study is to comprehensively analyse the different standards used for ampacity calculation. To achieve this, the research delves into understanding how various atmospheric variables impact and influence these standards. By examining the behaviour of each standard concerning the input variables, the study aims to gain valuable insights into how these calculations are affected by changes in atmospheric conditions.

3.4.1.2. Impact of the Altitude

The objective of this analysis is to investigate the impact of altitude on ampacity calculations for the transmission line. The study aims to assess whether altitude significantly influences the results and whether the availability of a terrain elevation atlas is necessary to accurately account for this impact. By examining the relationship between altitude and ampacity values, the research seeks to determine the relevance of

incorporating elevation data in the calculations and make informed decisions regarding the necessity of utilizing a terrain elevation atlas.

3.4.1.3. Impact of Emissivity and Solar Absorption Coefficients

A sensitive analysis of the emissivity and solar absorption coefficient is carried out at different temperatures of service to understand how they impact in the final ampacity calculation.

3.4.2. ANALYSIS OF THE DATA EQUIPMENT

By observing and comparing the data collected from the sensors and other data sources, it becomes possible to study the reliability of the equipment installed by both suppliers. This approach involves examining the variables gathered by both sets of equipment to ensure their coherence. Additionally, it allows for verification of the formulas employed for calculation and identification of any potential simplifications made. This process enables Iberdrola to gain a deeper understanding of the equipment they have installed, enabling them to address any issues with the suppliers and draw conclusions for future large-scale supplier contracts by considering the necessary considerations. Furthermore, it becomes possible to suggest to Iberdrola the utilization of safety coefficients, potential simplifications in calculation, the frequency of rating updates, and whether the installation of a sensor is necessary or if a predictive estimation suffices.

3.4.2.1. Reliability Analysis

The main aim of the reliability analysis is to assess the reliability of the providers' systems involved, as both experience periods of inactivity, leading to a lack of dynamic ratings. This is cause of system shutdowns, sensor malfunctions, and disruptions in data supply from the meteorological information provider.

The lack of continuous and reliable dynamic ratings poses a serious challenge, especially if there are plans to implement dynamic rating in the future. Unreliable dynamic ratings could result in the power transmission line being operated beyond its safe limits, leading to potential losses of valuable assets and possible power supply interruptions.

Another purpose of this analysis is to clean the data for the subsequent analysis, ensuring the use of reliable data.

3.4.2.2. Input Data Analysis

The success and accuracy of any project that involves ratings or data analysis heavily depend on the quality and credibility of the input data. One of the objectives of the project is to evaluate the trustworthiness of the ratings given by both suppliers by examining the data they utilize as input.

Since each team uses different approaches to collect the required data, it becomes imperative to scrutinize these methods to ensure their validity and appropriateness. By doing so, it can be determined whether the data collection methods chosen by each supplier are reliable and capable of producing accurate and meaningful results.

3.4.2.3. Type of Calculation

The objective of this section is to make a comparison between the ampacity calculations provided by different suppliers, with the primary goal of determining the consistency of their dynamic rating results for the same transmission line at a specific moment.

Additionally, another important aim is to calculate the ampacity using the data inputs provided by both suppliers, employing the three standards for comparison. This allows for an evaluation of the ratings provided by the suppliers in contrast to our own calculated results. The objective is to uncover any disparities between the outcomes, considering the possibility of undisclosed coefficients or other factors, and to identify any irregular data from the supplier's perspective.

3.4.2.4. Periodicity of the Rating

The analysis of rating variability is essential to determine how frequently it is necessary to update the rating. This analysis becomes crucial because if DLR is to be used for OPF, updating the rating minute by minute may not be practically feasible due to the rapid reconfiguration required in the grid.

Hence, the study focuses on evaluating the viability of updating the rating at different time intervals, such as 15 minutes, 30 minutes, or 1 hour. By doing so, it aims to compare these different update frequencies with the real-time rating to assess the degree of change observed.

Ultimately, this investigation seeks to strike a balance between the frequency of rating updates and the feasibility of grid reconfiguration, ensuring that the DLR implementation aligns with operational constraints while still offering significant benefits in terms of flexibility and optimal power flow management.

3.4.2.5. Emissivity and Solar Absorption Coefficients

The objective is to evaluate the feasibility of using default values i.e., the recommended coefficients of emissivity and absorption provided by standards, because most of the time knowing the actual coefficients of the transmission is challenging, as they change over the time. The study aims to determine if these default values can serve as reasonable substitutes in ampacity calculations, considering the potential difficulty in obtaining accurate coefficients for specific transmission lines. By conducting this evaluation, the research seeks to determine the accuracy and applicability of default values and assess their adequacy for practical use in ampacity calculations when actual coefficients are unavailable or challenging to obtain.

3.4.2.6. Solar Radiation

The objective is to determine the necessity of having a solar radiation sensor on the transmission line. This will be achieved by comparing the accuracy and reliability of ampacity calculations using estimated values for solar radiation against those obtained with actual sensor measurements. The study aims to assess whether the use of estimated values can provide sufficient accuracy in adjusting ampacity values, potentially offering a viable alternative to installing dedicated solar radiation sensors on the transmission line.

3.4.2.7. Simplified Wind Calculation

The objective is to develop a simplified method for estimating the wind speed and direction on the transmission line. This simplified approach is based on determining

whether there is wind or not and applying a predefined fixed value for each case. The method also allows for the parametrization of different conditions and include the option to use a parametrizable fixed angle value to consider wind direction.

3.4.2.8. Temperature Analysis

The primary objective of the temperature analysis is to determine the feasibility of using ambient temperature predictions instead of sensor measurements. The aim is to assess whether temperature predictions can provide sufficient accuracy for ampacity calculations, potentially eliminating the need for dedicated ambient temperature sensors.

Furthermore, a secondary objective is to explore the potential benefits of using the maximum temperature value between the actual temperature and a temperature estimation/prediction (forecast). By considering the maximum temperature value, the analysis seeks to anticipate potential temperature fluctuations and proactively address situations where higher temperatures are forecasted. This approach can help ensure the reliability and safety of ampacity calculations by accounting for expected temperature variations.

3.5. METHODOLOGY USED FOR THE ANALYSIS

First, an overview of the formulas used by the different standards is given. Then, the methodology used for each analysis is explained.

3.5.1. STANDARDS' FORMULAS

This study employs steady-state formulas. As mentioned earlier, all the standards are built upon Equation 1, the heat balance equation, for ampacity calculation. Consequently, the conductor current in Amperes is defined by the following heat exchange equation:

$$I = \sqrt{\frac{P_{rad} + P_{conv} - P_{sol}}{R_T}}$$

Where:

- R_T is the electrical resistance of the conductor in alternating current at temperature T.

- P_{sol} is the heat gain from solar radiation.
- P_{rad} is the heat loss due to radiation.

To calculate the conductor's current, it is necessary to determine the alternating current resistance at the operating temperature:

$$R_T = R_{T_{25^\circ C}} + (T - 25) \cdot \frac{R_{T_{75^\circ C}} - R_{T_{25^\circ C}}}{75 - 25}$$

The values of $R_{T_{25^\circ C}}$ and $R_{T_{75^\circ C}}$ are specific to each conductor. T represents the operating temperature in $^\circ C$. Resistance values are expressed in Ω/m .

3.5.1.1. IEEE

In this section is summarized the standard IEEE for calculating the ampacity at steady state [31].

3.5.1.1.1. Heat absorbed from solar radiation

The calculation of heat absorbed by the conductor is formulated as follows:

$$P_{sol} = \alpha \cdot D \cdot Q_{se} \cdot \sin(\theta)$$

Where:

- α is the coefficient of solar radiation absorption.
- D is the diameter of the conductor (m).
- Q_{se} is the global solar radiation intensity (incident and reflected) (W/m^2).
- θ is the angle of solar incidence.

The value of P_{sol} is expressed in W/m .

The angle of solar incidence is defined by:

$$\theta = \arccos [\cos(H_c) \cdot \cos(Z_c - Z_1)]$$

Where:

- H_c is the sun's altitude (from 0° to 90°).

- Z_c is the sun's azimuth in degrees.
- Z_1 is the azimuth of the line in degrees.

The correction of solar radiation based on the line's altitude follows the following formula:

$$Q_{se} = K_{solar} \cdot Q_s$$

Where Q_s is the global solar radiation in W/m^2 , and this radiation can be estimated using a polynomial approximation described for clear and industrial atmosphere conditions.

The value of the K_{solar} coefficient is calculated using the following polynomial approximation:

$$K_{solar} = 1 + 1.148 \cdot 10^{-4} \cdot H_e - 1.108 \cdot 10^{-9} \cdot H_e^2$$

Here, H_e represents the altitude of the line in meters above sea level.

Altitude and solar azimuth calculations require knowledge of the line's average latitude, the day of the year, and solar time.

- The considered latitude (Lat) in the calculation is the line's average latitude in degrees.
- The day of the year (N) represents the day within the 365-day year, indicating the cumulative days since January 1st.
- Solar time (ω) is expressed as an angle in degrees, with solar noon at 0 degrees. For instance, during summer, solar noon is at 14:00, and every hour corresponds to a 15-degree angular variation. For instance, 9 AM corresponds to -75 degrees in the summer.

Solar declination (δ) in degrees is determined by an angle dependent on the day of the year and is formulated as follows:

$$\delta = 23.46 \cdot \sin \left[\frac{284 + N}{365} \cdot 360 \right]$$

Solar altitude (H_C) in degrees is defined by the following formula:

$$H_C = \arcsin [\cos(Lat) \cdot \cos(\delta) \cdot \cos(\omega) + \sin(Lat) \cdot \sin(\delta)]$$

Solar azimuth (Z_c) in degrees is defined by the following formula:

$$Z_c = C + \arctan(\chi)$$

Where:

$$\chi = \frac{\sin(\omega)}{\sin(Lat) \cdot \cos(\omega) - \cos(Lat) \cdot \tan(\delta)}$$

C depends on the variables χ and ω according to the following table:

Solar time ω	C when $\chi \geq 0$	C when $\chi < 0$
$-180 \leq \omega < 0$	0	180
$0 \leq \omega < 180$	180	360

Table 6: C parameter for Solar Azimuth calculation.

3.5.1.1.2. Convective Heat Dissipation

For calculating the heat dissipated by the conductor due to wind action, it is necessary to consider calculations for both natural and forced convection for weak or very weak winds, selecting the larger of the two results.

Forced Convection: Due to irregular behaviour in the case of light or strong winds, two heat dissipation formulas are established. In any case, the maximum of the results from the two equations is chosen. These equations are:

$$P_{conv1} = K_{angle} \cdot [1.01 + 1.35 \cdot N_{Re}^{0.52}] \cdot \lambda_f \cdot (T_s - T_a)$$

$$P_{conv2} = K_{angle} \cdot 0.754 \cdot N_{Re}^{0.6} \cdot \lambda_f \cdot (T_s - T_a)$$

Where:

- λ_f is the thermal conductivity of the air layer in contact with the conductor (W/ $^{\circ}$ C·m).
- T_s is the conductor's surface temperature ($^{\circ}$ C).

- T_a is the air temperature ($^{\circ}\text{C}$).
- N_{Re} is the Reynolds number K_{angle} is the angle of incidence coefficient.

The value of P_{conv} is expressed in W/m. The thermal conductivity in the boundary layer is determined as follows:

$$\lambda_f = 2.424 \cdot 10^{-2} + 7.477 \cdot 10^{-5} \cdot T_f - 4.407 \cdot 10^{-9} \cdot T_f^2$$

Assuming T_f , the temperature in the boundary layer, is the following average:

$$T_f = \frac{(T_s + T_a)}{2}$$

The Reynolds number is defined as follows:

$$N_{Re} = V \cdot \frac{D \cdot \gamma}{\mu_f}$$

Where:

- V is the wind speed (m/s).
- D is the conductor's diameter (m).
- μ_f is the dynamic viscosity of air ($\text{Pa}\cdot\text{s}$) and also in ($\text{kg}/\text{m}\cdot\text{s}$) as defined for forced convection:

$$\mu_f = \frac{1.458 \cdot 10^{-6} \cdot (T_f + 273)^{1.5}}{T_f + 383.4}$$

- This value depends on the temperature in the boundary layer defined above.
- Air density γ (kg/m^3) is defined by the following equation:

$$\gamma = \frac{1.293 - 1.525 \cdot 10^{-4} \cdot y + 6.379 \cdot 10^{-9} \cdot y^2}{1 + 0.00367 \cdot T_f}$$

This equation also depends on the temperature in the boundary layer, and altitude above sea level in meters, y .

The angle of incidence coefficient is calculated based on the angle between the wind and the conductor. A 90-degree angle corresponds to maximum heat dissipation. To evaluate

with a certain angle δ with respect to the conductor, calculate the corresponding coefficient according to the following formula:

$$K_{angle} = 1.194 - \cos(\phi) + 0.194 \cdot \cos(2 \cdot \phi) + 0.368 \cdot \sin(2 \cdot \phi)$$

Natural Convection: For calculating heat dissipated by natural convection, the following equation is used:

$$P_{CN} = 3.645 \cdot \gamma^{0.5} \cdot D^{0.75} \cdot (T_s - T_a)^{1.25}$$

Where:

- D is the conductor's diameter (m).
- T_s is the conductor's surface temperature ($^{\circ}\text{C}$).
- T_a is the air temperature ($^{\circ}\text{C}$) μf is the dynamic viscosity of air ($\text{Pa}\cdot\text{s}$) and also in ($\text{kg}/\text{m}\cdot\text{s}$) as defined for forced convection. Air density γ in (kg/m^3) as defined for forced convection.

For light winds, natural convection should be considered only when the heat dissipation is greater than that of forced convection.

Convective Heat Dissipation: Convective heat dissipation must be considered as the maximum of the heat obtained from both natural and forced convection in all cases.

$$P_{conv} = \max(P_{conv;forced}; P_{conv;natural})$$

The value of P_{conv} is expressed in W/m .

3.5.1.1.3. Radiative Heat Dissipation

For calculating heat dissipation due to conductor radiation, the following equation is used:

$$P_{rad} = 17.8 \cdot D \cdot \varepsilon \cdot \left[\left(\frac{T_s + 273}{100} \right)^4 - \left(\frac{T_a + 273}{100} \right)^4 \right]$$

Where:

- D is the conductor's diameter (m).
- ε is the emissivity coefficient with respect to a black body.

- T_s is the conductor's surface temperature ($^{\circ}\text{C}$).
- T_a is the air temperature ($^{\circ}\text{C}$).

The value of P_{rad} is expressed in W/m.

3.5.1.2. CIGRE 601

The main formulas of the standard CIGRE 601 are summarized [30].

3.5.1.2.1. Heat absorbed from solar radiation

The calculation of heat absorbed by the conductor is formulated as follows:

$$P_{sol} = \gamma \cdot D \cdot S_i$$

Where:

- γ is the coefficient of solar radiation absorption, typically set to 0.5 by default.
- D is the conductor's diameter (m).
- S_i is the intensity of global solar radiation (incident and reflected) (W/m^2).

The value of P_{sol} is expressed in W/m.

The value of the global radiation intensity is defined as follows:

$$S_i = I_B \cdot \left(\sin(\eta) + \frac{\pi}{2} \cdot F \cdot \sin(H_s) \right) + I_d \cdot \left(1 + \frac{\pi}{2} \cdot F \right)$$

Where:

- I_B is the direct solar radiation on a surface perpendicular to the sun (W/m^2).
- I_d is the diffuse solar radiation on a horizontal surface (W/m^2).
- F is the reflectance coefficient of the surface.
- η is the angle of incidence of the sun with respect to the conductor's axis in degrees.
- H_s is the solar altitude in degrees.

Direct solar radiation is defined by the following equation:

$$I_B = N_S \cdot \frac{1280 \cdot \sin(H_S)}{\sin(H_S) + 0.314}$$

Where H_S is the solar altitude in degrees and N_S is the clarity index ratio depending on the standard type of atmosphere.

To correct solar radiation based on altitude above sea level, the following equation should be used:

$$I_{By} = I_B \cdot \left[1 + 1,4 \cdot 10^{-4} \cdot y \cdot \left(\frac{1367}{I_B} - 1 \right) \right]$$

Where y is the altitude of the conductor line above sea level in meters.

Diffuse solar radiation is defined by the following equation:

$$I_d = (430,5 - 0,3288 \cdot I_B) \cdot \sin(H_S)$$

Solar declination (δ) in degrees is defined as an angle depending on the day of the year:

$$\delta = 23,3 \cdot \sin \left[\frac{284 + N}{365} \cdot 2 \cdot \pi \right]$$

Solar altitude H_S in degrees is defined by the following formula:

$$H_S = \arcsin [\cos(Lat) \cdot \cos(\delta) \cdot \cos(\omega) + \sin(Lat) \cdot \sin(\delta)]$$

Solar azimuth angle (Z_c) in degrees is defined by the following formula:

$$Z_c = \arcsin \left[\frac{\cos(\delta) \cdot \sin(\omega)}{\cos(H_S)} \right]$$

Angle of incidence of the sun with respect to the conductor's axis (η) is defined as:

$$\eta = \arccos [\cos(H_S) \cdot \cos(Z_c - \theta)]$$

3.5.1.2.2. Convective Heat Dissipation

For calculating the heat dissipated by the conductor due to wind action, both natural and forced convection calculations must be considered for weak or very weak winds. In both

cases, the formulation is the same, though the constants used may vary. The formula is as follows:

$$P_{conv} = \pi \cdot \lambda_f \cdot (T_s - T_a) \cdot Nu$$

Where:

- λ_f is the thermal conductivity of the air layer in contact with the conductor ($\text{W}/\text{°C}\cdot\text{m}$).
- T_s is the conductor's surface temperature ($^\circ\text{C}$).
- T_a is the air temperature ($^\circ\text{C}$).
- Nu is the Nusselt number.

The value of P_{conv} is expressed in W/m .

In both calculations, the thermal conductivity in the boundary layer is determined as follows:

$$\lambda_f = 2.368 \cdot 10^{-2} + 7.23 \cdot 10^{-5} \cdot T_f - 2.763 \cdot 10^{-8} \cdot T_f^2$$

Assuming that T_f , temperature in the boundary layer, is the average value:

$$T_f = \frac{(T_s + T_a)}{2}$$

The only variable depending on the type of convection is the Nusselt number. Depending on the type of convection, it is calculated as follows:

Forced Convection: For incident winds at a certain angle δ with respect to the conductor, firstly, the Nusselt number for perpendicular winds needs to be calculated.

a) Perpendicular wind

The Nusselt number is directly related to the Reynolds number. The Reynolds number is calculated as follows:

$$Re = V \cdot \frac{D}{\nu_f}$$

- V is the wind speed (m/s).
- D is the diameter of the conductor (m).
- ν_f is the kinematic viscosity of air (m^2/s).

The kinematic viscosity of air is calculated using dynamic viscosity μ_f and air density γ at the given temperature and altitude above sea level:

$$\nu_f = \frac{\mu_f}{\gamma}$$

The dynamic viscosity of air μ_f is defined by the following equation:

$$\mu_f = (17.239 + 4.635 \cdot 10^{-2} \cdot T_f - 2.03 \cdot 10^{-5} \cdot T_f^2) \cdot 10^{-6}$$

And it depends on the temperature of the boundary layer defined above.

The density of the air γ is defined by the following equation:

$$\gamma = \frac{1.293 - 1.525 \cdot 10^{-4} \cdot y + 6.379 \cdot 10^{-9} \cdot y^2}{1 + 0.00367 \cdot T_f}$$

Which also depends on the temperature of the previously defined boundary layer and the altitude with respect to sea level in meters.

Once the Reynolds number is obtained, to calculate the Nusselt number, consider the surface roughness of the conductor, defined by R_s :

$$R_s = \frac{d}{[2 \cdot (D - d)]}$$

Where D is the total diameter of the conductor and d is the diameter of the wires that make up the outer layer of the conductor.

Depending on the conductor's roughness, the coefficients B and n are extracted from the following tables:

Smooth conductors		
Re	B	n
35 – 5000	0.583	0.471
5000 – 50000	0.148	0.633
50000 – 200000	0.0208	0.814

Table 7: Coefficients B and n for smooth conductors.

ACSR Conductors with $R_S \leq 0.05$		
Re	B	n
100 – 2650	0.641	0.471
2650 – 50000	0.178	0.633

Table 8: Coefficients B and n for ACSR Conductors with $R_S \leq 0.05$.

ACSR Conductors with $R_S > 0.05$		
Re	B	n
100 – 2650	0.641	0.471
2650 – 50000	0.048	0.800

Table 9: Coefficients B and n for ACSR Conductors with $R_S > 0.05$.

Once the Reynolds number is obtained and the coefficients B and n are selected, the Nusselt number is calculated using the equation:

$$Nu_{perp} = B \cdot Re^n$$

This value corresponds to the maximum evaporation, which is the case for wind perpendicular to the conductor.

b) Wind with δ Direction

The reduction of the Nusselt number when the wind direction is not perpendicular to the conductor is based on equations that depend on the conductor type and angle.

The following equations can be applied when the Reynolds number $Re < 4000$.

For Smooth Conductors:

$$Nu_\delta = Nu_{perp} \cdot (\sin^2(\delta) + 0,0169 \cdot \cos^2(\delta))^{0.225}$$

For ACSR Conductors:

$$\text{If } \delta \leq 24^\circ \quad Nu_\delta = Nu_{perp} \cdot [0.42 + 0.68 \cdot (\sin(\delta))^{1.08}]$$

$$\text{If } \delta > 24^\circ \quad Nu_\delta = Nu_{perp} \cdot [0.42 + 0.58 \cdot (\sin(\delta))^{0.90}]$$

When wind speed is low ($V < 0.5$ m/s) and wind direction is not defined, assuming wind direction is 45° results in a reduction factor of 0.845 for ACSR conductors.

Natural Convection: When wind is assumed to be absent, the Nusselt number depends on the Grashof and Prandtl numbers. The Grashof number is defined as:

$$Gr = \frac{D^3 \cdot (T_s - T_a) \cdot g}{(T_f + 273) \cdot v_f^2}$$

Where:

- D is the diameter of the conductor (m).
- T_s is the conductor surface temperature ($^\circ\text{C}$).
- T_a is the air temperature ($^\circ\text{C}$).
- g is the acceleration due to gravity (9.807 m/s 2).
- T_f is the average temperature in the boundary layer.
- v_f is the kinematic viscosity of air (m 2 /s).

The Prandtl number is defined as follows:

$$Pr = c \cdot \frac{\mu_f}{\lambda_f}$$

Where:

- c is the specific heat of air (1005 J/kg· $^\circ\text{K}$).
- μ_f is the dynamic viscosity of air (Pa·s) and also in (kg/m·s).
- λ_f is the thermal conductivity of the air layer in contact with the conductor (W/ $^\circ\text{C}\cdot\text{m}$).

Based on the product of the Grashof and Prandtl numbers, coefficients are obtained from the table to define the Nusselt number:

<i>Range of Gr * Pr Values</i>	<i>A</i>	<i>m</i>
$10^{-1} - 10^2$	1.020	0.148
$10^2 - 10^4$	0.850	0.188
$10^4 - 10^7$	0.480	0.250
$10^7 - 10^{12}$	0.125	0.333

Table 10: A and m coefficients.

Finally, the Nusselt number is defined by the equation:

$$Nu_{nat} = A \cdot (Gr \cdot Pr)^m$$

For natural convection, the maximum angle the conductor makes with the horizontal, β , reduces the heat of natural convection. Depending on the conductor type and the maximum angle, these corrections are as follows:

For Smooth Conductors with $\beta < 60^\circ$: $Nu_\beta = Nu_{nat} \cdot (1 - 1.58 \cdot 10^{-4} \cdot \beta^{1.5})$

For ACSR Conductors with $\beta < 80^\circ$: $Nu_\beta = Nu_{nat} \cdot (1 - 1.76 \cdot 10^{-6} \cdot \beta^{2.5})$

Convective Heat Convective heat should be considered using the maximum values obtained from both natural and forced convection

$$P_{conv} = \max(P_{conv;forced}; P_{conv;natural})$$

Calculate the corresponding dissipated powers using the formula from the beginning of the section, each time with the corresponding Nusselt number, corrected as necessary.

3.5.1.2.3. Radiative Heat Dissipation

For calculating the heat dissipated due to radiation from the conductor, the following equation is used:

$$P_{rad} = \pi \cdot D \cdot \sigma_B \cdot \varepsilon \cdot [(T_s + 273)^4 - (T_a + 273)^4]$$

Where:

- D is the diameter of the conductor (m).
- σ_B is the Stefan-Boltzmann constant ($5.6697 * 10^{-8}$ W/m²·K⁴).
- ε is the emissivity coefficient relative to a blackbody.
- T_s is the conductor surface temperature (°C).
- T_a is the air temperature (°C).

The value of P_{rad} is expressed in W/m.

3.5.1.3. CIGRE 207

The main formulas from CIGRE 207 [35] are described below

3.5.1.3.1. Heat absorbed from solar radiation

The calculation of heat absorbed by the conductor is formulated as follows:

$$P_{sol} = \gamma \cdot D \cdot S_i$$

Where:

- γ is the coefficient of solar radiation absorption, typically set to 0.5 by default.
- D is the conductor's diameter (m).
- S_i is the intensity of global solar radiation (incident and reflected) (W/m²).

The value of P_{sol} is expressed in W/m.

The value of the global radiation intensity is defined as follows:

$$S_i = I_B \cdot \left(\sin(\eta) + \frac{\pi}{2} \cdot F \cdot \sin(H_s) \right) + I_d \cdot \left(\frac{\pi}{2} + \frac{\pi}{2} \cdot F \right)$$

Where:

- I_B is the direct solar radiation on a surface perpendicular to the sun (W/m²).
- I_d is the diffuse solar radiation on a horizontal surface (W/ m²).

- F is the reflectance coefficient of the surface.
- η is the angle of incidence of the sun with respect to the conductor's axis in degrees.
- H_s is the solar altitude in degrees.

Direct solar radiation is defined by the following equation:

$$I_B = \frac{1280 \cdot \sin(H_s)}{\sin(H_s) + 0.314}$$

Where H_s is the solar altitude in degrees.

To correct solar radiation based on altitude above sea level:

- I_B increases by 7-13% from sea level to 1000 m above sea level.
- I_B increases by 13-22% from sea level to 2000 m above sea level.

The highest value occurs in summer.

Diffuse solar radiation is defined by the following equation:

$$I_d = (570 - 0.47 \cdot I_B) \cdot \sin^{1.2}(H_s)$$

Solar declination (δ) in degrees is defined as an angle depending on the day of the year:

$$\delta = 23.4 \cdot \sin \left[\frac{284 + N}{365} \cdot 2 \cdot \pi \right]$$

Solar altitude H_s in degrees is defined by the following formula:

$$H_s = \arcsin [\cos(Lat) \cdot \cos(\delta) \cdot \cos(\omega) + \sin(Lat) \cdot \sin(\delta)]$$

Solar azimuth angle (Z_c) in degrees is defined by the following formula:

$$Z_c = \arcsin \left[\frac{\cos(\delta) \cdot \sin(\omega)}{\cos(H_s)} \right]$$

Angle of incidence of the sun with respect to the conductor's axis (η) is defined as:

$$\eta = \arccos [\cos(H_S) \cdot \cos(Z_C - \theta)]$$

θ is the azimuth of the line conductor in degrees.

3.5.1.3.2. Convective Heat Dissipation

For calculating the heat dissipated by the conductor due to wind action, both natural and forced convection calculations must be considered for weak or very weak winds. In both cases, the formulation is the same, though the constants used may vary. The formula is as follows:

$$P_{conv} = \pi \cdot \lambda_f \cdot (T_s - T_a) \cdot Nu$$

Where:

- λ_f is the thermal conductivity of the air layer in contact with the conductor (W/ $^{\circ}$ C·m).
- T_s is the conductor's surface temperature ($^{\circ}$ C).
- T_a is the air temperature ($^{\circ}$ C).
- Nu is the Nusselt number.

The value of P_{conv} is expressed in W/m.

In both calculations, the thermal conductivity in the boundary layer is determined as follows:

$$\lambda_f = 2,368 \cdot 10^{-2} + 7,23 \cdot 10^{-5} \cdot T_f - 2,763 \cdot 10^{-8} \cdot T_f^2$$

Assuming that T_f , temperature in the boundary layer, is the average value:

$$T_f = \frac{(T_s + T_a)}{2}$$

The only variable depending on the type of convection is the Nusselt number. Depending on the type of convection, it is calculated as follows:

Forced Convection: For incident winds at a certain angle δ with respect to the conductor, firstly, the Nusselt number for perpendicular winds needs to be calculated.

c) Perpendicular wind

The Nusselt number is directly related to the Reynolds number. The Reynolds number is calculated as follows:

$$Re = V \cdot \frac{D}{v_f}$$

- V is the wind speed (m/s).
- D is the diameter of the conductor (m).
- v_f is the kinematic viscosity of air (m^2/s).

The kinematic viscosity of air is calculated using dynamic viscosity μ_f and air density γ at the given temperature and altitude above sea level:

$$v_f = \frac{\mu_f}{\gamma}$$

The dynamic viscosity of air μ_f is defined by the following equation:

$$\mu_f = (17.239 + 4.635 \cdot 10^{-2} \cdot T_f - .03 \cdot 10^{-5} \cdot T_f^2) \cdot 10^{-6}$$

And it depends on the temperature of the boundary layer defined above.

The density of the air γ is defined by the following equation:

$$\gamma = \frac{1.293 - 1.525 \cdot 10^{-4} \cdot y + 6.379 \cdot 10^{-9} \cdot y^2}{1 + 0.00367 \cdot T_f}$$

Which also depends on the temperature of the previously defined boundary layer and the altitude with respect to sea level in meters.

Once the Reynolds number is obtained, to calculate the Nusselt number, consider the surface roughness of the conductor, defined by R_s :

$$R_s = \frac{d}{[2 \cdot (D - d)]}$$

Where D is the total diameter of the conductor and d is the diameter of the wires that make up the outer layer of the conductor.

Depending on the conductor's roughness, the coefficients B and n are extracted from the following table:

<i>Surface</i>	<i>Re</i>		<i>B</i>	<i>n</i>
	<i>from</i>	<i>to</i>		
Stranded all surfaces	10^2	$2.65 \cdot 10^3$	0.641	0.471
Stranded $R_s \leq 0.05$	$>2.65 \cdot 10^3$	$5 \cdot 10^4$	0.178	0.633
Stranded $R_s > 0.05$	$>2.65 \cdot 10^3$	$5 \cdot 10^4$	0.048	0.8

Table 11: Coefficients B and n.

Once the Reynolds number is obtained and the coefficients B and n are selected, the Nusselt number is calculated using the equation:

$$Nu_{perp} = B \cdot Re^n$$

This value corresponds to the maximum evaporation, which is the case for wind perpendicular to the conductor.

d) Wind with δ Direction

The reduction of the Nusselt number when the wind direction is not perpendicular to the conductor is based on equations that depend on the conductor type and angle:

$$\text{If } \delta \leq 24^\circ \quad Nu_\delta = Nu_{perp} \cdot [0.42 + 0.68 \cdot (\sin(\delta))^{1.08}]$$

$$\text{If } \delta > 24^\circ \quad Nu_\delta = Nu_{perp} \cdot [0.42 + 0.58 \cdot (\sin(\delta))^{0.90}]$$

When wind speed is low ($V < 0.5$ m/s) and wind direction is not defined, assuming wind direction is 45° results in a reduction factor of 0.55 for the Nu_{perp} .

Natural Convection: When wind is assumed to be absent, the Nusselt number depends on the Grashof and Prandtl numbers. The Grashof number is defined as:

$$Gr = \frac{D^3 \cdot (T_s - T_a) \cdot g}{(T_f + 273) \cdot \nu_f^2}$$

Where:

- D is the diameter of the conductor (m).
- T_s is the conductor surface temperature ($^\circ\text{C}$).
- T_a is the air temperature ($^\circ\text{C}$).
- g is the acceleration due to gravity (9.807 m/s^2).
- T_f is the average temperature in the boundary layer.
- ν_f is the kinematic viscosity of air (m^2/s).

The Prandtl number is defined as follows:

$$\text{Pr} = c \cdot \frac{\mu_f}{\lambda_f}$$

Where:

- c is the specific heat of air ($1005 \text{ J/kg}\cdot\text{K}$).
- μ_f is the dynamic viscosity of air ($\text{Pa}\cdot\text{s}$) and also in ($\text{kg/m}\cdot\text{s}$).
- λ_f is the thermal conductivity of the air layer in contact with the conductor ($\text{W}/\text{C}\cdot\text{m}$).

Based on the product of the Grashof and Prandtl numbers, coefficients are obtained from the table to define the Nusselt number:

Range of $Gr \cdot Pr$ Values	A	m
$10^2 - 10^4$	0.850	0.188
$10^4 - 10^6$	0.480	0.250

Table 12: A and m coefficients.

Finally, the Nusselt number is defined by the equation:

$$Nu_{nat} = A \cdot (Gr \cdot Pr)^m$$

Convective Heat Convective heat should be considered using the maximum values obtained from both natural and forced convection

$$P_{conv} = \max(P_{conv;forced}, P_{conv;natural})$$

Calculate the corresponding dissipated powers using the formula from the beginning of the section, each time with the corresponding Nusselt number, corrected as necessary.

3.5.1.3.3. Radiative Heat Dissipation

For calculating the heat dissipated due to radiation from the conductor, the following equation is used:

$$P_{rad} = \pi \cdot D \cdot \sigma_B \cdot \varepsilon \cdot [(T_s + 273)^4 - (T_a + 273)^4]$$

Where:

- D is the diameter of the conductor (m).
- σ_B is the Stefan-Boltzmann constant ($5.6697 \cdot 10^{-8}$ W/m²·K⁴).
- ε is the emissivity coefficient relative to a blackbody.
- T_s is the conductor surface temperature (°C).
- T_a is the air temperature (°C).

The value of P_{rad} is expressed in W/m.

3.5.2. ANALYSIS OF THE STANDARDS

3.5.2.1. Type of Formulation

The methodology aims to analyse the impact of input variables on the different standards for the ampacity calculation to compare them considering real data. For a specific moment in time given the input parameters from Table 13 a sensitivity analysis on the value of the parameter of interest (wind speed, wind angle, and temperature) is addressed.

Temperature	Wind speed	Wind direction	Solar radiation	Day	Hour
26 °C	2.02 m/s	90 °	566 W/m ²	11/06/2023	12:00:00

Table 13: Parameters for ampacity calculation.

3.5.2.2. Impact of the Altitude to the Line Ampacity

The methodology involved assessing the impact of line elevation on the ampacity of the transmission line. The input parameters considered are showed in the Table 14.

Temperature (°C)	26
Wind speed (m/s)	10
Wind direction (°)	90
Solar radiation (W/m²)	566
Day	11/06/2023
Hour	12:00:00
Roughness	0.04

Table 14: Parameters used for the altitude analysis.

The line elevation affects two parameters the solar heat gain and the convection cooling. The solar gain is affected because a major altitude, the effect of the radiation increases. The convection depends on the density of the air, which in turn this density depends on the altitude. At higher altitudes, the air density decreases, causing a negative impact on convective cooling. It can then be foreseen that at higher altitudes the ampacity of the line will be more restricted.

To investigate the impact on ampacity, the line's elevation was varied from 0 m to 1500 m above sea level. The study was performed under three different assumptions for the wind speed parameter: 0.5 m/s, 5 m/s, and 10 m/s. The ampacity variations concerning altitude are examined using IEEE, CIGRE 601, and CIGRE 207 standards.

3.5.2.3. Impact of the Emissivity and Absorption Coefficients

In this section, the focus is on studying the impact of coefficient variations. To accomplish this, the conditions from Table 14 are considered, and adjustments are made to the coefficients and the maximum operating temperature of the conductor.

3.5.3. ANALYSIS OF THE DATA EQUIPMENT

3.5.3.1. Reliability Analysis

The analysis of reliability is conducted in two stages. The first stage involves evaluating the reliability of the equipment's historical data for the entire year 2023 up to June. In the second stage, a more specific analysis is carried out for a particular period, spanning from March 8 to June 30, 2023. This specific period is chosen for subsequent analysis because it is the time when both systems exhibited the highest level of functionality and coincidence, making it ideal for meaningful comparisons. It is important to note that even during the selected period, there are still instances when one of the systems encountered issues.

The downtime for each system is identified by analysing timestamps and identifying intervals where ampacity values are not available or not given a reliable value because missing input data. The total number of minutes for the entire period is calculated by subtracting the start timestamp from the end timestamp. Simultaneously, the number of minutes without data available is determined by summing the downtime periods identified in the previous step.

The reliability percentage is then calculated by dividing the total minutes with data available by the total minutes of the analysis period and multiplying the result by 100, as the next formula shows:

$$\text{Reliability} (\%) = \frac{\text{Number of available data points}}{\text{Expected number of data points}} \cdot 100$$

This reliability percentage represents the proportion of time during which the systems provided ampacity values with valid input data.

3.5.3.2. Input Data Analysis

The methodology employed for this section consists of analysing and comparing the atmospheric variables used by the suppliers to calculate the rating.

Furthermore, data from a weather source, Open-Meteo [36], is collected in order to compare it with the data from the suppliers. This data is from the nearest meteorological station, located in Elche. The Table 15 shows the coordinates of the line and the coordinates of the meteorological station, in order to see the difference.

COORDINATES	Latitude	Longitude	Elevation
Line	38°	0.85°	47 m
Nearest meteorological station	38.30°	-0.7°	84 m

Table 15: Coordinates

The data comparison and analysis for the year 2023 were conducted from March 8, 2023, to June 30, 2023, the period mentioned before, as its reliability is higher.

The historical data from Open-Meteo is available on an hourly basis, so the hourly averages of the variables from the providers are calculated for comparison.

3.5.3.3. Type of Calculation

First a comparation between the ampacity values that the suppliers provide is made. The comparison is made with the data from the equipment for the period from March 8, 2023, to June 30, 2023, the same data as in the previous sections, but now focusing on the ampacity values.

Since the data from Supplier 1 is available minute by minute, for each five-minute interval in the dataset from Supplier 2, the corresponding value from Supplier 1 is used. For example, if Supplier 2 provides data at 12:05, 12:10, 12:15, and so on, the data from Supplier 1 at those specific minutes (12:05, 12:10, 12:15) is used in order to be able to compare.

Next, using the data input of the suppliers, the ampacity is calculated employing the different standards (IEEE, CIGRE 601, and CIGRE 207).

Subsequently, a comparison is made between my calculated results and those provided by the supplier, assuming they use one of these formulas.

3.5.3.4. Periodicity of the Rating

The aim of the periodicity analysis is to understand how often is necessary that the system generates the ampacity rating. This information is crucial for the OPF process, where minute-by-minute ratings might not be feasible. Three scenarios will be explored: providing the rating every 15 minutes, 30 minutes, and 1 hour.

To examine the periodicity of the measured and estimated ampacity of a line, the input data from GE, available minute by minute, is utilized, and the calculations of ampacity is carried out using the IEEE standard.

Within each scenario, the ampacity rating is computed in three ways: taking the average of the minute-by-minute ratings from the preceding period (e.g., 15 minutes), using the most restrictive ampacity value from the preceding period (i.e., the minimum ampacity of the past 15 minutes), and presenting the instantaneous value, representing the real-time rating every 15 minutes.

A comparison is made between the real-time ampacity values and the minute-by-minute ampacity to ascertain the level of reliability. If the real-time rating falls below the provided value, it suggests a potential safety concern, indicating that the given value may not be secure. This analysis helps evaluating the reliability of the ampacity ratings provided at different intervals and ensure that safe and accurate values are communicated during the OPF process.

3.5.3.5. Emissivity and Solar Absorption Coefficients

An evaluation of the use of default coefficient values given by the different standards is given. The next table shows the recommended values to be used when the actual values are unknown:

Coefficient	CIGRE 601	IEEE
Solar absorption	0.7	0.8
Emissivity	0.6	0.7

Table 16: Absorption and emissivity coefficients recommended by CIGRE 601 and IEEE standards.

For this analysis, atmospheric data from Supplier 1 for an entire day on June 11, 2023, is used. The calculated results are then be compared using the real coefficients of the line (solar absorption 0.6 and emissivity 0.5) against those using default coefficients.

3.5.3.6. Solar Radiation

If there is no sensor on the line to measure real solar radiation intensity, there are various ways to estimate this radiation. In this project, the following methods are studied:

1. Using the estimation provided by the different standards.
2. Using the prediction provided by a meteorological source, in this case Open-Meteo.
3. Use the historical maximum solar radiation data for the location of the lie and creating a sinusoidal parabolic function based on this value.

In this section, the solar radiation intensity estimated using the methods mentioned above is compared with the solar radiation measured by the sensor of the Supplier 1 that it is located on the proper line.

Subsequently, the impact in the final value of the ampacity is analysed. To calculate this ampacity, the IEEE standard is used.

3.5.3.7. Simplified Wind Calculation

The following simplifications are proposed:

- Simplification 1:

- Day + Wind speed $\geq \frac{15\text{km}}{\text{h}}$ → YES wind → Wind speed for formula: $\frac{1.2\text{m}}{\text{s}}$.
- Day + Wind speed $< \frac{15\text{km}}{\text{h}}$ → NO wind → Wind speed for formula: 0.6 m/s.
- Night → NO wind → Wind speed for formula: 0.6m/s.
- Wind direction = 15°.

- Simplification 2:

- Day + Wind speed $\geq \frac{9.36\text{ km}}{\text{h}}$ → YES wind → Wind speed for formula: $\frac{1.2\text{m}}{\text{s}}$.
- Day + Wind speed $< \frac{9.36\text{ km}}{\text{h}}$ → NO wind → Wind speed for formula: 0.2m/s.
- Night → NO wind → Wind speed for formula: 0.2m/s.
- Wind direction = 90°.

These simplifications are applied for the day on 14th April 2023, which has windy conditions, and complete data is available from both suppliers (no failures). It is used the three available data sets: Supplier 1, Supplier 2, and historical data collected from Open-Meteo.

3.5.3.8. Temperature Analysis

For this section, meteorological data from Supplier 1 and the prediction from Open Meteo is used. Two days are selected—one with low temperatures on 24th January 2023 and another with high temperatures on 25th June—to study both extremes. The ampacity calculations follow the IEEE standard.

Two cases are considered for the temperature used in the ampacity calculation:

1. Taking the predicted temperature and multiplying it by a safety factor based on the distance to the point being calculated ($K=1.1$ by default during the day, $K=1$ by default during the night).
2. Considering the maximum value among the current temperature measured by the sensor of Supplier 1, and the prediction.

Both results are compared with the ampacity calculation using the current temperature measured by Sensor 1.

4. RESULTS AND DISCUSSION

4.1. ANALYSIS OF THE STANDARDS

4.1.1. TYPE OF FORMULATION

In this section the results of the sensitivity analysis of the impact of the weather variables on the different ampacity standards is given.

4.1.1.1. Impact of the Wind speed

For the calculation of cooling power by convection, the consideration of conductor roughness (R_s) is accounted for in the CIGRE standards but not in the IEEE standards. In this study, two cases have been examined, one with $R_s=0.04$ and another with $R_s=0.08$, which closely aligns with our study line's roughness value of 0.083.

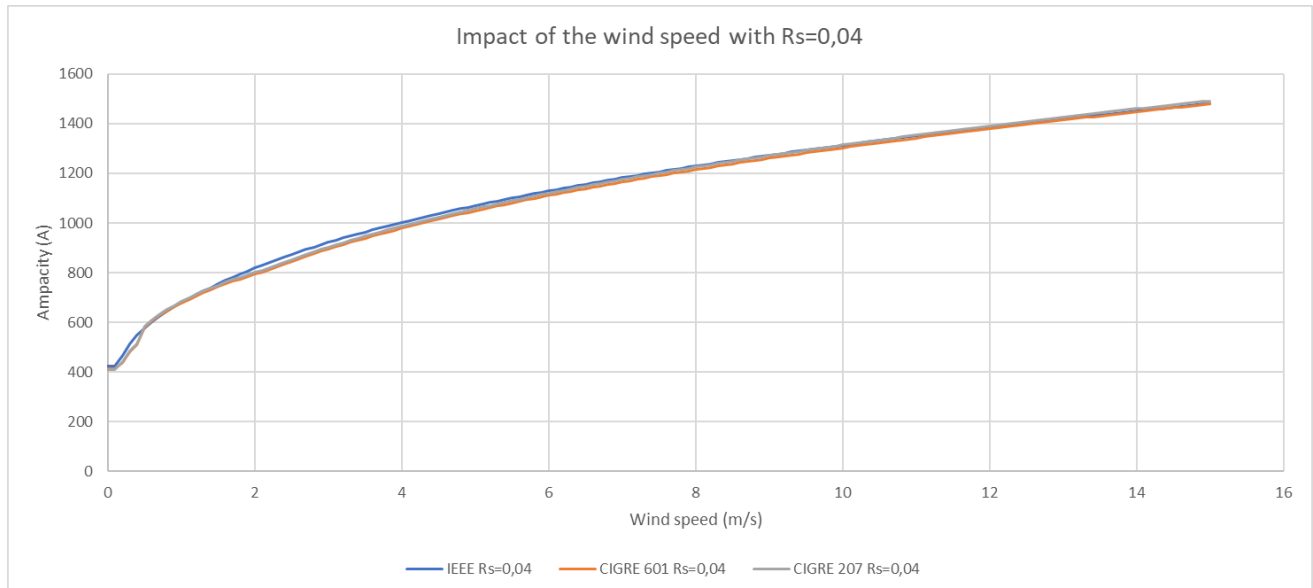


Figure 8: Wind speed analysis $R_s=0.04$

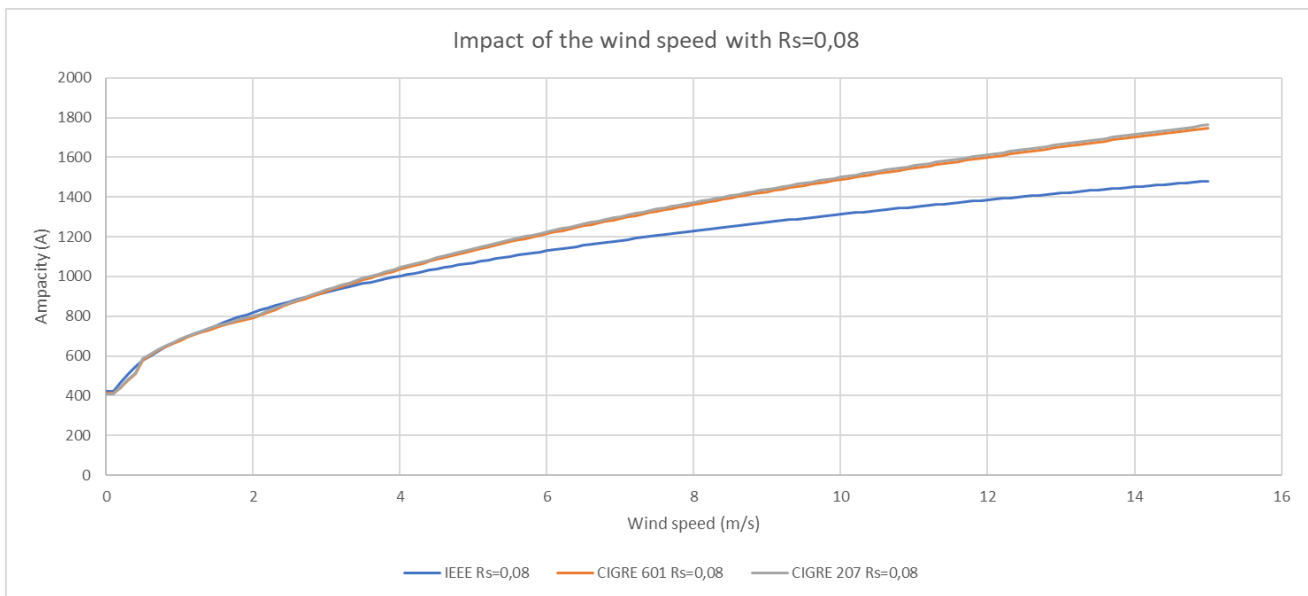


Figure 9: Wind speed analysis Rs=0.08

When considering $Rs=0.04$, Figure 13, there is little difference between the IEEE and CIGRE standards, with the maximum difference being 37.21 A between IEEE and CIGRE 601 at a wind speed of 0.4 m/s. The average difference between IEEE and CIGRE 601 is 13.78 A.

For $Rs=0.08$, at low wind speeds, the results from both standards are similar as Figure 9 shows. Nonetheless, around 3 m/s wind speed, the difference between IEEE and CIGRE starts to increase significantly, reaching a maximum difference of 267.35 A at a wind speed of 15 m/s. The average difference is 121.26 A between IEEE and CIGRE 601, much more than when $Rs=0.04$. This is due to the fact that with $Rs>0.05$, the CIGRE standards use higher coefficients to calculate the Nusselt Number, assuming that the convective cooling effect is higher in a rough conductor.

4.1.1.2. Impact of the Wind Direction

In this analysis, the parameters remain fixed, and the variable being varied is the wind direction over the transmission line.

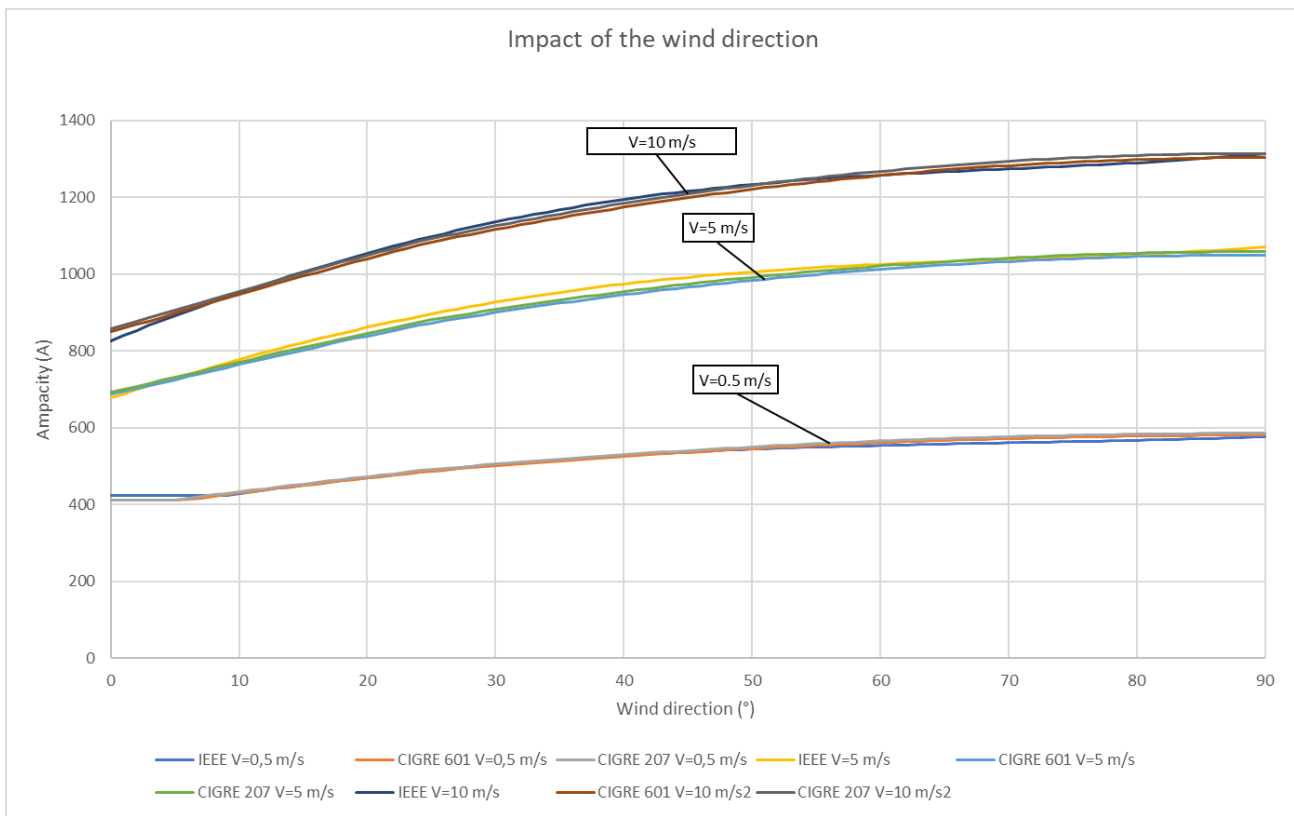


Figure 10: Wind direction analysis

The results depicted in Figure 10 show minimal changes among the different standards as the wind angle varies from 0 to 90 degrees. The average difference between IEEE and CIGRE 601 is 5.29 A, 16.30 A, and 10.91 A at wind speeds of 0.5 m/s, 5 m/s, and 10 m/s, respectively.

The differences between the standards can be attributed to the way they consider the wind angle. In the CIGRE standard, the impact of the wind angle on ampacity depends on whether the wind angle is greater than 24 degrees or not:

$$\text{If } \delta \leq 24^\circ \quad Nu_\delta = Nu_{perp} \cdot [0.42 + 0.68 \cdot (\sin(\delta))^{1.08}]$$

$$\text{If } \delta > 24^\circ \quad Nu_\delta = Nu_{perp} \cdot [0.42 + 0.58 \cdot (\sin(\delta))^{0.90}]$$

Conversely, the IEEE standard adopts a different approach to handle the wind attack angle. Instead of using a fixed threshold like CIGRE, the IEEE standard continually adjusts the constant multiplier based on the wind attack angle. This dynamic approach

means that even slight variations in the wind direction can result in variations in the calculated ampacity, making it a more sensitive method to account for wind angle effects

4.1.1.3. Impact of the Temperature

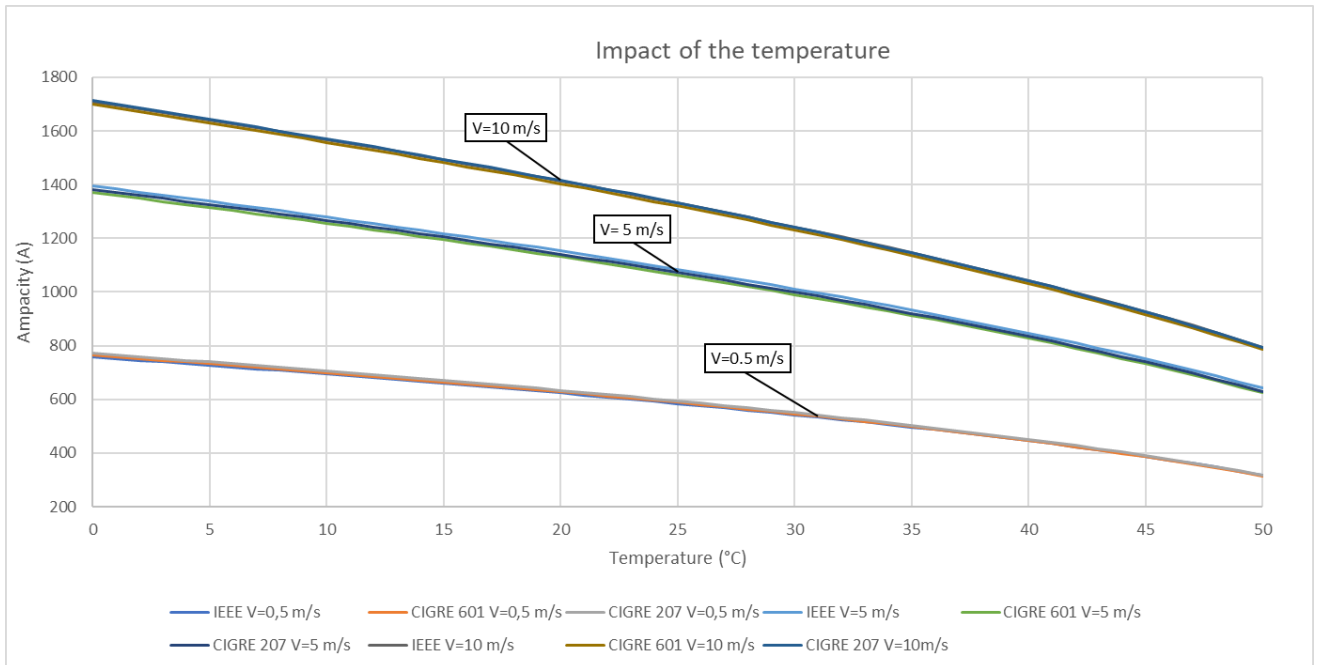


Figure 11: Temperature analysis

The analysis reveals minimal variation among the standards when the temperature is varied, with the average differences being 3.54 A, 21.18 A and 10.30 A at wind speeds of 0.5 m/s, 5 m/s, and 10 m/s, respectively. It is evident that higher temperatures result in lower ampacity values as Figure 11 shows. Both standards consider temperature as a crucial factor in the calculation of cooling convection, as lower temperatures allow for more cooling. Additionally, temperature significantly affects radiated heating, where heat is transferred from higher to lower temperatures. Consequently, in colder ambient conditions, the cable is allowed to transfer more heat to the surroundings. Moreover, it is observed that at higher wind speeds, the impact of temperature becomes more pronounced, as indicated by the more defined envelope in the results.

The analysis of the impact of solar radiation is studied later in a specific section dedicated to this aspect.

4.1.2. IMPACT OF THE ALTITUDE

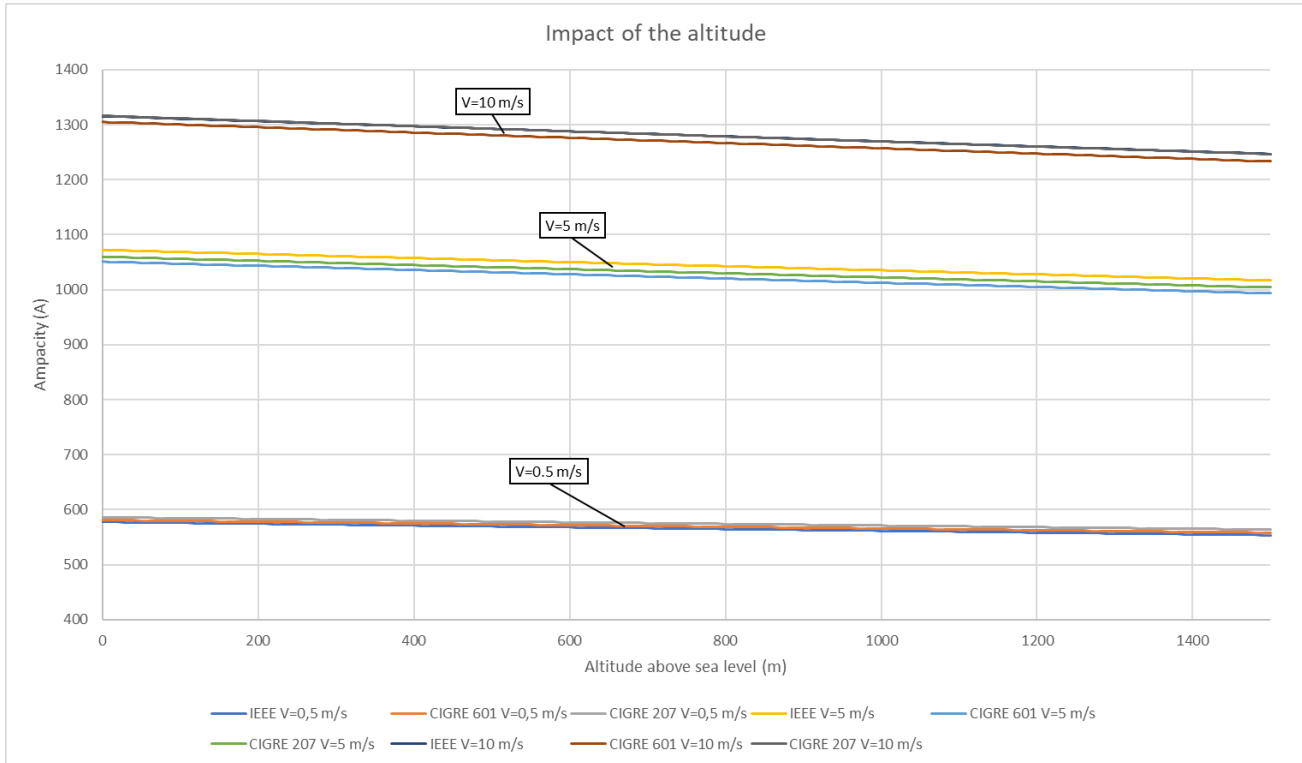


Figure 12: Impact of the altitude in the ampacity calculation

The Figure 12 shows how the ampacity varies when increasing the altitude, considering different wind speeds according to the mentioned standards (IEEE, CIGRE 601, and CIGRE 207).

Effectively, the results show that ampacity decreases with increasing altitude having the same weather conditions. As the transmission line elevation rises, the cooling mechanisms, such as convection, become less efficient due to the decrease in air density at higher altitudes. As the altitude parameters embeds the air density parameter in the studied formulas, the line's ability to dissipate heat reduces, leading to a lower ampacity.

The data from the study indicate that the ampacity variations due to altitude are more pronounced at higher wind speeds. This is likely because higher wind speeds enhance convective cooling, and when coupled with the impact of altitude on cooling effectiveness, the ampacity reduction becomes more significant.

IEEE V=0,5 m/s	CIGRE 601 V=0,5 m/s	CIGRE 207 V=0,5 m/s	IEEE V=5 m/s	CIGRE 601 V=5 m/s	CIGRE 207 V=5 m/s	IEEE V=10 m/s	CIGRE 601 V=10 m/s	CIGRE 207 V=10 m/s
4.2%	4.0%	3.8%	5.2%	5.5%	5.3%	5.2%	5.5%	5.3%

Table 17: Decrement in ampacity between 0 and 1500 meters of altitude.

The Table 17 illustrates the decrement in ampacity observed between 0 and 1500 meters of altitude for the various standards at different wind speeds. The maximum decrements in ampacity observed were around 5%, but this was under the most extreme conditions, with an elevation of 1000 meters and high wind speeds. Despite this, it is suggested to consider studying the altitude in specific zones for a more comprehensive analysis.

According to the Royal Decree 223/2008, the regulation on technical conditions for overhead lines, there are three zones on altitude above the sea level: Zone A (altitude less than 500 meters above sea level), Zone B (altitude between 500 and 1000 meters), and Zone C (altitude above 1000 meters) [37]. The study examined the maximum decrement that can occur in each zone, i.e., the decrement for every 500 meters increases in altitude..)[37]. The study examined the maximum decrement that can occur in each zone, i.e., the decrement for every 500 meters increases in altitude.

IEEE V=0,5 m/s	CIGRE 601 V=0,5 m/s	CIGRE 207 V=0,5 m/s	IEEE V=5 m/s	CIGRE 601 V=5 m/s	CIGRE 207 V=5 m/s	IEEE V=10 m/s	CIGRE 601 V=10 m/s	CIGRE 207 V=10 m/s
1.4%	1.3%	1.3%	1.8%	1.9%	1.8%	1.8%	1.9%	1.8%

Table 18: Decrement in ampacity when increasing 500 meters in altitude

The results in Table 18 revealed that the decrement that occurs in 500 meters (which this is the maximum altitude that can vary in each of the zones) at low wind speeds is around 1.5%, and at high wind speeds, it was around 2%. This difference is minimal, suggesting that it is not necessary to use an atlas for precise altitude data. Instead, for simplicity, assuming the minimum altitude value of the respective zone (500 meters for Zone B) can be considered, as the ampacity variations were not significantly different between the boundaries of each zone. However, if a more conservative approach is desired, the higher limit (1000 meters in this case) can also be considered. Thus, the use

of an atlas may not be necessary to estimate the ampacity at different altitudes within the identified zones.

4.1.3. IMPACT OF THE EMISSIVITY AND ABSORPTION COEFFICIENTS

		<i>IEEE calculation</i>						
Solar absorption		0.9	0.8	0.7	0.6	0.5	0.4	0.3
Emissivity		0.8	0.7	0.6	0.5	0.4	0.3	0.2
Temperature of Service (°C)	100	1122.1	1112.4	1102.5	1092.6	1082.5	1072.4	1062.2
	80	974.0	967.4	960.7	954.1	947.3	940.5	933.7
	65	833.3	829.5	825.6	821.8	817.9	814.0	810.0
	50	646.2	646.1	646.0	645.8	645.7	645.6	645.4
	40	467.1	471.2	475.3	479.4	483.4	487.4	491.3

Table 19: Ampacity values (A) varying the solar absorption and emissivity coefficients with different temperature of service using the IEEE standard for ampacity calculation.

		<i>CIGRE 601 calculation</i>						
Solar absorption		0.9	0.8	0.7	0.6	0.5	0.4	0.3
Emissivity		0.8	0.7	0.6	0.5	0.4	0.3	0.2
Temperature of Service (°C)	100	1096.4	1086.8	1077.1	1067.3	1057.4	1047.4	1037.4
	80	947.0	940.7	934.4	928.0	921.6	915.1	908.6
	65	805.9	802.6	799.2	795.8	792.4	789.0	785.6
	50	618.1	618.8	619.5	620.2	620.9	621.6	622.3
	40	439.1	444.7	450.2	455.7	461.1	466.4	471.7

Table 20: Ampacity values (A) varying the solar absorption and emissivity coefficients with different temperature of service using the CIGRE 601 standard for ampacity calculation.

		<i>CIGRE 207 calculation</i>						
Solar absorption		0,9	0,8	0,7	0,6	0,5	0,4	0,3
Emissivity		0,8	0,7	0,6	0,5	0,4	0,3	0,2
Temperature of Service (°C)	100	1105,9	1096,4	1086,7	1077,1	1067,3	1057,4	1047,4
	80	955,0	948,8	942,5	936,2	929,8	923,4	916,9
	65	812,9	809,6	806,2	802,9	799,5	796,1	792,7
	50	623,7	624,3	625,0	625,7	626,4	627,1	627,8
	40	444,0	449,5	455,0	460,4	465,7	471,0	476,2

Table 21: Ampacity values (A) varying the solar absorption and emissivity coefficients with different temperature of service using the CIGRE 207 standard for ampacity calculation.

The tables from above show the ampacity values varying the solar absorption and emissivity coefficients with the temperature of service of the cable. There are three tables, in each one of them the ampacity is calculated with a different standard: IEEE, CIGRE 601 and CIGRE 207. It can be observed that regardless of the formula used for calculation, the same pattern is consistently followed. For moderate service temperatures, there is minimal impact on ampacity values, with the change between the two extremes (solar absorption=0.9 and emissivity=0.8) and (solar absorption=0.3 and emissivity=0.2) being 2.79% and 0.12% for $T_s=65^\circ\text{C}$ and $T_s=50^\circ\text{C}$, respectively, in the case of IEEE calculations. For higher temperatures, the variation is greater, amounting to 5.34% and 4.14% for $T_s=100^\circ\text{C}$ and $T_s=80^\circ\text{C}$, respectively.

On the other hand, when the service temperature is higher, emissivity has a greater impact than solar absorption. The reason for that is that the emissivity coefficient ε , impacts more the power radiated when the difference of temperatures between the cable and the surrounding is greater, as the formula shows:

$$P_{rad} \propto \varepsilon * (T_s - T_a)$$

As a result, as the coefficient of emissivity increases the permissible ampacity rises because the radiated power to the environment also increases. Conversely, when the service temperature is lower ($T=40^\circ\text{C}$) and closer to the ambient temperature, the radiated power has less influence, and solar absorbed power becomes more significant. Hence, as the coefficients increase, the absorption coefficient has a more substantial impact, causing the cable to absorb more solar power and thus reducing the ampacity.

4.2. ANALYSIS OF THE DATA EQUIPMENT

4.2.1. RELIABILITY

Table 22 and Table 23 show the results of the reliability analyses for both suppliers. These reliability percentages indicate the proportion of available data during each period in relation to the total expected data, providing insights into the system's ability to consistently provide ampacity values during operational hours.

SUPPLIER 1	<i>January 1st to June 29th</i>	<i>March 8th to June 29th</i>
Data points that should have been available during the period	259,200	168,840
Data points lost (downtime)	45,050	14,406
Data points available	214,150	154,434
Reliability	82.6%	91.5%

Table 22: Reliability analysis for Supplier 1

SUPPLIER 2	<i>January 1st to June 29th</i>	<i>March 8th to June 29th</i>
Data points that should have been available during the period	43,239	32,737
Data points lost (downtime)	22,454	11,952
Data points available	20,785	20,785
Reliability	48.1%	63.5%

Table 23: Reliability analysis for Supplier 2

During March 8th to June 29th, the reliability of both suppliers increases, indicating improved performance during that time frame.

On the other hand, it is evident that Supplier 2 consistently exhibits lower overall reliability compared to Supplier 1. The reason behind this disparity lies in the

characteristics of Supplier 2's system. For Supplier 1, the data points lost primarily correspond to periods when their equipment is not functioning correctly, resulting in downtime. These periods are relatively straightforward to identify, as they are instances when the system is completely inactive. However, for Supplier 2, the situation is more complex. In addition to the periods when the entire equipment is non-operational, this supplier also experiences failures when the vibration sensor does not communicate. Furthermore, the challenge is compounded by instances when there are connectivity issues with the external provider.

It's important to note that during moments when an atmospheric variable is missing—whether due to sensor failures or communication problems with the external provider—Supplier 2 continues to provide a default rating. However, this default rating is not accurate, as it lacks essential input variables.

4.2.2. DATA INPUT: WEATHER VARIABLES

The comparison of the weather variables is conducted, taking into account the diverse sources and collection methods for each data point. The data was obtained from various origins: Supplier 's 1 input data is taken from the sensors installed on the tower, Supplier 2's wind speed data is calculated from the vibration sensor installed on the line and the rest from an external supplier and the data from Open-Meteo is from the nearest meteorological station with different coordinates from the line. This diversity in data sources necessitated careful consideration of the potential impacts on the comparison process.

	Temperature (°C)			Wind speed (m/s)			Solar radiation (W/m²)		
	IEEE / CIGRE		Open-Meteo	IEEE / CIGRE		Open-Meteo	IEEE / CIGRE		Open-Meteo
	Supplier 1	Supplier 2		Supplier 1	Supplier 2		Supplier 1	Supplier 2	
Average	20.08	23.00	19.75	0.48	1.14	2.90	201.32	366.48	208.34
Standard deviation	5.35	6.49	5.02	0.38	0.46	1.56	276.37	391.91	268.15
Range	29.30	39.12	26.30	2.50	3.50	8.99	1134.00	1030.41	857.00
Maximum	34.60	46.12	33.90	2.50	4.06	8.99	1134.00	1030.41	857.00
Minimum	5.30	7.00	7.60	0.00	0.56	0.00	0.00	0.00	0.00

Table 24: Statistical results of both Suppliers and Open-Meteo data set inputs

The Table 24 displays the statistical results, including average, standard deviation, range (maximum and minimum), for the different atmospheric variables from the three input datasets. Figure 13 and Figure 14, shows the temperature, wind speed and solar radiation over the time of the three datasets.

Notably, wind direction was excluded from the analysis due to its dependence on the sensor's position. Additionally, Supplier 2 measured effective wind direction, which is always perpendicular to the transmission line.

Finally, it is observed in the graphs a disruption in the equipment of Supplier 1, evident from a one-week period of inactivity.

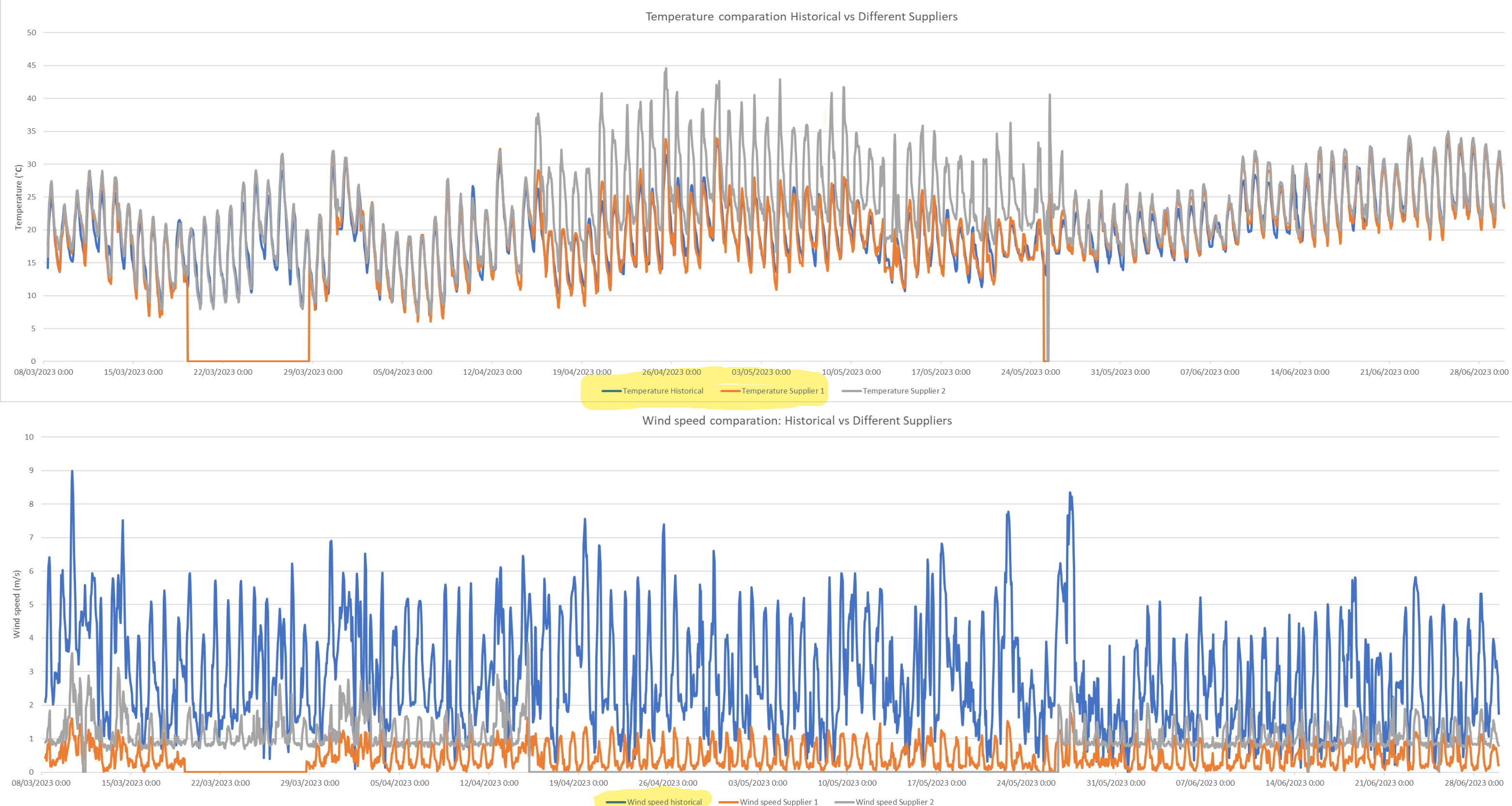


Figure 13: Temperature and Wind speed of the Supplier 1, Supplier 2 and Open-Meteo data sets.

Solar radiation comparation: Historical vs Different Suppliers



Figure 14: Solar radiation of the Supplier 1, Supplier 2 and Open-Meteo data sets.

4.2.2.1. Temperature measurements

Regarding ambient temperature, a similarity is observed between Supplier 1 and the data from Open-Meteo. However, a notable difference in the temperature data from Supplier 2 is evident, consistently showing higher values compared to the other suppliers. As previously mentioned, Supplier 1 collects data from an on-site weather station, Open Meteo gathers data from the nearest weather station, and Supplier 2 acquires data from an external provider with an unspecified station location. The similarity between temperatures from Open Meteo and Supplier 1 could imply that the Open Meteo weather station is closer to the line, while Supplier 2's data may be from a station located farther away.

4.2.2.2. Wind speed measurements

In terms of wind speed, there are important findings to note. Apart from the previously mentioned equipment disruption of Supplier 1, there was also a prolonged period of inactivity in the vibration sensor of Supplier 2, as evident from Figure 13. It is important to note that these periods are excluded for the statistical computation presented in the Table 24.

Additionally, the wind speed recorded by Open-Meteo consistently exceeded that of the suppliers. Both suppliers installed the wind sensors in the line or in the towers, which suggests that their wind data is more reliable. However, this suggestion can be called into question because surprisingly, both suppliers' wind measurements indicated very low wind speeds. Supplier 1's wind speed never exceeded 3 m/s, while Supplier 2 only occasionally reached this threshold, as Figure 13 shows. It is highly unlikely that there was never any wind on the transmission line, given that 3 m/s is considered a minimal wind speed. This raises doubts about the accuracy and reliability of the wind sensors' measurements.

On the other hand, Supplier 2 only measured the effective wind speed, considering it the most influential component, while Supplier 1 also factored in the wind angle. On this basis, it might be expected that the wind magnitude of Supplier 1 to be greater than that of Supplier 2, given that Supplier 2 accounted for only one component. Surprisingly, this

was not the case, as Supplier 2 consistently recorded higher wind speeds. This difference in wind speed measurements can be attributed to the fact that at equal wind conditions, wind at higher altitudes is always more effective due to the absence of ground and surrounding obstacles (such as trees) that introduce additional resistance. This variation in height could have contributed to the observed differences in wind speed readings between the two suppliers.

Taking all these aspects into consideration, it became crucial to carefully assess the accuracy and reliability of the wind speed data from both suppliers, as both reports very low wind speeds. The observed differences could be attributed to various factors, such as sensor calibration, sensor placement, and data processing methods. Addressing these discrepancies is of utmost importance to ensure the credibility of the wind speed data used in subsequent analyses and decision-making processes.

4.2.2.3. Solar radiation measurements

Regarding solar radiation, a similar pattern to the temperature emerged. Supplier 2 tends to report higher values compared to the other suppliers, while **Supplier 1 and Open Meteo data exhibited greater similarity**. The differences observed in solar radiation readings, may also be influenced by the location and characteristics of the meteorological station used by Supplier 2. Also, there was a disruption in the radiation sensor of Supplier 1 during March as it can be seen in the figure.

4.2.2.4. Key remarks on measurements reliability

In the comparison Table 25 between Supplier 1 and Supplier 2, the performances of their measurements are juxtaposed, providing a quick overview of the assessment results.

<i>Measurements</i>	<i>Similar</i>	<i>Different</i>
Wind speed		All
Ambient temperature	Supplier 1 and Open-Meteo	Supplier 2

<i>Measurements</i>	<i>Similar</i>	<i>Different</i>
Solar radiation	Supplier 1 and Open-Meteo	Supplier 2

Table 25: Similar and different measurements.

Regarding temperature and solar radiation measurements, Supplier 1 and Open-Meteo data show better agreement than Supplier 2's data. Supplier 2's higher values may be due to its reliance on data from a separate meteorological source, rather than having temperature and solar radiation sensors directly on the transmission line. It is possible that the meteorological station is located in a sunnier area compared to the location where Supplier 1 has its sensors (the tower of the line) and where Open-Meteo's station is placed, which could explain the differences in the recorded data.

As for wind measurements, both Supplier 1 and Supplier 2 have sensors installed, which should ideally provide more reliable data as they are being measurement on-site. However, surprisingly, both suppliers' wind speed data shows very low values, raising doubts about the accuracy of their measurements. This brings into question the reliability of the wind data provided by both suppliers.

4.2.3. TYPE OF CALCULATION

4.2.3.1. Suppliers' Ampacity Comparation

	<i>Ampacity (A)</i>	
	Supplier 1	Supplier 2
Average	582.08	623.49
Standard deviation	176.90	304.17
Range	575.50	288.64
Maximum	917.50	743.12
Minimum	342.00	454.48

Table 26: Statistical results of the ampacity values given by both Suppliers.

The Table 26 shows the statical results for the ampacity given by the different providers. The ampacity value provided by the Supplier 2 is consistently greater than the value given

by the Supplier 1 in most instances. The reason for that is that, as showed before, Supplier 2 is using higher wind speeds values than Supplier 1 for its calculations, resulting in higher ampacity values.

On the other hand, the ampacity values from Supplier 2 exhibit a wider dispersion around the average, as indicated by the higher standard deviation. But surprisingly, the variation between the maximum and minimum ampacity values is more pronounced in Supplier 1, indicating a greater range of variability in their results.

As mentioned before, Supplier 2 still given the dynamic rating even when it is missing an atmospheric data input. For the statistical analysis, these incomplete data points were removed. However, to provide a comprehensive view, two figures were created: the Figure 15 a) includes the ampacity values with incomplete atmospheric variables, while the Figure 15 b) excludes these data points. This comparison allows for a visual understanding of the impact of incomplete data on Supplier 2's ampacity values.

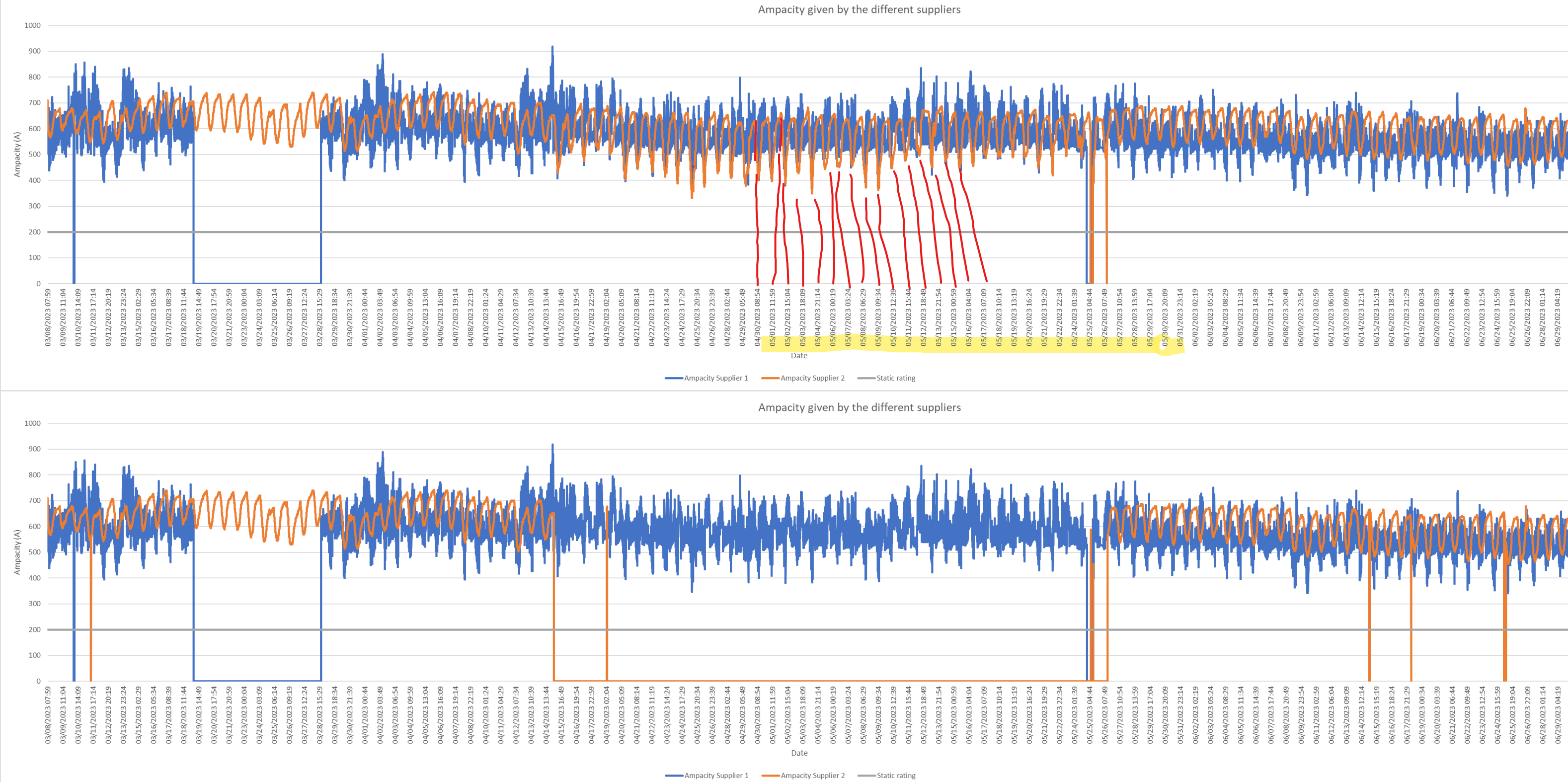


Figure 15: Dynamic rating values given by both Suppliers and static rating of the line a) include Supplier 2' points missing an input data b) excluding these points

4.2.3.2. Ampacity Calculation Using Suppliers' Input Data

4.2.3.2.1. Supplier 1

	IEEE	CIGRE	CIGRE
		601	207
Average of the difference	-2.13%	-1.42%	-0.93%

Table 27: Difference between the ampacity suppliers' value and the ampacity calculated by using their input data.

The Table 27 displays the percentage difference between our calculations and the values provided by Supplier 1. It should be noted that Supplier 1 adopts the CIGRE 207 standard, which accounts for the minimal deviation observed in their results compared to ours. The persistent difference of 1.19% could potentially be attributed to the application of specific safety coefficients by Supplier 1 in their calculations.

It is noteworthy that all our calculations consistently yield higher ampacity values compared to those provided by Supplier 1. This difference could be attributed to the safety coefficient in their calculations, which may lead to variations in the final results.

4.2.3.2.2. Supplier 2

	IEEE	CIGRE	CIGRE
		601	207
Average of the difference	21.18%	20.49%	21.52%

Table 28: Difference between the ampacity supplier 2 value and the ampacity calculated by using their input data.

Table 28 shows how the ampacities calculated using Supplier 2 weather input data are significantly different and higher than the ampacity provided by the supplier. This might suggest that they are using another calculation method for ampacity. It has been assumed that they use the indirect method, but they could potentially be using the direct method, calculating ampacity through sag or clearance. In [38], it is mentioned that this supplier

determines real-time sag data based on conductor vibrations measurement, implying that they use sag for ampacity calculation.

4.2.4. PERIODICITY OF THE RATING

At the time of study the periodicity, knowing the time duration in which the calculated ampacity exceeds the real-time ampacity is crucial because it helps determine whether the cable's thermal limits can withstand the operating conditions.

When the calculated ampacity consistently exceeds the real-time ampacity over extended periods, it indicates that the cable might be operating at or near its thermal limits for a significant portion of time. This prolonged exposure to high currents and temperatures can lead to excessive heating of the cable, potentially causing thermal degradation, insulation damage, or even cable failure.

On the other hand, if the given ampacity occasionally exceeds the real-time ampacity for short durations, it might not pose a significant risk as long as it stays within safe limits. These occasional deviations are normal and can be tolerated by the cable without adverse effects.

	15 MIN			30 MIN			1 HOUR		
	Average	Minimum	Instantaneous	Average	Minimum	Instantaneous	Average	Minimum	Instantaneous
Average	4,92	2,79	4,66	5,68	3,31	4,94	6,44	3,68	5,93
Maximum	140	14	14	141	29	29	144	57	59
Median	2	1	1	2	2	2	2	2	2

Table 29: Statistics of the time in minutes when the ampacity given different frequencies (15 min, 30 min, and 1 hour) exceeds the real-time ampacity.

The Table 29 presents the results of the time (minutes) when the ampacity rating calculations for three different scenarios: providing the rating every 15 minutes, 30 minutes, and 1 hour, exceeds the real-time ampacity. The calculations were performed using three methods: taking the average of minute-by-minute ratings from the preceding time period, using the most restrictive ampacity value from the preceding time period, and presenting the instantaneous real-time rating for each time.

When the average ampacity rating from the preceding period is considered, the highest average values are observed for the 1-hour scenario, followed by the 30-minute scenario and the 15-minute scenario. However, the differences are not very high, as it is the average time of each of the periods that the given ampacity exceed the real one, but it does not account for how many times occurs. It is evident that in the case of given the minimum value from the preceding period reduces the times that it occurs.

The median time duration, in almost all cases, is 2 minutes. This means that the cable is able to withstand these durations without the calculated ampacity exceeding the real-time ampacity.

The critical time periods occur when the ampacity starts to decrease for extended durations. In such cases, providing the value of the average of the preceding period, the minimum value, or the instantaneous value would still result in a higher ampacity rating than that of the subsequent period, as the ampacity is decreasing.

In this scenario of decreasing ampacity, combining on-site measurements with forecasted data can be effective in anticipating ampacity decreases. It's possible to select the lower ampacity value calculated from both on-site measurements and forecasts. Another approach is to apply a safety factor to the calculated ampacity when a decrease is detected between periods, reducing the duration during which the given ampacity exceeds the actual one.

Overall, the results demonstrate that the ampacity ratings can vary based on different calculation methods and time intervals. The choice of scenario and calculation approach will depend on the specific requirements of the OPF process and the desired level of conservatism in the system's operation.

4.2.5. EMISSIVITY AND SOLAR ABSORPTION COEFFICIENTS

Having understood the variation of ampacity with coefficients in 4.1.3, this knowledge is applied to our study line. The conductor coefficients for this line are: Solar Absorption=0.6 and Emissivity=0.5, with a service temperature of 65°C. The ampacity value has been calculated for a full day using both the actual coefficients of the line and the coefficients

recommended by IEEE (Solar Absorption=0.7, Emissivity=0.6) and CIGRE 601 (solar absorption=0.8, emissivity=0.7). The Table 30 displays the absolute variation in ampacity when comparing the results with the calculation using the actual coefficients. Notably, the variations are more significant when using the coefficients recommended by IEEE compared to the recommendations of CIGRE 601. This discrepancy arises because the coefficients recommended by IEEE differ more from the actual coefficients of our study line.

	<i>IEEE</i>	<i>CIGRE 601</i>	<i>CIGRE 207</i>
Solar absorption=0.7 Emissivity=0.6 (CIGRE 601 recommendation)	2.18%	2.10%	2.09%
Solar absorption=0.8 Emissivity=0.7 (IEEE recommendation)	4.30%	4.14%	4.12%

Table 30: Comparison of ampacity values using default and actual coefficients - Average absolute difference

In the Figure 16, the calculated ampacity using IEEE coefficients, both the actual ones from the line and the recommended ones, during the entire day is presented. The Figure 17 displays the difference between them. It can be observed that the difference is not constant and changes during time, more significant changes are observed during the night, mainly due to lower ambient temperatures, leading to a greater disparity with the conductor's temperatures. Consequently, as the emissivity coefficient increases, the ampacity rises, with no solar power effect during night-time. This effect gradually diminishes as the temperature increases and solar radiation becomes present, as the radiated power has less influence. The variation amounts to 4.30%, as shown in the table.

A similar pattern is observed with CIGRE 601 as Figure 18 and Figure 19, but the variation is less significant, 2.09%, as mentioned earlier.

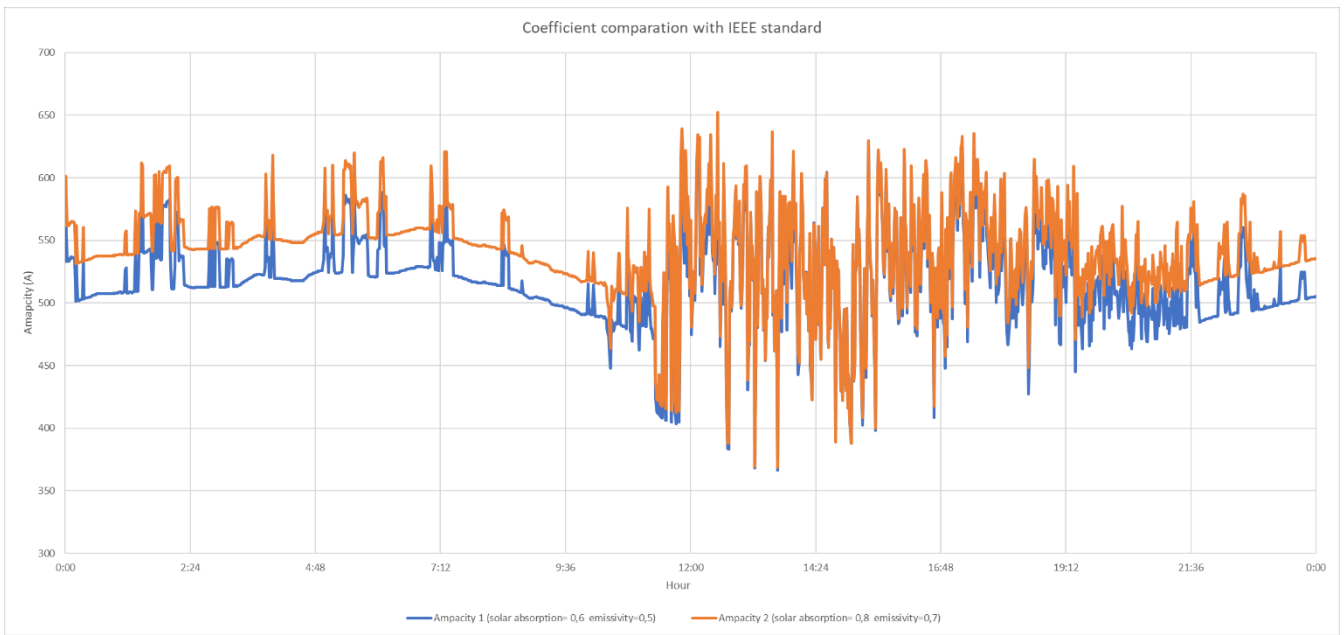


Figure 16: Ampacity comparison between ampacity calculated with actual line coefficients and ampacity calculated with IEEE recommended coefficients.

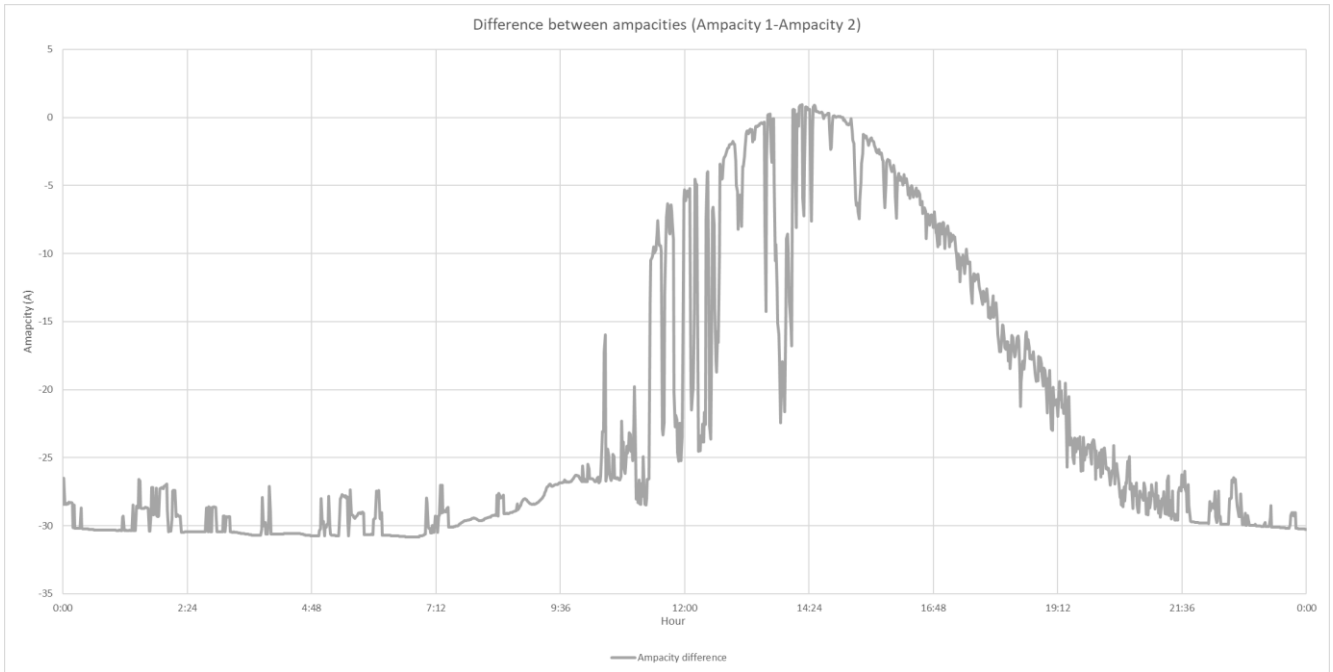


Figure 17: Difference between ampacity calculated with actual line coefficients and ampacity calculated with IEEE recommended coefficients.

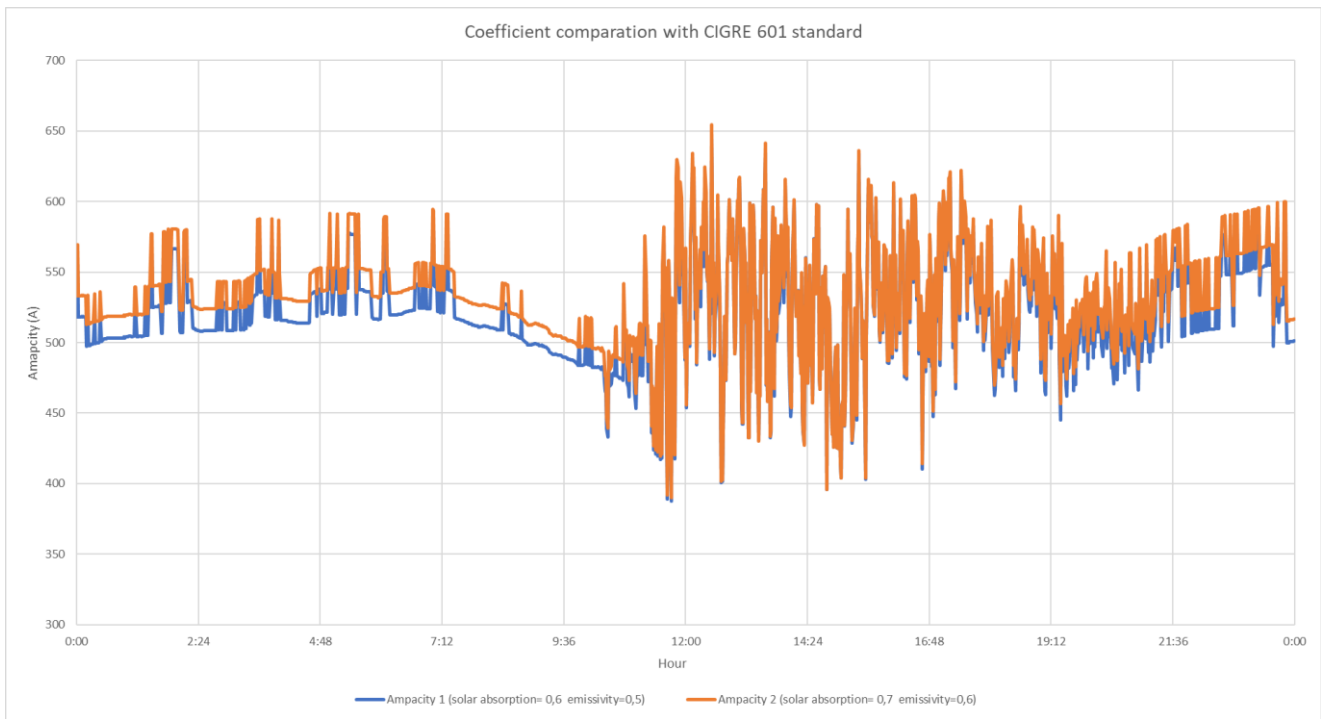


Figure 18: Ampacity comparison between ampacity calculated with actual line coefficients and ampacity calculated with CIGRE 601 recommended coefficients.

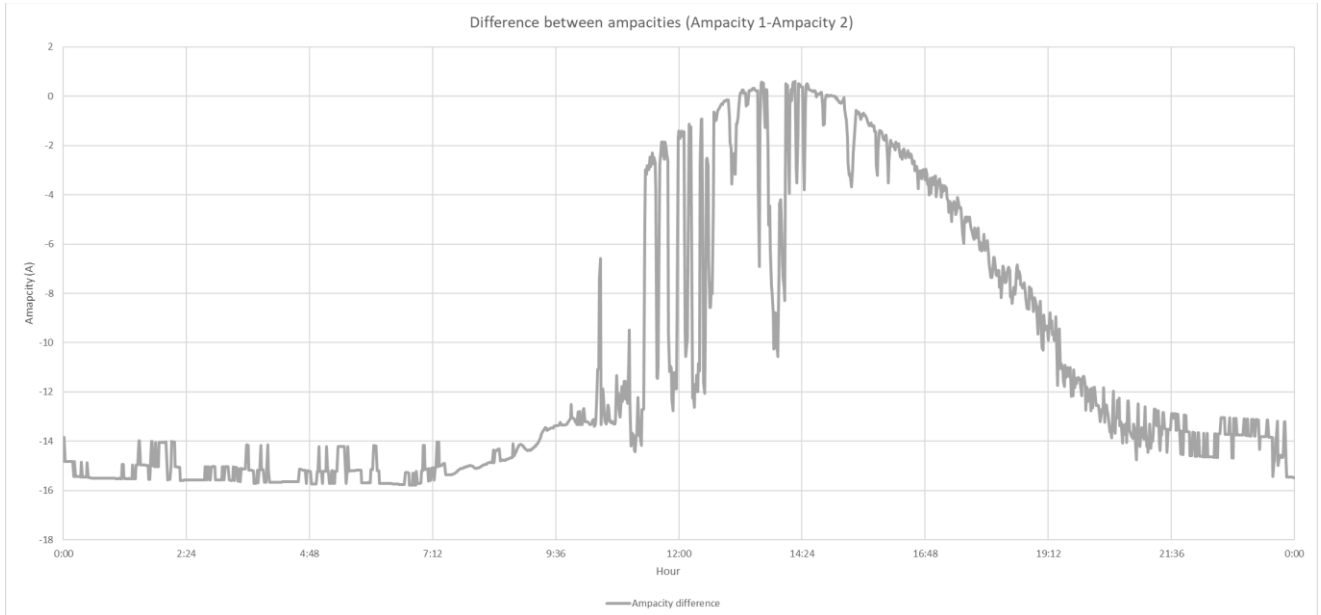


Figure 19: Difference between ampacity calculated with actual line coefficients and ampacity calculated with CIGRE 601 recommended coefficients.

4.3. SOLAR RADIATION

The Figure 20 shows solar radiation throughout the entire day. It depicts the solar radiation measured by the sensor (Qsensor), the solar radiation estimated using the IEEE formula (Q1), the solar radiation estimated using the CIGRE 601 formula (Q2), the solar radiation predicted by Open-Meteo (Q3), and finally, the radiation estimated based on historical maximum radiation (Q4).

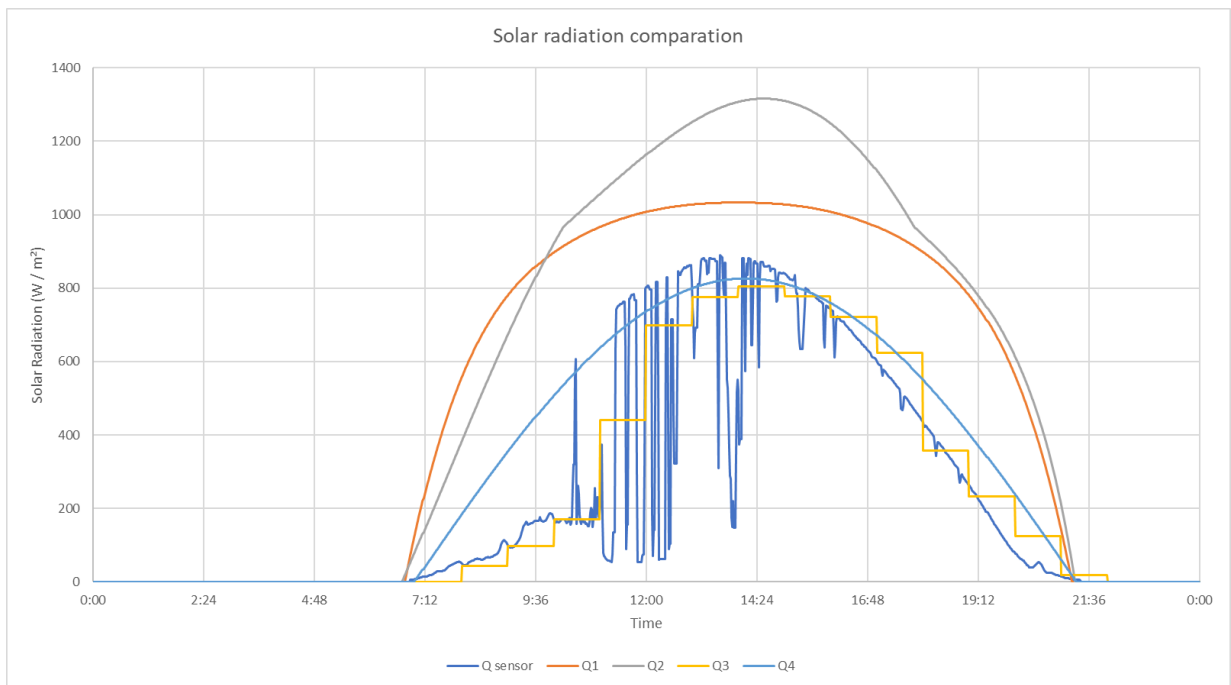


Figure 20: Solar radiation estimated by different ways and Solar radiation measured with the sensor.

As observed, the largest difference in solar radiation lies with Q1 and Q2, which are the estimated values based on standards. The predicted values, Q3, and the values estimated based on the maximum solar radiation, Q4, resemble the real values more closely.

The Table 31 presents the absolute percentage difference between the estimated and the measure solar radiation values, as well as the variation in the final ampacity calculation when using the sensor's measurement and the estimated values. Although there is a considerable difference between the estimated values and the measurement of solar radiation, its influence on the ampacity calculation is not significant.

Among the different estimated solar radiation values (Q1, Q2, Q3, and Q4), Q3, which represents the solar radiation predicted, exhibits the least variation. Specifically, the variation in Q3 is 52.04% compared to the actual measured solar radiation and the ampacity calculation using Q3 as an input show only a 0.93% variation compared to the calculation based on the actual measured solar radiation.

	<i>Q1</i>	<i>Q2</i>	<i>Q3</i>	<i>Q4</i>
Solar radiation variation	255.95%	252.79%	52.04%	93.28%
Ampacity variation	4.25%	6.30%	0.93%	1.57%

Table 31: Absolute percentage difference between the estimated and the measure solar radiation values.

Based on the information provided, it seems that using the predicted solar radiation (Q3) or estimating it based on historical values (Q4) can yield reasonably accurate results for the final ampacity calculation. Thus, it is possible to dispense with the use of a sensor.

4.4. SIMPLIFIED WIND CALCULATION

The Figure 21 displays the wind measured by Supplier 1 and the wind with the proposed simplifications. As observed, it consistently falls under the no-wind condition (0.6 m/s and 0.2 m/s in simplifications 1 and 2, respectively) since the limit is never exceeded at any time. This is because the measurements from Supplier 1 are strangely very low at all times, as said before.

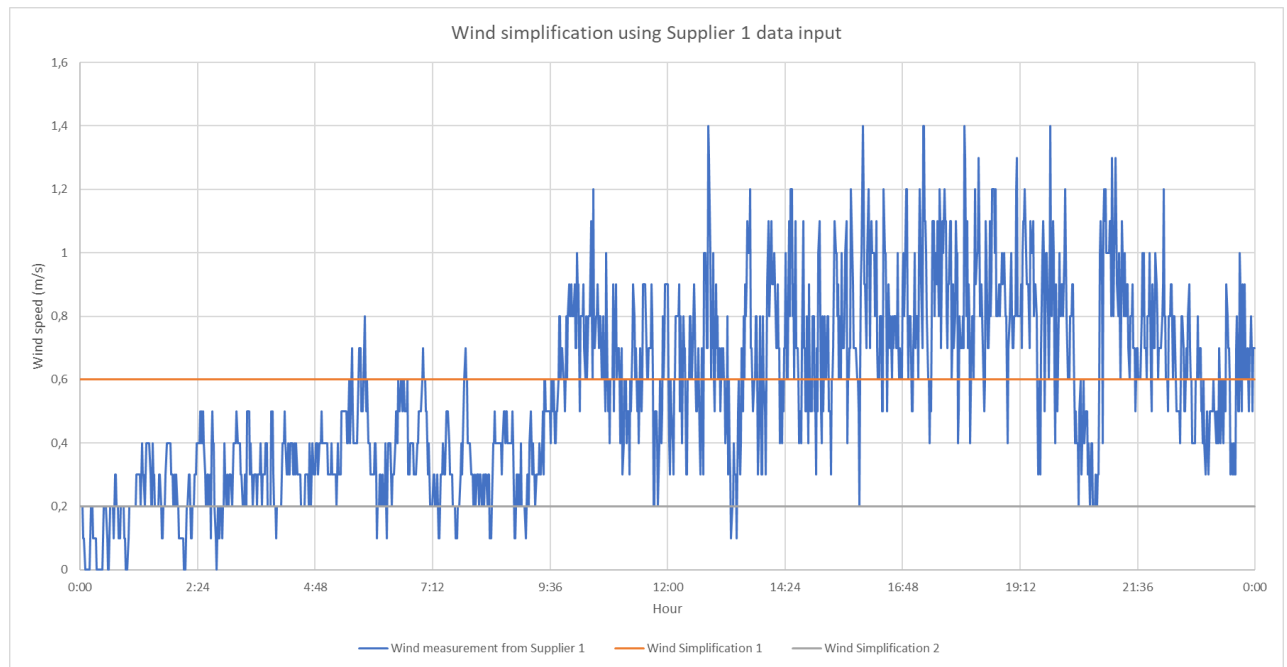


Figure 21: Wind simplification using Supplier 1 data input.

The Figure 22 displays the ampacities calculated with real wind data and with simplified wind data. The ampacities with the simplifications appear very similar because during no wind conditions one simplification assumes greater wind speed (0.6 m/s compared to 0.2 m/s), but on the other hand assumes lower wind direction (15° and 90° , respectively), so it is compensated in the final calculation of the convection power. The issue with data from Supplier 1 is the significant variation from one minute to another. The simplified wind approach manages to smooth out the curve, but during the night, the ampacity value given exceeds the real value. This could be because the assumed wind data during the night in the simplifications is relatively higher compared to the one that the sensor measures, although in reality, 0.6 m/s is considered a light breeze. The problem might indeed lie in the measurement of wind data by Supplier 1, which consistently appears very low.

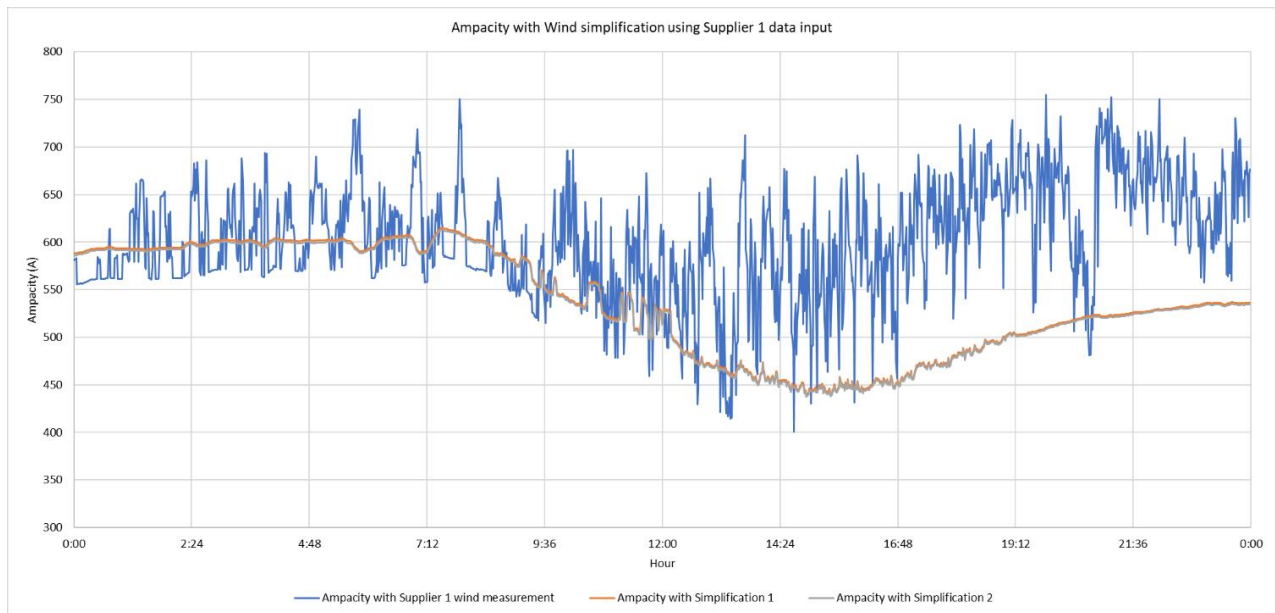


Figure 22: Ampacity with wind simplification using Supplier 1 data input.

Using the data input from Supplier 2 for the wind simplification yields a similar result as with Supplier 1, as it can be seen in the Figure 23. Throughout the entire time period, the measured wind never exceeds the thresholds required to be considered as "there is wind," resulting in both simplifications consistently indicating the absence of wind.

Considering that both Supplier 1 and Supplier 2's data consistently fall below the wind thresholds set in the simplifications, it raises concerns about the accuracy or reliability of the wind measurements from both sources.

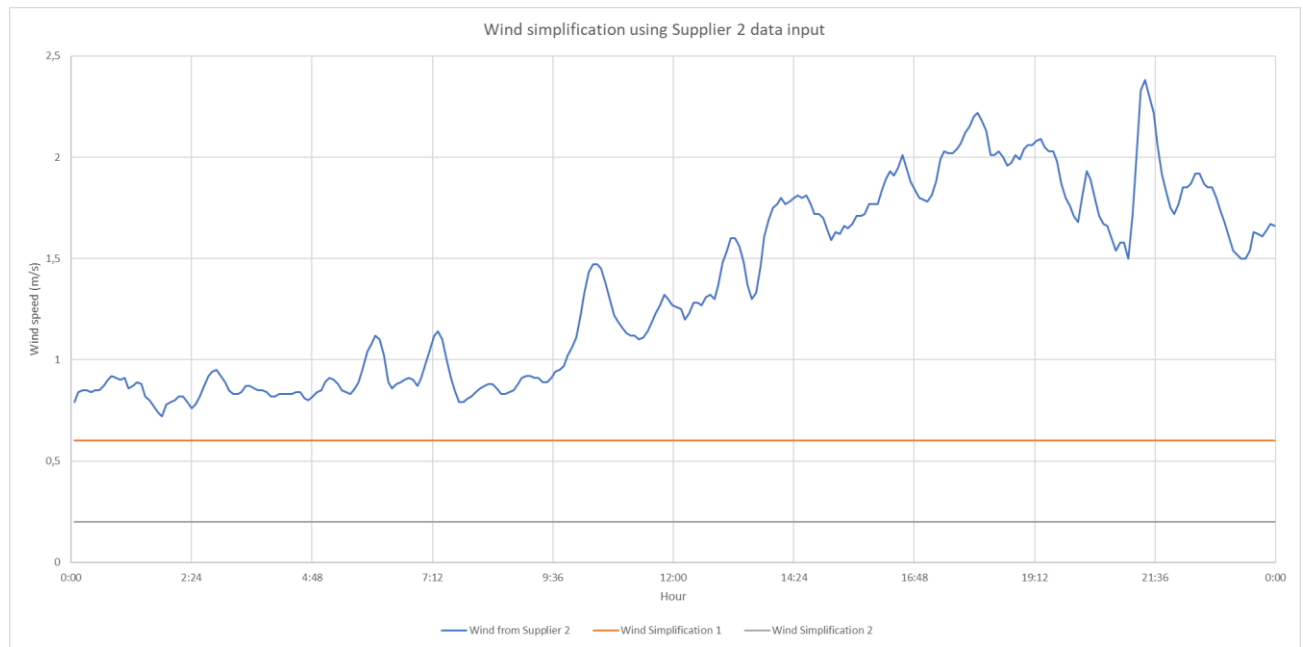


Figure 23: Wind simplification using Supplier 2 data input.

Upon examining the ampacity Figure 24, it is evident that at no point, when using wind data with the simplifications, does the calculated ampacity exceed the one calculated with the measured wind data. This discrepancy arises because, as seen in the Figure 23, a lower wind speed is assumed compared to the actual wind speed present at all times. The ampacity with both simplifications is very similar, for the same reason explained earlier with Supplier 1.

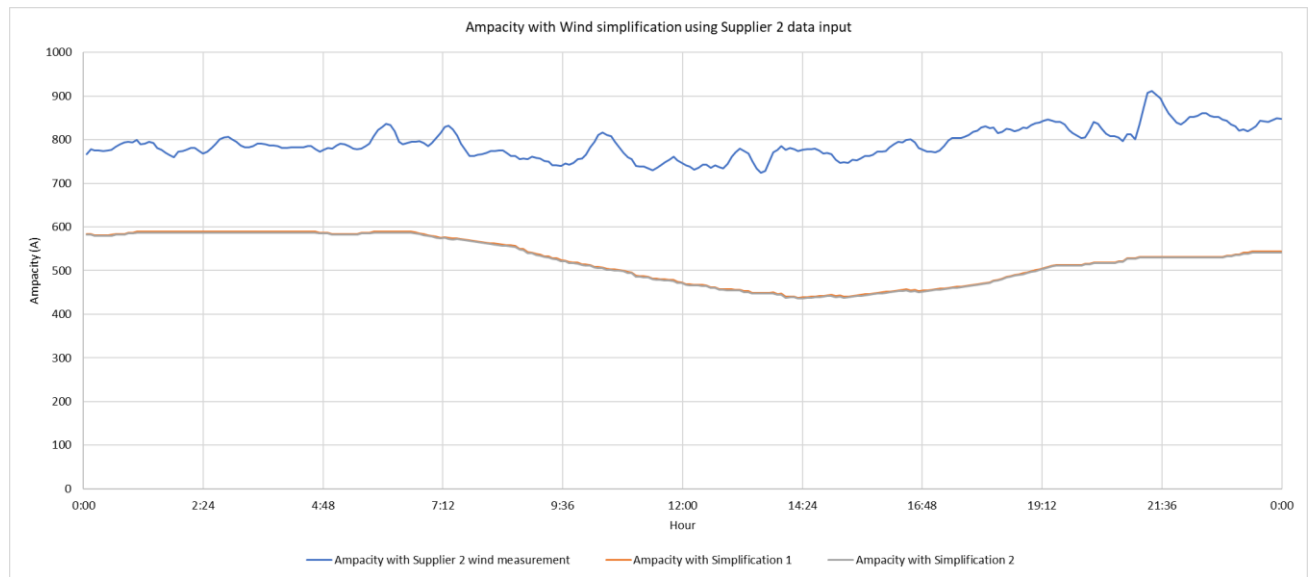


Figure 24: Ampacity with wind simplification using Supplier 2 data input.

When historical data is used, wind values are higher, and the thresholds set in the simplifications for determining the presence of wind are exceeded. As observed, when the thresholds are surpassed, it is considered that wind is present. In such cases, the assumed wind speed for both simplifications is 1.2 m/s, which is a very conservative value.

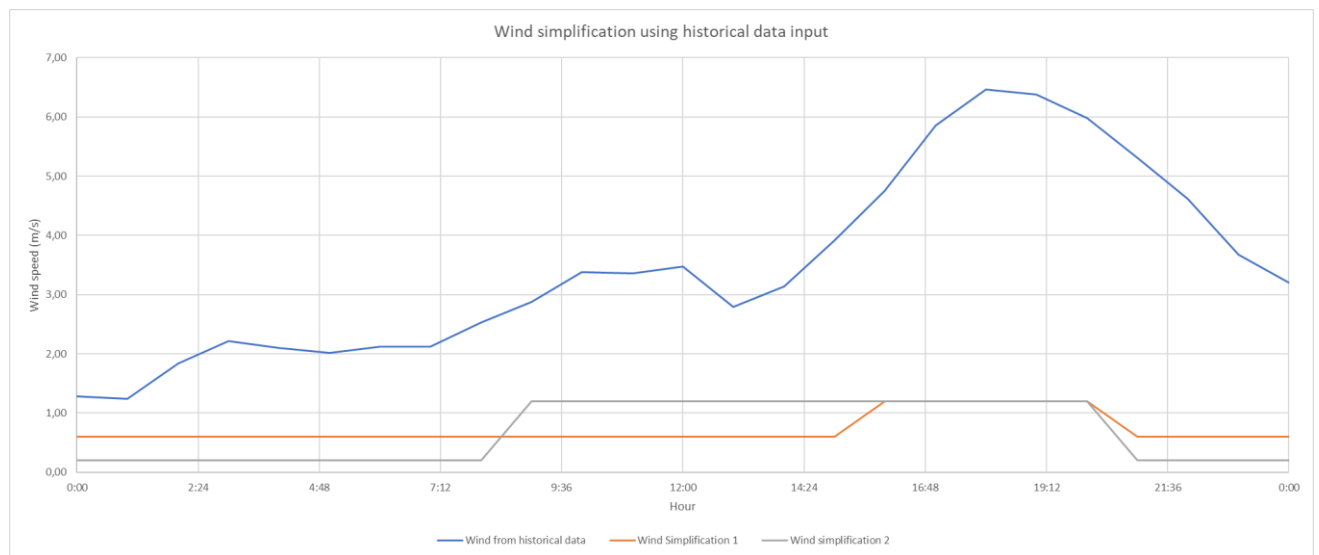


Figure 25: Wind simplification using historical data from Open-Meteo as data input.

The conservative values assumed in both simplifications ensure that ampacity calculations are carried out with caution. This approach helps maintain safety margins and ensures that the calculated ampacity values are not underestimated, even in the presence of more severe wind conditions.

As observed, simplification 2 tends to align more closely with the ampacity calculated using the non-simplified wind data. This suggests that simplification 2 provides a better approximation of the actual ampacity under real wind conditions compared to simplification 1.

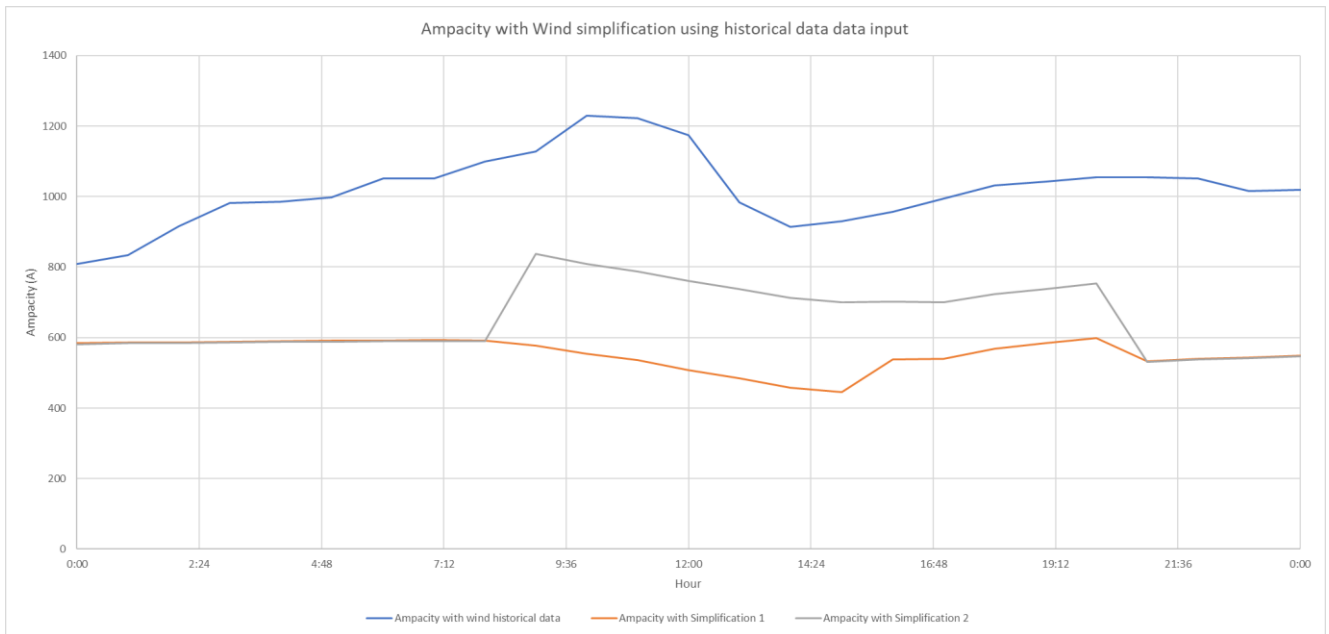


Figure 26: Ampacity with wind simplification using historical data from Open-Meteo as data input.

In the Table 32, the absolute average differences in both assumed wind speed and ampacity are recorded when comparing the two simplifications with the non-simplified data. This is provided for the three sets of data input: Supplier 1, Supplier 2, and historical data.

	<i>Supplier 1</i>		<i>Supplier 2</i>		<i>Historical data</i>	
	Simplification 1	Simplification 2	Simplification 1	Simplification 2	Simplification 1	Simplification 2
Wind speed difference (m/s)	0.13	0.37	0.76	1.16	2.75	2.79
Ampacity difference (%)	12.60%	12.73%	33.67%	33.92%	45.20%	35.52%

Table 32: Differences between the simplified and non-simplified approaches.

As observed, these simplifications are effective when having relatively high wind speeds, happen with the historical data. In this case, it has been possible to analyse the impact of these simplifications better. As seen in Table 32, simplification 2 optimizes the obtained ampacity better, differing by 35.52% from the non-simplified ampacity. This value could be further optimized by assuming fewer conservative values.

4.5. TEMPERATURE ANALYSIS

4.5.1. DAY OF LOWER TEMPERATURE

The Figure 27 displays the temperature measured by the sensor of Supplier 1 and the predicted temperature multiplied by the coefficient mentioned earlier, with $K = 1$ during the night and $K = 1.1$ during the day 23rd January 2023. It can be observed that the predicted temperature during the night is higher than the one measured by the sensor, whereas the predicted temperature during the day is lower than the measured temperature. As a result, when multiplying the predicted temperature by the coefficient of 1.1 during the day, it aligns more closely with the actual temperature.

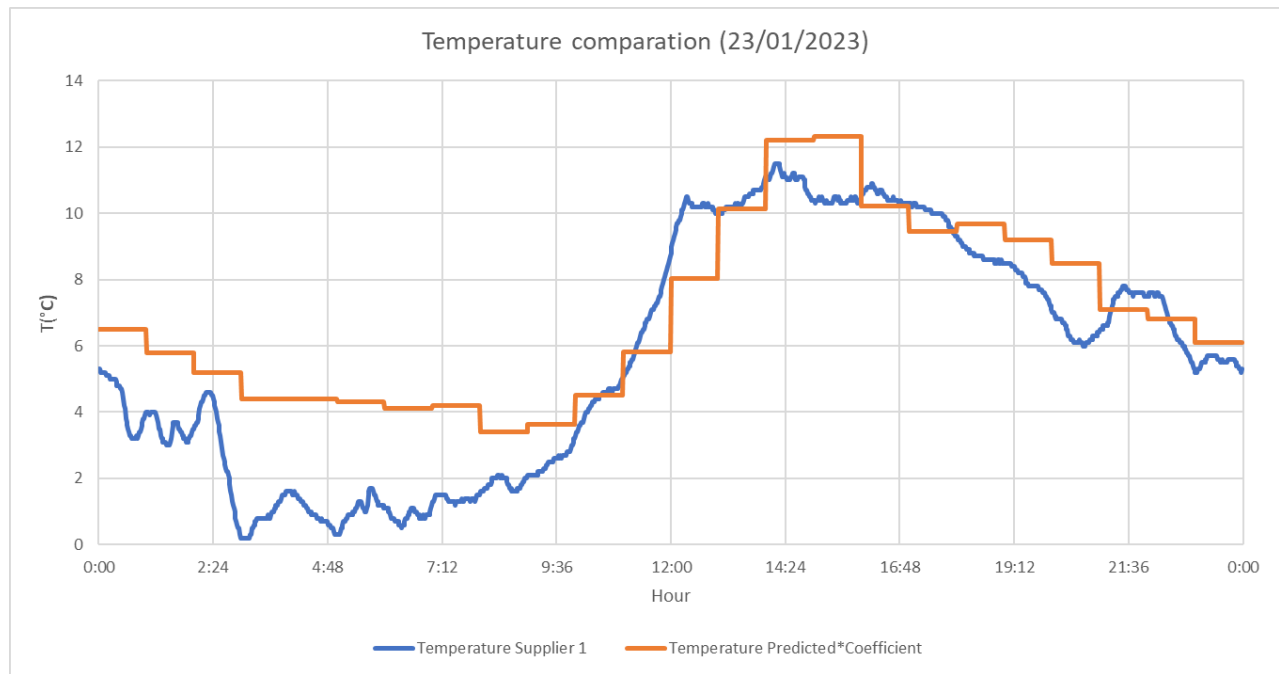


Figure 27: Comparation between temperature measured and predicted with coefficient applied for the day 23/01/2023.

When comparing ampacity values, Figure 28, it is important to identify the moments when the ampacity calculated with the prediction multiply by the coefficient is greater than the ampacity calculated with the actual temperature. These moments occur when the predicted temperature multiply by the coefficient is lower than the actual temperature, but as observed in the previous graph, these instances are infrequent.

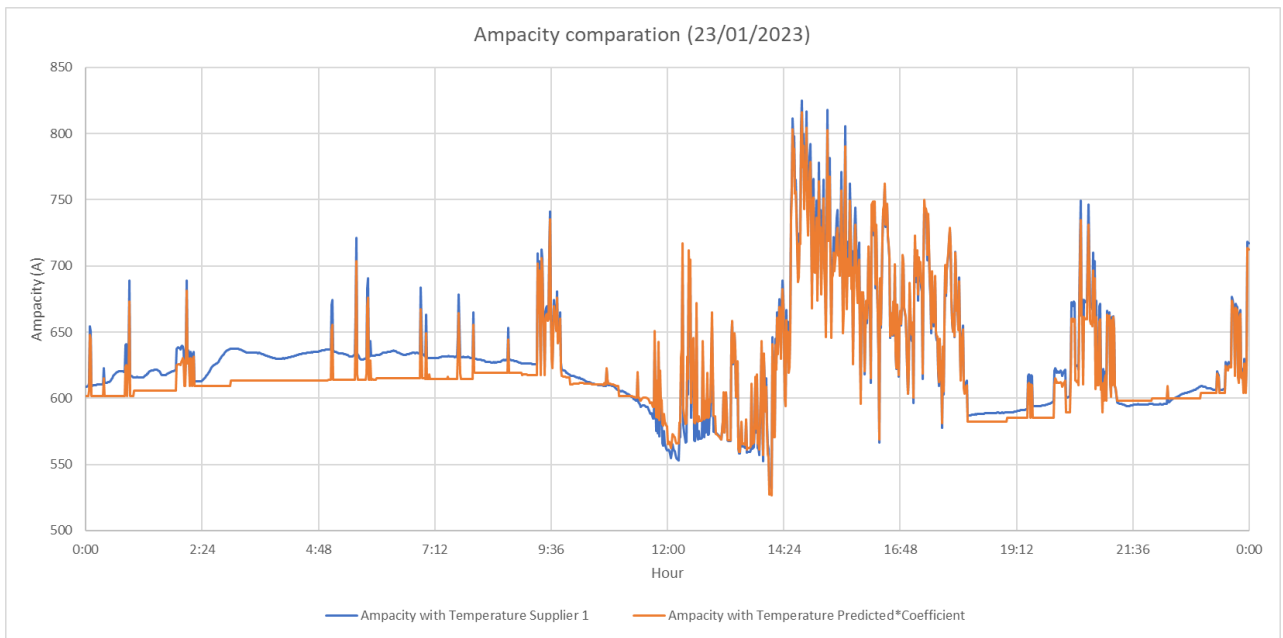


Figure 28: Comparation between the ampacity calculated with measured temperature and the ampacity calculated with temperature predicted with coefficient applied for the day 23/01/2023.

Additionally, ampacity calculations are performed using the higher of the predicted and measured temperatures. This way it ensures a conservative approach and helps to anticipate sudden changes in temperature.

The Table 33, shows the absolute average temperature differences (in °C) between the real temperature and the ones used in the calculations: the predicted temperature with the coefficients and the maximum between the predicted and the measured. Furthermore, the percentage difference in the final ampacity calculation in both cases is given. As observed, there is minimal variation in both temperature and ampacity values in both cases.

	<i>Predicted*Coefficient</i>	<i>Maximum</i>
Temperatures difference (°C)	1.20	1.28
Ampacity difference (%)	1.5%	1.1%

Table 33: Differences between the parameterized methods and the non-parametrized one for the day 23/01/2023.

4.5.2. DAY OF HIGHER TEMPERATURE

In this section, the day studied is the 25th of June 2023. In Figure 29, it can be seen that as observed in the previous case, during the night, the predicted temperatures are overestimated compared to the actual temperatures, confirming that using K=1 is sufficient and conservative. However, during the day, the predicted temperatures align quite well with the real temperatures and applying the coefficient of 1.1 makes them even higher, resulting in a more conservative estimation.

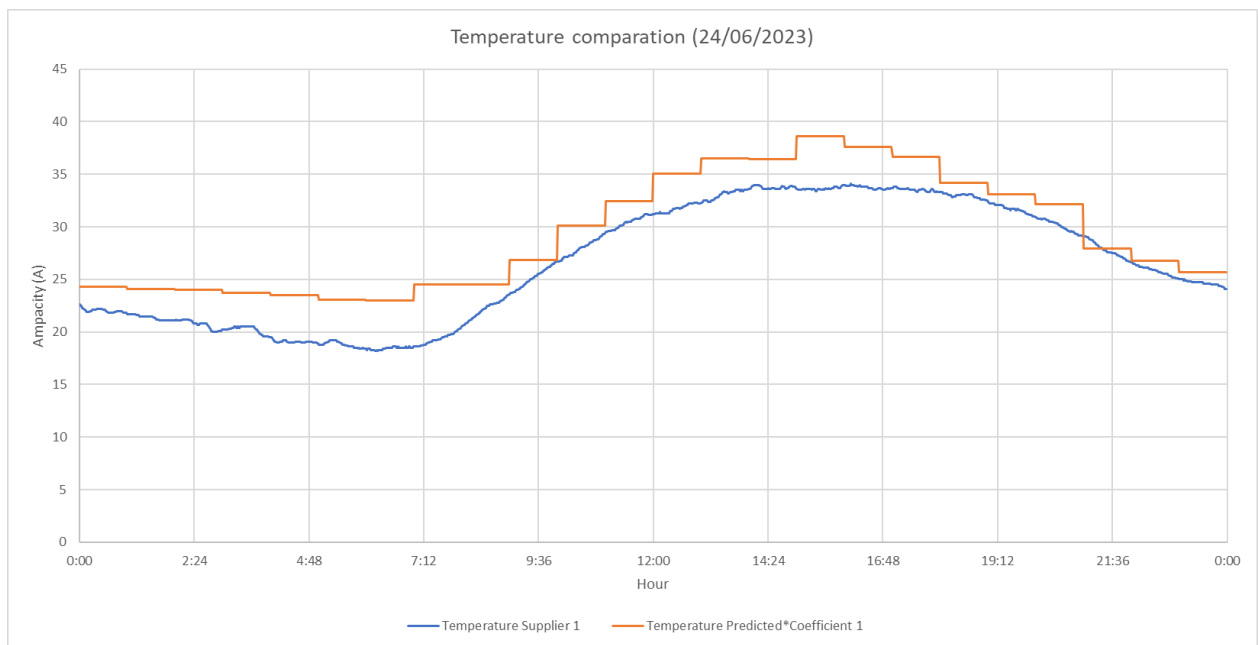


Figure 29: Comparation between temperature measured and predicted with coefficient applied for the day 24/06/2023.

In the Table 34, the differences are shown. As the predicted temperature aligns very well with the real temperature, when choosing the maximum between the two (predicted and measured), the differences are lower compared to when applying the coefficient. Using the coefficient would lead to a more conservative estimation than necessary in this case.

	<i>Predicted*</i>	<i>Coefficient</i>	<i>Maximum</i>
Temperatures difference (°C)		2.81	1.40
Ampacity difference (%)		4.4%	1.81%

Table 34: Differences between the parameterized methods and the non-parametrized one for the day

24/01/2023.

The analysis confirms that both methods of temperature consideration, either using the predicted temperature with a coefficient or selecting the higher temperature value, result in relatively small differences in ampacity calculations. Additionally, it is confirmed that in the case of using the predicted temperature multiplied by coefficients, which would be applicable when a temperature sensor is not available, the chosen coefficients provide a safe and reliable estimation.

5. CONCLUSIONS

While various studies have demonstrated that DLR can genuinely enhance the capacity of power lines at most of the times, its application across an entire network like that of Iberdrola entails a significant journey. This journey requires ensuring the system's complete reliability and safety, as any failure could result in substantial economic losses, such as the potential breakdown of a power line. The initial step toward implementing DLR within the company has involved the installation of pilot equipment by two different suppliers across some lines. This project has focused on analysing the data of these equipment. This analysis has been conducted with a forward-looking perspective: envisioning DLR as an input parameter for the Optimal Power Flow (OPF), aiming to enhance network flexibility. After all, DLR holds little value without a tool like the OPF. Having additional capacity is meaningless if you lack the knowledge of how and when to leverage it. Consequently, the following key conclusions from the conducted analyses are detailed below:

1. DLR is alternative to network reinforcement since it is a solution that can be quickly adopted. While the network reinforcement needs a long process that may last several years.
2. The reliability of the existing DLR pilot equipment is suboptimal, with Supplier 1 showing 82.6% reliability and Supplier 2 showing 48.1% reliability from January to June 2023.
3. **The wind speed measured by both equipment is too low, barely reaching 3 m/s, which raises doubts about the reliability of the measurements.**
4. Temperature and solar radiation measurements from Supplier 1 closely align with the historical data of Open-meteo data, while those from Supplier 2 show more significant discrepancies.

-
5. The capacity calculations using Suppliers' input variables differ from their reported ampacities, suggesting the utilization of unknown coefficients, simplifications, or methods by the suppliers.
 6. It is necessary to engage in discussions with the suppliers of the pilot equipment for several reasons. Firstly, to address the issue of frequent equipment breakdowns and their unreliability. Secondly, to verify the accuracy of their measurements for ambient variables, especially considering that the wind speed measured by both suppliers is too low. Thirdly, to request information on the coefficients and simplifications utilized in their calculations is also essential for a comprehensive evaluation.
 7. In the case of Supplier 2, it might be prudent to suggest changing his meteorological provider to obtain more accurate measurements for temperature and solar radiation that align better with the actual conditions of the transmission line. Furthermore, a clarification is needed on whether they employ a direct or indirect method for rating calculations, as the provision of rating without a complete set of atmospheric variables seems incongruent and as the calculation of the rating using its input data employing the three different standards does not match with the rating that they give.
 8. For Supplier 1, it is important to point out that the CIGRE 207 standard used for calculations is outdated and may not yield accurate results.
 9. Regarding the impact of variables on ampacity calculations using IEEE and CIGRE 601 standards, both generally produce similar results except for moderate to high wind speeds (above 3.5 m/s) with high conductor roughness (greater than 0.05). In such cases, CIGRE 601 yields higher ampacity values due to its consideration of conductor roughness, unlike IEEE.
 10. The CIGRE 207 standard is outdated, and the preferable options are to use the IEEE or CIGRE 601 standards.

-
11. The altitude of the transmission line above sea level has minimal impact on ampacity calculations. If the exact altitude is unknown, it is acceptable and conservative, to use the higher value of the altitude zone based on regulation on technical conditions for overhead lines encompassing the line's location.
 12. Absorption and emissivity coefficients significantly influence ampacity calculations when conductor service temperatures are high (80°-100°) because the higher difference between the ambient and conductor temperatures. However, for moderate service temperatures (common in most cases), using default coefficients recommended by the standards suffices.
 13. Solar radiation sensors are unnecessary as predictions or estimations provide reliable results.
 14. A priori, wind measurement on site the line is indeed important, but its reliability is crucial. As an alternative, wind forecasts can be used, but considering that wind conditions vary significantly across different locations. The meteorological station should ideally be in close proximity to the line, or a safety factor could be applied based on the distance between them to account for potential discrepancies.
 15. If it is decided to measure the wind on site, there are two possibilities for wind measurement and need to be studied to see which one is more cost-effective:
 - a. On-Site Wind Speed Measurement (Effective Wind Speed) as used by Supplier 2: Provides the effective wind speed but requires line shutdown and maintenance involves climbing the line. By adopting this method, there is no need for a separate wind direction sensor.
 - b. Wind Speed and Wind Direction Sensors on Towers as used by Supplier 1: Requires both wind and direction sensors but eliminates the need for line shutdown and maintenance in the proper line. However, it measures wind at the tower, not the exact line wind.

-
16. Proposed simplifications for wind are useful when wind speeds are reasonably high and exceed the simplification thresholds. Simplification 2 optimizes ampacity more effectively than Simplification 1, and further investigation could explore less conservative simplifications.
 17. An ambient temperature sensor is unnecessary as ambient temperature prediction with applied coefficients yields reliable results. A cable temperature sensor is neither necessary, as it is no need for the ampacity calculation. However, they can be installed at control points in the network to verify that the measured cable temperature corresponds to the expected ampacity result. For instance, at monitored points in the network where maintenance challenges are reduced, such as main substations.
 19. For anticipating temperature changes to reduce ampacity variation in OPF, temperature sensors can be installed to use the maximum temperature between sensor measurements and predictions in ampacity calculations.
 20. Periodicity is a crucial parameter to consider for using DLR as an input for the OPF. The challenge of periodicity arises when ampacity decreases over an extended period, leading the provided rating, whether average, minimum, or instantaneous for the timeframe, to surpass the actual rating. In such a scenario of ampacity decline, a potential solution could involve combining on-site measurements with predicted measurements or applying a safety factor when detecting this ampacity decrease.

In conclusion, equipment reliability is an absolute necessity, and engaging in discussions with both suppliers to review their equipment is crucial. When implementing DLR, variables like solar radiation and ambient temperature do not require on-site measurements, whereas the need for wind measurements should be evaluated for potential placement on all lines or just critical ones. Combining on-site measurements with forecasted data can anticipate abrupt changes in ampacity and provide support if measurement sensors fail. The frequency of data collection is a key parameter for OPF, necessitating further investigation based on the desired level of system security. These conclusions are expected to guide the future

deployment of DLR within Iberdrola. The subsequent section provides recommendations for key steps that the company should consider in formulating the deployment plan for 2030.

6. PLAN 2030

The term "Plan 2030" is not a complete plan in itself, but rather a compilation of essential steps that need to be considered when developing and executing the deployment plan for Dynamic Line Rating (DLR) through Dynamic Smart Protection (DSP) and Dynamic Thermal Rating (DTR). It serves as a comprehensive roadmap to guide the process of implementing DLR in Iberdrola's power grid network. While these steps may not necessarily follow a strict chronological order, they are all crucial elements that need to be considered for the successful deployment of this technology.

1. **Analysis of Existing DLR Pilot Equipment:** Conduct a comprehensive analysis of the existing pilot equipment, which serves as the foundation for this project. Evaluate the reliability and performance of these equipment installations, review the input variables used in their rating calculations, and identify patterns or trends in their historical data. This analysis will form the basis for determining the necessary improvements and adaptations for full-scale implementation.
2. **Engage with Suppliers:** Collaborate with the suppliers of the pilot equipment to address the issues related to frequent disruptions in their operation found in the previous step. Request these suppliers to verify and validate their environmental measurements, especially the recorded wind speeds, which have shown concerns regarding their accuracy. Also, urge the suppliers to calibrate their sensors regularly and ensure the reliability of the weather data provided if on-site measurements are not available.
3. **DLR Calculation Approach:** Based on the findings from Step 1, determine the most suitable approach for calculating DLR. This involves making decisions on several key aspects:
 - Decide which variables are critical to be measured in real-time, with wind speed being a primary focus.

-
- Select the preferred standard to be used for calculating ampacity, evaluating options like IEEE or CIGRE 601.
 - Consider potential simplifications or parameterizations in the rating calculation process to optimize efficiency.
 - Determine the periodicity for updating DLR values, ensuring it aligns with the capabilities of the Optimum Power Flow (OPF) calculations.
4. **Data Verification:** Establish robust data verification procedures to ensure the integrity of input variables. Develop mechanisms for detecting inconsistent measurements and address potential errors promptly. Even, considering the option of categorizing stations as "unreliable" when necessary.
5. **Evaluate the necessity of on-site wind measurements:** If it is necessary for all lines or only critical ones, considering the potential to utilize forecasts with safety coefficients for other lines.
6. **Select Optimal Wind Measurement Approach:** If it decided to measure the wind on-site, thoroughly explore the two viable options for wind speed measurement and evaluate their advantages and challenges:
- a. On-Site Wind Speed Measurement (Effective Wind Speed): Analyse the benefits of accurate on-site wind speed measurement, but also assess the impact of required line stoppages for installation and maintenance, as well as potential risks for personnel maintenance as they must work in the line with high voltages.
 - b. Wind Speed and Wind Direction Sensors on Towers: Examine the benefits of measuring wind speed and direction from the towers, which eliminates line stoppages. However, consider the trade-off of not having measurements from the exact line location.

-
5. **Methods for Rating Validation:** Devise effective methods for validating the calculated ratings. Consider installing temperature sensors on the line to verify that the calculated temperature aligns with the actual conductor intensity.
 6. **Contracting Suppliers:** Select a reliable and experienced contractor to supply the necessary sensors and weather data. Ensure that the chosen supplier meets the specific requirements and quality standards necessary for successful DLR implementation.
 7. **Contingency Plan:** Develop a comprehensive contingency plan to proactively manage potential equipment failures and disruptions. Outline procedures for quick response and recovery to minimize downtime and maintain grid stability.
 8. **Placement of Sensors:** Strategically determine the number and placement of sensors on each line, considering their significant length and specific characteristics. Prioritize the selection of the most restrictive rating when multiple sensors are deployed on a single line.
 9. **SCADA Integration:** Establish robust protocols and interfaces for transmitting sensor and weather data to the SCADA system. Ensure seamless integration for real-time monitoring and control.
 10. **Develop OPF Application:** Develop a sophisticated OPF application to effectively incorporate DLR into network reconfiguration strategies. Optimize the power system's operation by utilizing DLR to dynamically adjust line ratings, improving grid efficiency and reliability.
 11. **Analyse DLR forecast:** This encompasses not only the forecasted measurements (as it has been done in this project) but also the potential provision of information about the expected rating in the upcoming hours. This approach can prove valuable for the planning of scheduled tasks. For instance, if a line needs to be disconnected tonight, having knowledge of the projected network status at that moment could aid in redirecting the flow efficiently. Furthermore, this information can be beneficial for

generating alerts by anticipating overloads in specific lines within a specific time frame based on the current network situation.

12. **Maintenance, Inventory, and Averias Plan:** Create detailed plans for sensor calibration, maintenance, and inventory management. Establish schedules for regular maintenance activities and inventory checks to ensure optimal equipment performance.
13. **Cost Analysis:** Conduct a thorough cost analysis, considering not only the initial setup costs but also the operational expenses and expected durability of the equipment. Assess the long-term economic benefits and ensure a cost-effective implementation strategy.
14. **Risk Analysis:** Conduct a risk analysis to identify and evaluate potential risks associated with DLR implementation. Focus on the risk of inaccurately calculated DLR ratings leading to line overloading and damage. Consider the significant financial losses and operational disruptions due to power line failures. Evaluate risks related to DLR equipment reliability, data accuracy, and compatibility with SCADA. Develop mitigation strategies and contingency plans, such as enhanced equipment redundancy and regular calibration. Regularly monitor and review risk analysis to address potential threats and safeguard valuable power grid assets.
15. **Plan for Future Considerations:** Investigate opportunities for future enhancements, including the utilization of machine learning algorithms to enhance weather inputs for DLR. For instance, in cases where a weather station provides specific wind and temperature data, machine learning could be employed to estimate corresponding line conditions. This approach could be particularly useful in instances where sensor data is missing or unreliable, demonstrating a commitment to ongoing improvement and innovation.

The initial step: “Analysis of Existing DLR Pilot Equipment” has been completed in this project. The derived outcomes are expected to contribute to the prospective deployment of DLR.

To sum up, the Plan 2030 encompasses essential phases for Iberdrola's DLR deployment strategy. Adhering to these steps will establish a solid foundation for the effective implementation of DLR in the power grid network.

7. BIBLIOGRAPHY

- [1] ‘Acuerdo de París sobre el Cambio Climático’, Feb. 03, 2023. <https://www.consilium.europa.eu/es/policies/climate-change/paris-agreement/> (accessed Jun. 19, 2023).
- [2] ‘EUuniversal_D1.3_Challenges-and-opportunities-for-electricity-grids-and-markets.pdf’. Accessed: Aug. 12, 2023. [Online]. Available: https://euniversal.eu/wp-content/uploads/2021/08/EUuniversal_D1.3_Challenges-and-opportunities-for-electricity-grids-and-markets.pdf
- [3] ‘Las energías renovables podrían alcanzar el 50% del “mix” de generación eléctrica en España en 2023 | Red Eléctrica’. <https://www.ree.es/es/sala-de-prensa/actualidad/nota-de-prensa/2023/03/las-energias-renovables-podrian-alcanzar-50porciento-del-mix-de-generacion-electrica-en-espana-en-2023> (accessed May 25, 2023).
- [4] R. Mínguez, R. Martínez, M. Manana, A. Arroyo, R. Domingo, and A. Laso, ‘Dynamic management in overhead lines: A successful case of reducing restrictions in renewable energy sources integration’, *Electr. Power Syst. Res.*, vol. 173, pp. 135–142, Aug. 2019, doi: 10.1016/j.epsr.2019.03.023.
- [5] L. Rácz, G. Gabor, and B. Németh, ‘Different Approaches of Dynamic Line Rating Calculations’, in *2019 7th International Youth Conference on Energy (IYCE)*, Jul. 2019, pp. 1–6. doi: 10.1109/IYCE45807.2019.8991570.
- [6] ‘Repotenciación: la gran renovación del parque renovable en España’, *El Periódico de la Energía*, Mar. 21, 2023. <https://elperiodicodelaenergia.com/repotenciacion-la-gran-renovacion-del-parque-renovable-en-espana/> (accessed May 29, 2023).
- [7] A. Sendin, J. Matanza, and R. Ferrús, *Smart Grid Telecommunications: Fundamentals and Technologies in the 5G Era*. Hoboken, NJ, 2021.
- [8] B.-G. Risi, F. Riganti-Fulginei, and A. Laudani, ‘Modern Techniques for the Optimal Power Flow Problem: State of the Art’, *Energies*, vol. 15, no. 17, 2022, doi: 10.3390/en15176387.
- [9] A. De Paola, D. Angeli, and G. Strbac, ‘Scheduling of Wind Farms for Optimal Frequency Response and Energy Recovery’, *IEEE Trans. Control Syst. Technol.*, vol. 24, no. 5, pp. 1764–1778, Sep. 2016, doi: 10.1109/TCST.2016.2514839.
- [10] F. Gómez, J. M. De María, D. Puertas, A. Baïri, and R. Granizo, ‘Numerical study of the thermal behaviour of bare overhead conductors in electrical power lines’, Jan. 2011.
- [11] M. Simms and L. Meegahapola, ‘Comparative analysis of dynamic line rating models and feasibility to minimise energy losses in wind rich power networks’, *Energy Convers. Manag.*, vol. 75, pp. 11–20, Nov. 2013, doi: 10.1016/j.enconman.2013.06.003.

-
- [12] D. J. Spoor and J. P. Roberts, ‘Development and experimental validation of a weather-based dynamic line rating system’, in *2011 IEEE PES Innovative Smart Grid Technologies*, Nov. 2011, pp. 1–7. doi: 10.1109/ISGT-Asia.2011.6257099.
 - [13] R. Martínez, A. Arroyo, M. Mañana, P. Bernardo, R. Minguez, and R. Garrote, ‘A comparison of different methodologies for rating definition in overhead lines’, *Renew. Energy Power Qual. J.*, pp. 806–810, May 2016, doi: 10.24084/repqj14.470.
 - [14] T. Yip, C. An, G. Lloyd, M. Aten, and B. Ferri, ‘Dynamic line rating protection for wind farm connections’, in *2009 CIGRE/IEEE PES Joint Symposium Integration of Wide-Scale Renewable Resources Into the Power Delivery System*, Jul. 2009, pp. 1–5.
 - [15] C. A. E. Realpe, ‘Using the concept of dynamic line rating to facilitate the integration of variable renewable energy and to optimize the expansion of the German power grid’.
 - [16] T. Song and J. Teh, ‘Dynamic thermal line rating model of conductor based on prediction of meteorological parameters’, *Electr. Power Syst. Res.*, vol. 224, p. 109726, Nov. 2023, doi: 10.1016/j.epsr.2023.109726.
 - [17] ‘Congressional_DLR_Report_June2019_final_508_0.pdf’. Accessed: May 29, 2023. [Online]. Available: https://www.energy.gov/sites/prod/files/2019/08/f66/Congressional_DLR_Report_June2019_final_508_0.pdf
 - [18] M. Kanálik, A. Margitová, J. Urbanský, and L. Beňa, ‘Temperature Calculation of Overhead Power Line Conductors According to the CIGRE Technical Brochure 207’, in *2019 20th International Scientific Conference on Electric Power Engineering (EPE)*, May 2019, pp. 1–5. doi: 10.1109/EPE.2019.8778173.
 - [19] A. Arroyo *et al.*, ‘Comparison between IEEE and CIGRE Thermal Behaviour Standards and Measured Temperature on a 132-kV Overhead Power Line’, *Energies*, vol. 8, no. 12, Art. no. 12, Dec. 2015, doi: 10.3390/en81212391.
 - [20] S. Karimi, P. Musilek, and A. M. Knight, ‘Dynamic thermal rating of transmission lines: A review’, *Renew. Sustain. Energy Rev.*, vol. 91, pp. 600–612, Aug. 2018, doi: 10.1016/j.rser.2018.04.001.
 - [21] G. Blumberg and C. Weber, ‘Impact of dynamic line rating on redispatch’, in *2019 16th International Conference on the European Energy Market (EEM)*, Sep. 2019, pp. 1–6. doi: 10.1109/EEM.2019.8916513.
 - [22] S. Klyapovskiy, S. You, A. Michiorri, G. Kariniotakis, and H. W. Bindner, ‘Incorporating flexibility options into distribution grid reinforcement planning: A techno-economic framework approach’, *Appl. Energy*, vol. 254, p. 113662, Nov. 2019, doi: 10.1016/j.apenergy.2019.113662.
 - [23] C. Castel, ‘Dynamic Line Rating for overhead lines – V6’.
 - [24] ‘Oncor_DLR_Case_Study_05-20-14_FINAL.pdf’. Accessed: Jun. 29, 2023. [Online]. Available:

https://www.energy.gov/sites/prod/files/2016/12/f34/Oncor_DLR_Case_Study_05-20-14_FINAL.pdf

- [25] ‘Dynamic Line Rating: Innovation Landscape Brief’.
- [26] J. S. Jones, ‘Energinet’s dynamic line rating improves capacity up to 30%’, *Smart Energy International*, Jun. 01, 2023. <https://www.smart-energy.com/industry-sectors/energy-grid-management/energineets-dynamic-line-rating-improves-overhead-capacity-by-up-to-30/> (accessed Jun. 29, 2023).
- [27] ‘National Grid trials new technology which allows more renewable power to flow through existing power lines | National Grid Group’. <https://www.nationalgrid.com/national-grid-trials-new-technology-which-allows-more-renewable-power-flow-through-existing-power> (accessed Jun. 29, 2023).
- [28] ‘acer-decision-06-2022-on-the-first-amendment-of-the-core-intraday-ccm.pdf’. Accessed: Jul. 06, 2023. [Online]. Available: <https://www.sepsas.sk/media/5569/acer-decision-06-2022-on-the-first-amendment-of-the-core-intraday-ccm.pdf>
- [29] D. Hardman, N. Murdoch, and J. Berry, ‘THE BENEFITS AND DESIGN OF A DYNAMIC PROTECTION SYSTEM FOR THE DISTRIBUTION NETWORK’, 2019.
- [30] ‘Guide for thermal rating calculations of overhead lines’, *e-cigre*. <https://e-cigre.org/publication/601-guide-for-thermal-rating-calculations-of-overhead-lines> (accessed May 25, 2023).
- [31] ‘IEEE Standard for Calculating the Current-Temperature Relationship of Bare Overhead Conductors’, *IEEE Std 738-2012 Revis. IEEE Std 738-2006 - Inc. IEEE Std 738-2012 Cor 1-2013*, pp. 1–72, Dec. 2013, doi: 10.1109/IEEESTD.2013.6692858.
- [32] A. T, ‘Sag & Tension in overhead Line? - Definition & Factors Affecting it’, *Circuit Globe*, May 25, 2016. <https://circuitglobe.com/sag-and-tension.html> (accessed Aug. 12, 2023).
- [33] S. Abbott, S. Abdelkader, L. Bryans, and D. Flynn, ‘Experimental validation and comparison of IEEE and CIGRE dynamic line models’, in *45th International Universities Power Engineering Conference UPEC2010*, Aug. 2010, pp. 1–5.
- [34] I. A. S. Rincón, ‘Análisis de Metodologías Para el Cálculo de la Ampacidad en Conductores Desnudos’.
- [35] ‘207.Thermal behaviour of Overhead line conductors.pdf’. Accessed: Aug. 16, 2023. [Online]. Available: <https://cigreindia.org/CIGRE%20Lib/Tech.%20Brochure/207.Thermal%20behaviour%20of%20Overhead%20line%20conductors.pdf>
- [36] ‘Free Open-Source Weather API | Open-Meteo.com’. <https://open-meteo.com/> (accessed Aug. 01, 2023).
- [37] ‘Machine Translation of “Royal Decree 223/2008 Of 15 February, Laying Down The Regulations On Technical Conditions And Guarantees Of Security In ...” (Spain)’.

<https://www.global-regulation.com/translation/spain/1444584/royal-decree-223-2008-of-15-february%252c-laying-down-the-regulations-on-technical-conditions-and-guarantees-of-security-in-high-voltage-power-lines-and.html> (accessed Aug. 02, 2023).

- [38] K. Morozovska and P. Hilber, ‘Study of the Monitoring Systems for Dynamic Line Rating’, *Energy Procedia*, vol. 105, pp. 2557–2562, May 2017, doi: 10.1016/j.egypro.2017.03.735.

ANNEX I: ALIGNMENT WITH THE SUSTAINABLE DEVELOPMENT GOALS (SDGs)

Countries around the world are increasingly committing themselves and setting more ambitious targets in the fight against climate change. This growing concern is reflected in conferences and agreements between nations, such as the United Nations Climate Change Conference (COP26), as well as in the Sustainable Development Goals (SDGs) of the 2030 Agenda.

COP26 was held in Glasgow in 2021 and brought together 120 world leaders, who reached agreements on a number of critical measures. These included limiting global temperature rise, reducing carbon emissions by 45% and phasing out fossil fuels, among many others.

The SDGs, also known as the Global Goals, are a set of 17 interconnected goals established by the United Nations in 2015. They cover a wide range of sustainable development issues, such as poverty eradication, gender equality, climate action, education and health, among others. The SDGs provide a comprehensive framework to address the world's most pressing challenges and ensure a sustainable and equitable future for all.

Our main focus is on SDG 7, which aims to ensure universal access to affordable, reliable, sustainable and modern energy. However, it is important to bear in mind that the Sustainable Development Goals (SDGs) are interconnected and progress on one can have a positive impact on the others. By working towards SDG 7 and promoting access to clean and sustainable energy, we indirectly contribute to achieving the broader global targets outlined in the SDGs.

To effectively address SDG 7, it is crucial to establish an efficient electricity grid that relies on environmentally friendly energy sources. This aligns with the goal of decarbonization, which aims to reduce the carbon footprint and mitigate the negative impacts of climate

change. By transitioning to renewable and zero-emission energy sources, we can ensure a sustainable and greener future while promoting economic growth and social well-being.

Therefore, renewable energy plays a key role in reducing the carbon footprint. The Spanish Electric Network (Red Eléctrica Española, REE) estimates that by 2023, 50% of the energy generated in Spain will be renewable [3], signifying significant progress in energy transition. Spain boasts one of the highest installed capacities for renewable energy after Germany.

However, the high integration of renewables into the electrical power system poses a challenge for Transmission System Operators (TSOs) and Distribution System Operators (DSOs). Renewable energies are unpredictable and require a more flexible operation of the electric system. It's important to explain that due to grid safety considerations, there are instances where the full energy generated by renewables cannot be introduced, resulting in curtailment. For example, in 2015, wind energy accounted for 20% of the country's energy capacity, but only 0.3% of this energy could be introduced due to limitations in the transmission and distribution network capacity [4].

Therefore, it is necessary to increase the capacity of the grid to enable the integration of renewables. To achieve this, Dynamic Line Rating (DLR) has emerged as a viable solution, as it allows optimizing existing power lines and eliminates the need for constructing new ones. This solution is both environmentally friendly and cost-effective compared to building new infrastructure. A practical example can be seen in the case [4], where the DSO managed to increase injected wind energy into the grid by 70.9 GWh, resulting in a total savings of 7,800 tons of CO₂ emissions through DLR.

In conclusion, DLR proves to be a beneficial solution for increasing grid capacity and integrating renewables. It offers environmental advantages and cost savings compared to traditional approaches, making it a valuable tool in the pursuit of sustainable energy systems.